QUASI-PHASEMATCHED WAVEGUIDES FOR INFRARED NONLINEAR OPTICS USING GaAs/Ge/GaAs HETEROEPITAXY

A DISSERTATION

SUBMITTED TO THE DEPARTMENT OF APPLIED PHYSICS

AND THE COMMITTEE ON GRADUATE STUDIES

OF STANFORD UNIVERSITY

IN PARTIAL FULFILLMENT OF THE REQUIREMENTS FOR THE DEGREE OF

DOCTOR OF PHILOSOPHY

Christopher Barrowclough Ebert

November 1998

UMI Number: 9924419

UMI Microform 9924419
Copyright 1999, by UMI Company. All rights reserved.

This microform edition is protected against unauthorized
copying under Title 17, United States Code.

UMI
300 North Zeeb Road
Ann Arbor, MI 48103

© Copyright by Christopher Barrowclough Ebert 1999
All Rights Reserved

I certify that I have read this dissertation and that in my opinion it is fully adequate, in scope and quality, as a dissertation for the degree of Doctor of Philosophy.

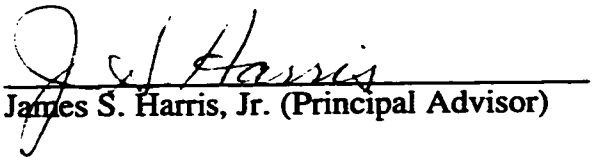

James S. Harris, Jr. (Principal Advisor)

I certify that I have read this dissertation and that in my opinion it is fully adequate, in scope and quality, as a dissertation for the degree of Doctor of Philosophy.

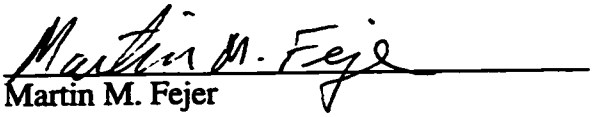

Martin M. Fejer

I certify that I have read this dissertation and that in my opinion it is fully adequate, in scope and quality, as a dissertation for the degree of Doctor of Philosophy.

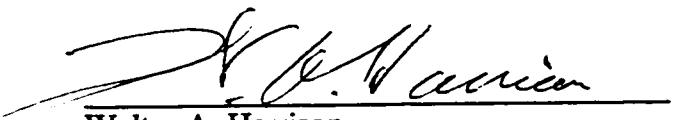

Walter A. Harrison

Approved for the University Committee on Graduate Studies

ABSTRACT

Coherent light sources with wavelengths in the mid-infrared (mid-IR) region of the spectrum have many potential applications, ranging from airborne countermeasures to wavelength conversion for Wavelength-Division Multiplexing. Although lasers exist in this spectral region, they suffer from many practical limitations, including limited wavelength tuning or the need for cryogenic cooling. A mid- to far-IR output can be generated by mixing two near-IR beams in a material which exhibits a strong nonlinear susceptibility, where the generated light is at the difference of the two applied frequencies. Because this difference frequency field and the applied near-IR fields travel at different frequencies, due to material dispersion, the two will slip out of phase after a finite length (known as the coherence length) and power will flow back into the applied beams, rather than the desired output beam. Quasiphasematching is a method whereby the sign of the nonlinear coefficient is reversed every coherence length, ensuring a monotonic transfer of power into the desired output.

Gallium Arsenide (GaAs) has many properties that make it a desirable material for nonlinear optical mixing. Specifically, GaAs has a large nonlinear coefficient, a wide transparency range, a mature and well-developed materials technology, and the possibility for direct integration of near-IR laser diode sources on the same substrate. GaAs lacks, however, a convenient method of phasematching the nonlinear interaction. The sign of the nonlinear coefficient in GaAs is determined by the direction of the Ga-As bonds in the zincblende crystal structure. By reversing the sublattice allocation - by interchanging the position of the Ga and As atoms - it is possible to reverse the sign of the nonlinear coefficient.

We have achieved this desired effect through the use of polar-on-nonpolar epitaxy. Due to the reduced symmetry of the polar material, it is possible for both phases of GaAs to nucleate on a nonpolar material, such as Ge. Under the proper conditions, the correct phase of GaAs can be grown on a Ge interlayer. To produce the desired devices, a

thin layer of Ge is epitaxially grown via MBE on a GaAs wafer, followed by a layer of GaAs of opposite orientation as that of the substrate. Through a process of lithography and selective etching, alternating regions of the GaAs wafer are exposed. The wafer is then introduced into the MBE chamber for regrowth of the necessary waveguiding layers.

Material results demonstrating control of the GaAs orientation, using only epitaxial techniques, will be presented. We have found that a combination of temperature and substrate misorientation direction determines the phase of the epilayer GaAs. In addition, the boundary propagation between two regions of opposite phase is examined, due to its impact on device performance. Finally, preliminary second harmonic generation data using waveguides fabricated on all-epitaxial orientation-patterned GaAs will be presented.

ACKNOWLEDGEMENTS

First of all, I would like to thank Prof. Harris for serving as my advisor during my studies here at Stanford. I have truly come to appreciate the experience of working in his group, especially the diverse set of challenges and opportunities that are rarely found elsewhere. And I have come to learn that when it matters, Prof. Harris will be there for you.

I would also like to thank Prof. Fejer for serving as a 'co-advisor' for me. His advice and experience are always valuable, and often gave a me a new way of looking at problems and looking for solutions. The collaboration between the Fejer and Harris groups has been especially fruitful and rewarding, and I am glad to have had the pleasure of working with him. My sincere gratitide also goes to Prof. Harrison for several helpful discussions and reading my thesis, and to Prof. Feigelson and Prof. Moler for serving on my orals committee.

My time at Stanford has been made enjoyable because of the people here. My Applied Physics classmates (Adrian Butscher, Dario Falquier, Peter Giles, Duncan Steward, Tim Stowe, and Paul White) helped through the first year of problem sets, and beyond. I also appreciate the camaraderie of the Ginzton crowd, whether from softball during the summer or just wasting time at 10:00 doughnuts. Krishnan Parameswaran has always been around to talk hockey or baseball, or run the OSA, and Patric Torreau has been invaluable in helping with the optical measurements in this thesis.

I've had the wonderful opportunity to work with some of the staff here at Stanford, and I've enjoyed the interaction. Special thanks goes to Ken Williams, Sandy Meyer, Bob Wheeler and the CIS crew (Keith Gaul, Pat Burke, Jose Solorzano, Luke Meisenbach, Karl Brandt, and Len Booth). Gail Chun-Creech and Lu Miao were instrumental over the years in keeping the group running, and Paula Perron of Applied Physics was especially helpful in keeping everything in order.

The fellow students in the Harris group, both past and present, were an invaluable part of this thesis. Herman Chui introduced me to MBE growth and nonlinear optics, and Michael Larson was particularly instrumental in teaching me the proper use and

care of the equipment. Glenn Solomon has been a wonderful resource of knowledge of the days past. Wayne Martin and Vijit Sabnis have kept my e-mail coming over the years, while Chien-Chung Lin, Thierry Pinguet, and Sylvia Spruytte have been a great help in the new lab. Tzu-Fang Huang, Cheng-yu Hung, Renan Milo, Barbara Paldus, and Fred Sugihwo have also been helpful through the years. Special mention goes to Chris Coldren, both for his technical help in getting the MBE machines operational again, but also for his insights and intuition on a great number of problems.

A place of honor in this thesis goes to Loren Eyres, my co-worker on this project. It was his idea of using GaAs/Ge/GaAs heteroepitaxy that led to this project, and it is because of his determination and perseverance that we were able to accomplish what we did. But more importantly, he has been a great friend over the years, and that's what I'll remember most.

Last but not least, I would like to thank those people, although not here at Stanford, that are also an integral part of this thesis. This includes the teachers, coaches, and mentors I've had over the years, from grade school through the University, since each of them has made some contribution to my development, that no matter how small, is still vital to who I am today. And finally, this thesis is dedicated to my family and friends back home, in thanks for providing me safe refuge for rest and relaxation during my studies.

TABLE OF CONTENTS

1. INTRODUCTION AND MOTIVATION 1
1.1 INFRARED OPTICS 1
1.1.1 Current Infrared Sources 2
1.2 NONLINEAR OPTICS 5
1.3 GALLIUM ARSENIDE 7
1.4 ORGANIZATION 8
2. NONLINEAR OPTICS AND WAVEGUIDE FUNDAMENTALS 10
2.1 PHYSICS OF NONLINEAR OPTICS 11
2.2 NONLINEAR OPTICAL EQUATIONS 13
2.2.1 Phasematching 17
2.3 SUM-FREQUENCY GENERATION AND DIFFERENCE-FREQUENCY GENERATION 22
2.4 WAVEGUIDES 23
2.5 CONCLUSION 27
3. APPROACH 28
3.1 ALTERNATIVE APPROACHES 29
3.1.1 Quasi-Phasematching 32
3.2 Ge/GaAs APPROACH 35
3.3 CONCLUSION 38
4. MOLECULAR BEAM EPITAXY 39
4.1 MBE MECHANICS 40
4.2 GaAs MBE 42
4.3 RHEED 47
4.4 Ge EPITAXY 50
4.5 REGROWTH 50
5. ANTIPHASE GROWTH: BACKGROUND, RESULTS AND DISCUSSION 53
5.1 BACKGROUND 53
5.2 ANTIPHASE GROWTH 60
5.3 TEST STRUCTURE 63

5.4 DISCUSSION OF ANTIPHASE GROWTH 70
5.5 CONCLUSION 72
6. GROWTH OF ORIENTATION-PATTERNED WAVEGUIDES AND NONLINEAR OPTICAL RESULTS 75
6.1 TEMPLATE GROWTH 75
6.1.1 Buffer Layer Studies 76
6.1.2 Template Design 76
6.2 TEMPLATE PATTERNING AND REGROWTH PREPARATION 77
6.2.1 Alternative Template Designs 79
6.3 REGROWTH 80
6.4 PHASE-BOUNDARY PROPAGATION 81
6.5 WAVEGUIDE GROWTH 83
6.6 WAVEGUIDE FABRICATION 85
6.7 NONLINEAR OPTICAL MEASUREMENTS 86
6.7.1 Loss Mechanisms in Orientation-Patterned GaAs Waveguides 89
6.8 CONCLUSION 91
7. FUTURE WORK AND CONCLUSION 93
7.1 FUTURE WORK 93
7.2 ACCOMPLISHMENTS AND CONCLUSION 95
8. BIBLIOGRAPHY 97

LIST OF TABLES

Number *Page*

Table 1. Growth conditions for various samples grown for antiphase growth studies.... 70

LIST OF FIGURES

Number *Page*

Figure 1.1. Applications and sources in the infrared region of the optical spectrum 4
Figure 1.2. Schematic of nonlinear optical conversion processes.....6
Figure 2.1. Noncentrosymmetric potential energy function.. 12
Figure 2.2. $Sinc^2(L/L_c)$ curve showing reduced conversion away from phasematching condition..... 18
Figure 2.3. Indices of refraction for a negative uniaxial crystal.. 19
Figure 2.4. Schematic of a quasi-phasematched structure. 20
Figure 2.5. Nonlinear output versus length for different phasematching conditions 21
Figure 2.6. Energy-conservation diagrams..... 22
Figure 2.7. Schematic of an Optical Parametric Oscillator 23
Figure 2.8. Schematic of a waveguide structure 24
Figure 2.9. Diagram showing TE and TM waves for waveguides fabricated on (001) GaAs..... 27
Figure 3.1. Birefringence of AlAs/GaAs multilayer stacks, and oxidized AlAs/GaAs stacks, as a function of (oxidized) AlAs duty cycle.. 31
Figure 3.2. GaAs lattice viewed along two different directions 33
Figure 3.3. Process diagram of wafer-bonding method for creating orientation-patterned structures..... 35
Figure 3.4. Schematic of a GaAs/Ge/GaAs heterostucture with GaAs phases antiphase to one another..... 36
Figure 3.5. Process flow for creating orientation-patterned waveguides using all-epitaxial methods 37
Figure 4.1. Schematic of an MBE machine..... 42
Figure 4.2. Step-flow growth vs. island nucleation..... 43
Figure 4.3. Schematic of growth on a surface misoriented towards (111)A..... 45
Figure 4.4. Schematic of growth on a surface misoriented towards (111)B..... 45
Figure 4.5. Co-evaporation vs. MEE..... 46
Figure 4.6. Schematic of Ewald sphere..... 48
Figure 4.7. Proposed model of (2x4) surface reconstruction during GaAs growth. 49

Figure 5.1. Antiphase Boundary (APB) and Antiphase Domains (APDs)..... 54
Figure 5.2. Schematic of growth of GaAs/Ge/GaAs heterostructures..... 59
Figure 5.3. RHEED pictures before and after Ge deposition..... 61
Figure 5.4. Etch profiles for features defined along in-plane [110] and [1-10] directions of a (001) wafer..... 62
Figure 5.5. Schematic of test structure used for antiphase growth studies..... 64
Figure 5.6. Cross section of film nucleated at 350° C. 65
Figure 5.7. Cross-section of film nucleated at 500° C..... 66
Figure 5.8. Cross-section of film nucleated at 400° C..... 67
Figure 5.9. Cross-section views of samples containing layers of alternating phase..... 69
Figure 5.10. Step- vs. Terrace-nucleation model..... 72
Figure 6.1. Schematic of template structure used for patterned regrowth..... 77
Figure 6.2. Etch sequence used to pattern templates..... 78
Figure 6.3. Cross-section of orientation-patterned GaAs film grown via MOCVD using a wafer-bonded template..... 81
Figure 6.4. SEM micrograph of anisotropically etched orientation-patterned GaAs film. 82
Figure 6.5. Waveguide structure used for SHG of 1550 nm pump. 83
Figure 6.6. Cross section SEM micrograph of orientation-patterned GaAs film..... 84
Figure 6.7. Profile of a waveguide fabricated in orientation-patterned GaAs..... 85
Figure 6.8. Schematic of setup used to measure SHG..... 86
Figure 6.9. SHG Phasematching peaks for three different gratings..... 87
Figure 6.10. Plot showing predicted phasematching period vs. wavelength..... 88
Figure 6.11. Output power vs. Input power for SHG..... 89
Figure 6.12. Loss (in dB/cm) for waveguides..... 91

1. INTRODUCTION AND MOTIVATION

Although many applications exist for infrared optics, the scarcity of intense, coherent sources is a limiting factor towards the realization of many systems such as chemical sensors or eyesafe laser radar. For many wavelengths, such as the familiar red light of a He-Ne laser, it is possible to fabricate a laser to directly generate the light of interest, and provide a source with the desired coherence and power requirements. For many regions of the optical spectrum, however, there is a lack of suitable materials with the necessary properties for lasing. By taking advantage of the nonlinear properties of certain materials, it is possible to convert light from an easily-generated frequency into the desired frequency.[1] One potential material for realizing this conversion is Gallium Arsenide - GaAs. Although GaAs is widely used for its electronic and optoelectronic properties for devices such as transistors or semiconductor diode lasers, it has many other characteristics that makes it useful, and even desirable, for certain nonlinear optical applications.

As implied by the title of this work, three questions relevant to the research presented here need to be discussed: What is the interest in Infrared Optics?, Why use nonlinear optical techniques?, and Why use GaAs?

1.1 INFRARED OPTICS

First of all, what is the interest in infrared optics and infrared sources? One wide-ranging use of infrared optics involves spectroscopic applications. Many gases, such as NO, CF_4, NH_3, and most hydrocarbons all have strong absorption features in the infrared region of the spectrum, as illustrated in Figure 1.1(a). A suitable infrared source, tuned to an absorption line for one of these molecules, provides a sensitive method of determining concentrations by measuring how much light is attenuated by the sample. Such a device would be useful for pollution control or process monitoring. For instance, a sensor that analyzed automobile exhaust for pollutants could be used to feed back information to the engine for cleaner operation. Alternatively, a source tuned to the glucose

absorption line (9-10 μm) could be used to measure blood sugar levels and control insulin for diabetics, perhaps even without drawing blood from the patient.[2, 3]

Another significant use of infrared light involves fiber optic communication systems, such as are commonly used for long-distance telephone calls. These typically are centered around the regions of minimum dispersion (1.3 μm) or minimum loss (1.55 μm) in silica-based fibers. One technique for increasing the data rate through a fiber is Wavelength Division Multiplexing (WDM) whereby several wavelengths are used to transmit data concurrently through the fiber, instead of just one. In order to realize such a system, however, techniques for routing data from one wavelength to another must be developed. Present schemes involve detecting the data at one wavelength and converting it to an electrical signal, which is then used to drive a source at the desired new wavelength. Several disadvantages of such a system are readily apparent, primarily the power required for such a conversion, and the time required, since electrical processes are relatively slow as compared to optical processes. An all-optical method could avoid most, if not all, of these problems.[4]

Many other potential applications exist for infrared optics, as can also be seen in Figure 1.1(a). Laser radar systems could take advantage of the atmospheric windows (regions of low absorption) at 3-5 μm and 8-12 μm, allowing for the detection and tracking of remote objects.[5] Such a system could also be made eye-safe, since the necessary powers would not be dangerous to vision at these wavelengths. Another important use is for airborne countermeasures. An intense infrared signal, in the proper spectral region, could be made to appear as a hot jet engine to a heat-seeking missile and thus used to decoy the missile away from an aircraft.

1.1.1 Current Infrared Sources

Figure 1.1(b) illustrates many of the coherent, infrared sources that are presently available. In the near-infrared (near-IR -- 800 nm - 2 μm), it is possible to make efficient semiconductor diode lasers, and these have in fact found many applications, including optical data storage (CDs) and as sources for optical fiber communication systems. Lasers using materials lattice-matched to GaAs usually operate in the 600 nm - 1

μm region, while using InGaAsP lattice-matched to InP allows the wavelength region to be extended out to 1.3 - 1.55 μm. Semiconductor lasers with wavelengths spanning the region of 3-34 μm also exist, particularly ones employing the lead salt (PbSnTe and PbSSe) material system.[6] For example, GaInSb/InAs superlattice lasers are capable of emitting 3-5 μm radiation, while strained-quantum well lasers using InAsSb/InAlAs are capable of emitting in the 4.5 μm region.[2, 7] For wavelengths greater than 3 μm, IV-VI lead salt lasers, such as PbSe/PbSrSe are expected to have an advantage over III-V compounds, particulary with respect to Auger recombination.[8] These lasers operate, however, in the 40 - 160K temperature range. Operation of diode lasers further out in the IR is made difficult by increasing amounts of Auger recombination. As the bandgap of the semiconductor decreases, the amount on nonradiative recombination between the holes and electrons becomes increasingly significant, especially at room temperature. As a result, the energy given up through the recombination process goes into phonons, or lattice heating, instead of photons. Operation at cryogenic temperature decreases this effect, but significantly increases the complication of packaging and operation of such a device.

Recent developments at Bell Labs by Faist et al. have brought solid-state mid-IR lasers one step closer to reality, in the form of quantum cascade lasers.[9] This laser, instead of using interband recombination, uses intersubband recombination created by cleverly engineering the energy levels in coupled quantum wells. In addition, due to the 'cascading' nature, each electron can result in the production of 20 photons, as opposed to the 1:1 photon: electron correspondence in traditional diode lasers. Currently, quantum cascade lasers span the wavelength region from 4 to 11 μm, with the output being selected by the design of quantum well structure, and not through a change in materials.[10] In addition, operation at room temperature has been achieved, although only in a pulsed mode and not yet in a CW mode.[11] Single-mode operation and narrow linewidth, necessary for spectroscopic applications, can be achieved through the use of DBR grating mirrors.[12] Because of the incredible complexity of this structure with hundreds of epilayers, however, it is still questionable whether it will find use in any other than high-end applications.

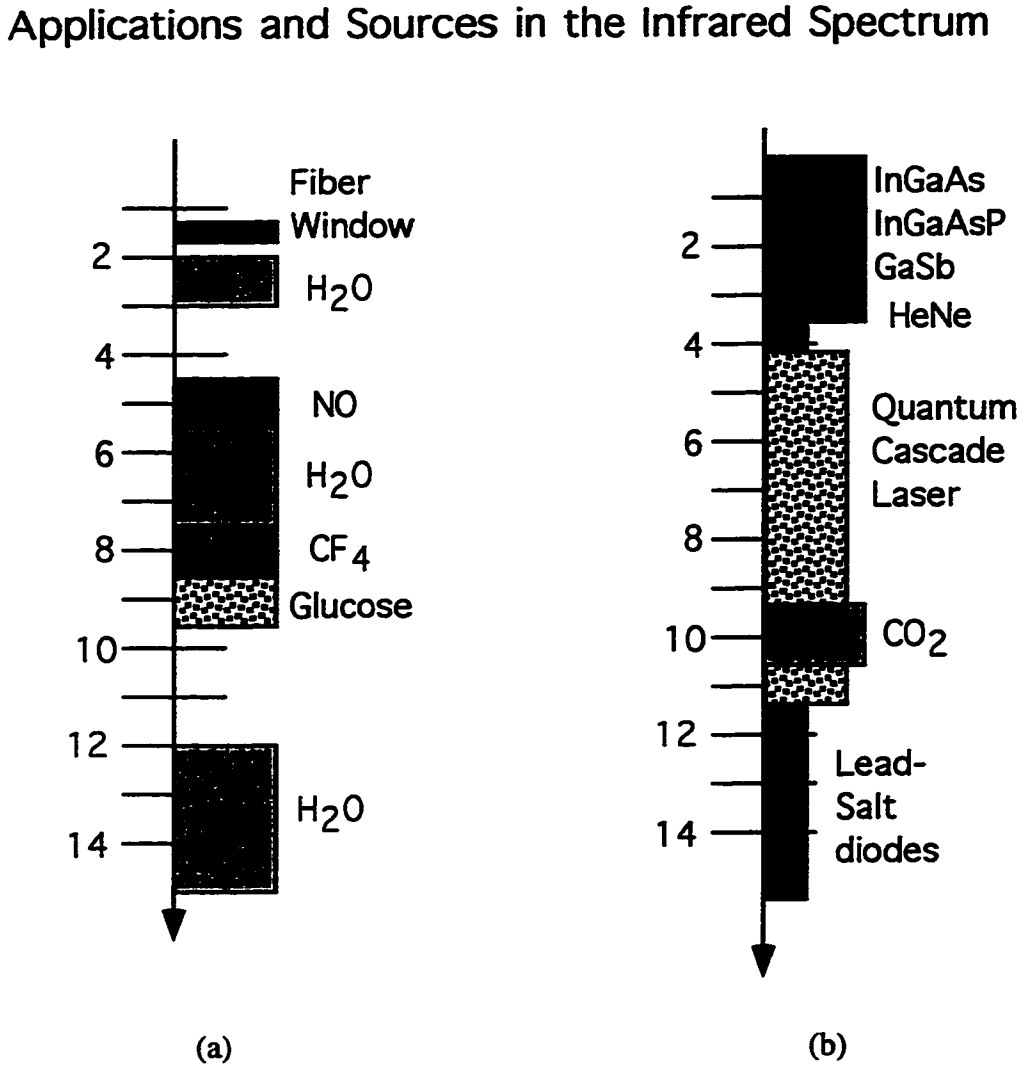

Figure 1.1. Applications (a) and sources (b) in the infrared region of the optical spectrum.

Most solid-state lasers operate in the near-infrared region of the spectrum, between 1 and 2 μm. Nd:YAG lasers, with a wavelength of 1.064 μm, are commonly used for high-power applications, while erbium-doped fiber lasers operate around the technologically significant 1.55 μm region. In addition to the familiar 632.8 nm red line, a He-Ne laser can also be made to operate at 3.39 μm. Further out in the IR spectrum at 10.6 μm, the CO_2 gas laser is available as a source. Gas lasers, however, are relatively

large, inefficient, and fragile when compared to their solid-state counterparts, although they are capable of large powers. In addition, most of these sources lack any significant tunability in their lasing wavelength. These and other sources are illustrated in Figure 1.1.

1.2 NONLINEAR OPTICS

It is possible, however, to take advantage of the availability of solid-state diode lasers in the near-IR in order to generate mid- to far-IR radiation. This is done through nonlinear optical techniques, specifically Difference Frequency Mixing, or DFG. This process is shown schematically in Figure 1.2. In a medium with a strong nonlinear response, intense radiation will induce a polarization in the material proportional to the strength of the radiation field squared, tripled, or even higher powers. This induced polarization will then act as a source for radiation at a higher harmonic of the original field. In the case of two or more fields, sum or difference frequencies are also possible. Under certain conditions, it is necessary to input only one wavelength, known as the pump. Two longer wavelength beams will then build up spontaneously, in a process known as parametric generation.

Nonlinear optical techniques are currently being used in a wide variety of material and wavelength combinations. Green light (532 nm) can be easily generated through Second Harmonic Generation (SHG) of Nd:YAG lasers (1064 nm), as schematically illustrated also in Figure 1.2. Lithium niobate is commonly used for the generation of near- to mid-IR tunable radiation. Commercial products containing doubling or tripling crystals, along with tunable Optical Parametric Oscillators (OPOs), are widely available and used in a variety of applications.[13] The limitations on extending these techniques to the regions of interest in the infrared will be discussed.

Thus, one possible approach to generating intense, coherent beams of mid- to far-IR radiation would be take advantage of the parametric generation process, driven by a near-IR diode laser. The nonlinear medium would be used to convert 2 μm radiation into 4 μm light . In order to generate the large amounts of optical power (necessary for countermeasure applications), an array of such devices could be fabricated in parallel, ideally all on the same substrate. Such an approach also has the advantage of tunability

through the slight variation of critical parameters, such as angle or input wavelength. For instance, a small tuning range in the pump wavelength results in significant tuning of the output. For the case of DFG of 8 μm light from 1.3 μm and 1.55 μm diodes, a tuning range of 50 Å on the 1.3 μm pump would result in an output tuning range of almost 200 nm. Such tuning ranges would be extremely useful for spectroscopic techniques.

For WDM applications, such a nonlinear technique could be used to optically shift data from one wavelength channel to another. For example, mixing a data channel at 1.55 + Δ μm with a 755 nm pump, would result in a DFG frequency of 1.55 - Δ μm. Slight tuning of the pump could be used to shift one channel into any appropriate channel. Since the process would be all-optical, speed or latency issues would not arise. Furthermore, multiple channels could be processed simultaneously, with minimal crosstalk. In addition, the shifted channel would be the phase-conjugate of the input channel. This fact could be used to correct dispersion errors by propagating the phase-conjugated signal through a comparable length of fiber as the original signal, thus cancelling out the original dispersion. Accordingly, such an all-optical router would be a useful device for WDM systems.

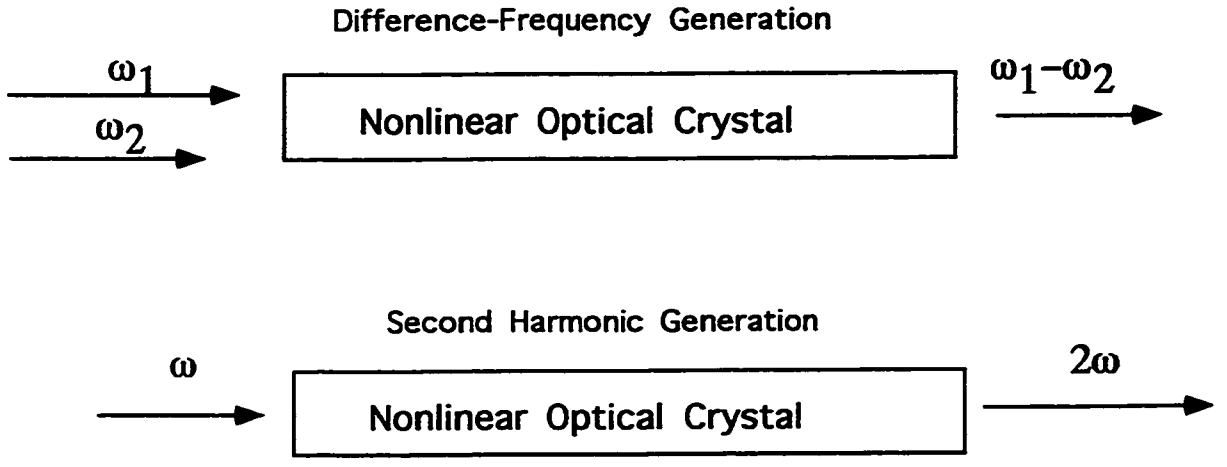

Figure 1.2. Schematic of nonlinear optical conversion processes, illustrating both difference-frequency generation (top) and second harmonic generation (bottom).

1.3 GALLIUM ARSENIDE

In order to successfully implement these nonlinear techniques, a suitable material fulfilling three requirements must be found. First, the material must have a large second-order nonlinear response for DFG to occur. Due to symmetry considerations, any centrosymmetric material will not have the necessary second-order nonlinear response, but only odd-order responses (i.e. third, fifth, etc.). Accordingly, the material must be noncentrosymmetric, or not possess inversion symmetry, which eliminates the major semiconductor Si and such common materials as amorphous solids, liquids, and gases.

Second, the material must be transparent for all wavelengths or frequencies involved in the interaction. Any loss at either the pump or signal wavelengths seriously reduces the conversion efficiency of the nonlinear process. Many useful nonlinear materials, such as lithium niobate, have strong absorption in the infrared beginning at about 5 μm, precluding their use in the longer wavelength region of the spectrum.

And third, there must be a way of phasematching the interaction. Due to refractive index dispersion present in all materials, waves of differing frequency travel through the material at different speeds. As a result, a phase difference accumulates between the waves, resulting in a decrease in conversion efficiency. In order for a nonlinear interaction to efficiently convert power from one frequency into another, there must be some way of compensating, or phasematching, for this shift between the different waves

One suitable material for nonlinear optics in the near- to far-IR is GaAs. GaAs has a very large nonlinear coefficient, especially when compared to many other materials commonly used for nonlinear optics. A useful figure of merit for nonlinear materials is d^2/n^3, where d is the effective nonlinear coefficient, and n is the material index of refraction. Accordingly, GaAs has a figure of merit approximately three times larger than that of lithium niobate (~250 pm^2/V^2 vs. 84 pm^2/V^2). In addition, GaAs is also transparent for all the wavelengths of interest (~1-10 μm). A technique for phasematching GaAs is the main subject of this thesis. In addition, processing technology for GaAs is well-developed, allowing the use of known techniques in device fabrication. Furthermore, being an important opto-electronic material, the use of GaAs holds the promise of direct integration of the nonlinear device with the sources themselves. This may be achieved

either through multiple epitaxial growths and fabrications, or through bonding techniques where devices fabricated on separate substrates are integrated with the nonlinear optical devices.

Accordingly, it was decided to use GaAs-based materials for the generation of infrared light through nonlinear optical techniques. Two potential applications were selected as goals. One was for a wavelength converter for 1.55 μm light, as discussed above, for WDM applications. Although such devices can be fabricated using existing materials, such as Periodically Poled Lithium Niobate (PPLN), the resulting conversion process is not polarization independent. Since such a converter will be used in a fiber optic system, polarization-retaining fiber would be necessary to allow use of a PPLN converter, so such a device is not compatible with the existing optical fiber infrastructure. Because of the symmetry of the nonlinear tensor in GaAs, however, the wavelength conversion efficiency will be polarization independent, thus allowing a GaAs-based converter to be used without a costly replacement of fibers. The second was an Optical Parametric Oscillator (OPO), pumped at 2 μm, for the generation of 4 μm light for airborne countermeasures. Because of the flexibility of the QPM method, however, this change is relatively minor, and almost all of the research performed can be applied equally to both topics.

The work for this thesis is focussed upon fabricating GaAs structures capable of producing mid-infrared light through nonlinear techniques. The bulk of the work presented here is concentrated on the materials work involved, since this was the major obstacle to realizing the desired goal. Since nonlinear optics is a technique that was chosen to help achieve a desired goal (generation of mid-infrared light), well-established methods pioneered in other materials were employed. In contrast, much of the materials work necessary for this project was relatively undeveloped, so that is where most of the significant research occurred.

1.4 ORGANIZATION

The organization of this thesis is as follows: Chapter 2 will discuss the nonlinear optics and waveguide theory neccesary for understanding the rest of the work. Chapter 3 will be a more detailed explanantion of the exact approach used, along with some

background information concerning alternatives. Chapter 4 will present the necessary material background data and discuss the epitaxial growth technique employed. Chapter 5 will present the fundamental materials results, while Chapters 6 will discuss both the growth results and the optical results. Chapter 7 will be a conclusion and discussion of future work that could be peformed, using this thesis as a starting point.

2. NONLINEAR OPTICS AND WAVEGUIDE FUNDAMENTALS

Nonlinear optics is the study of effects caused by the nonlinear polarization response of a material in the optical frequency range. These effects include frequency mixing, the electro-optic effect, and an intensity-dependent index of refraction. In constrast, linear effects such as reflection and refraction are due to the linear polarization response of the material. In order for nonlinear effects to become evident, the applied field usually needs to be on the order of 1 kV/cm. This requires a beam intensity of about 2.5 kW/cm^2.[14] Thus, it was not until the invention of the laser by Maiman in 1960, which is capable of producing such an intense beam, that the field of nonlinear optics was widely studied.[15] The first nonlinear optical experiments were peformed shortly afterwards by Franken in 1961.[1]

2.1 PHYSICS OF NONLINEAR OPTICS

If the atoms of a material are treated as a collection of harmonic oscillators (Lorentz model), then the application of a time-varying field will cause the electrons to vibrate at the applied frequency in their (parabolic) potential. This is the typical linear polarization response of a material. The parabolic potential for an atom is only an approximation, however, and begins to break down for large displacements from the equilibrium position. When the applied field is strong enough, and the potential significantly nonparabolic, then nonlinear effects will occur. Figure 2.1 illustrates the case of a noncentrosymmetric potential, where the deviations from the parabolic potential can be seen. In addition to the fundamental frequency, components at various harmonics will also be present in the polarization term. This is caused by the addition of a nonlinear restoring force to the potential. Depending on the symmetry of the material, either all harmonics or only odd harmonics may be allowed. Furthermore, if two or more frequencies are applied, then mixing between the various terms can also occur, resulting in polarization components at sum- and difference- frequencies.[16]

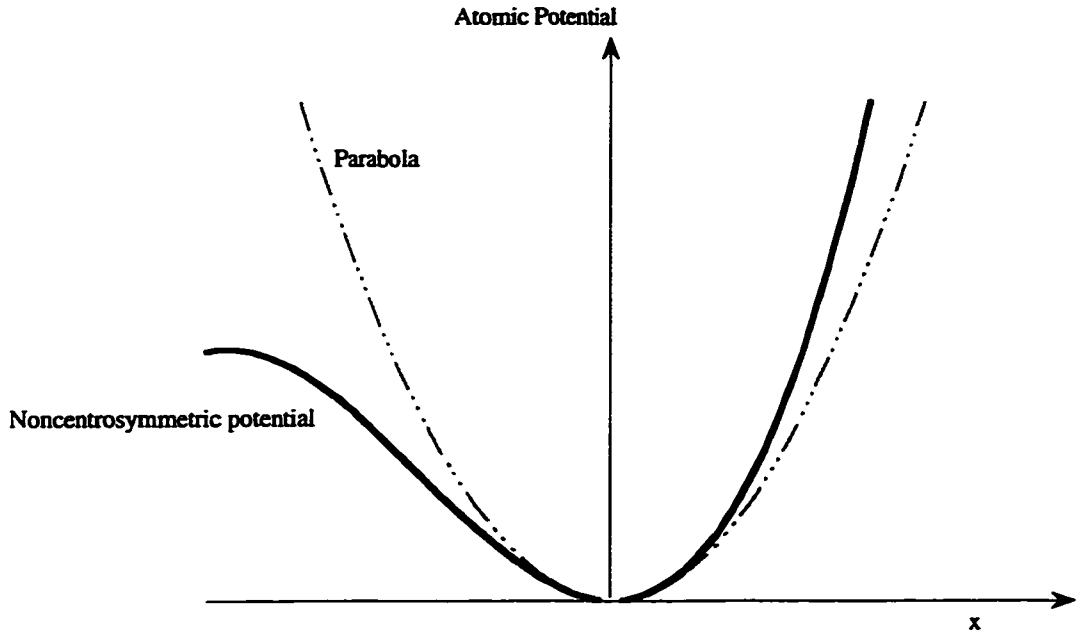

Figure 2.1. Noncentrosymmetric potential energy function. For small displacements from equilibrium a parabolic approximation is valid, however for larger displacements higher-order approximations are necessary.

This polarization, both the linear and nonlinear parts, then acts as a source of electromagnetic radiation for the wave equation, according to Larmor's theorem, which states that accelerated charges act as a source of electromagnetic radiation. The linear response of the medium is treated through the formalism of the dielectric constant, since it occurs at the same frequency as the applied field. The nonlinear response results in electrical fields at new frequencies, which is usually the desired goal in nonlinear optics. The efficiency of this process depends largely on the phase relationship between the induced polarization and the radiated field.

2.2 NONLINEAR OPTICAL EQUATIONS

For a nonlinear optical medium the polarization dependence on the electric field should be written as

$$P_i = \varepsilon_0(\sum_j \chi_{ij}^{(1)} E_j + \sum_{jk} \chi_{ijk}^{(2)} E_j E_k + \sum_{jkl} \chi_{ijkl}^{(3)} E_j E_k E_l + \ldots) \tag{2.1}$$

Linear effects are due to $\chi^{(1)}$, while nonlinear effects are due to $\chi^{(2)}$ and $\chi^{(3)}$. It is often convenient to separate the linear part of the polarization from the nonlinear portion:

$$\vec{P}^{tot} = \vec{P}^{lin} + \vec{P}^{NL} \tag{2.2}$$

The nonlinear portion is then found to be

$$P_i^{NL} = \varepsilon_0(\sum_{jk} \chi_{ijk}^{(2)} E_j E_k + \sum_{jkl} \chi_{ijkl}^{(3)} E_j E_k E_l + \ldots) \tag{2.3}$$

Assuming fields of the form

$$\vec{E}(\omega) = \vec{A}(\omega) e^{-i(\omega t - \mathbf{k}_\omega \cdot \mathbf{r})} \tag{2.4}$$

where ω is the frequency of the electric field and $\mathbf{k}_\omega = n\omega/c$ is the appropriate wavevector.

For two applied fields, $\mathbf{E}(\omega_1)$ and $\mathbf{E}(\omega_2)$, the frequency portion of the nonlinear polarization due to second-order effects becomes

$$P_i^{NL} = \varepsilon_0(\sum_j \chi_{ijj}^{(2)} (A_j(\omega_1))^2 e^{-i2\omega_1 t} + \sum_j \chi_{ijj}^{(2)} (A_j(\omega_2))^2 e^{-i2\omega_2 t} +$$
$$\sum_{jk} \chi_{ijk}^{(2)} A_j(\omega_1) A_k(\omega_2) e^{-i(\omega_1+\omega_2)t} + \sum_{jk} \chi_{ijk}^{(2)} A_j(\omega_1) A_k^*(\omega_2) e^{-i(\omega_1-\omega_2)t} +$$
$$\text{D.C. terms} + \text{complex conjugates}) \tag{2.5}$$

For a time-varying electric field, the nonlinear part of the polarization will now have a DC response (optical rectification), and a time-varying response at frequency

2ω due to the cross-terms in the product of the electric fields. If two applied fields of differing frequency (ω_1 and ω_2) are present, then the nonlinear part of the polarization will also have frequency components corresponding to $\omega_1+\omega_2$ and $\omega_1-\omega_2$ (due to the complex representation of the fields). The extension to three or more fields is clear, resulting in a large combination of possible terms. Since the applications relevant to this work involve only three frequency components (two applied and one generated) and second-order ($\chi^{(2)}$) effects, only those will be treated in the discussion below. The effects of the linear polarization are typically taken into account by the index of refraction. The wave sees a phase shift, relative to free space, as it travels through the medium. In a sense, the wave is inducing a polarization, which in turns radiates at the fundamental frequency. The phase shift is due to the time delay in this process.

The nonlinear coefficient $\chi^{(2)}_{ijk}$ is actually a function of three related arguments: ω_1, ω_2, and $\omega_3=\omega_1+\omega_2$, with negative frequencies being allowed. Accordingly, it is often written as $\chi^{(2)}_{ijk}(\omega_3; \omega_1, \omega_2)$ in order to emphasize the dependence of ω_3 on $\omega_1$and ω_2. Furthermore, since interchanging the last two arguments does not change the induced polarization in any way, by definition $\chi^{(2)}_{ijk}(\omega_3; \omega_1, \omega_2)=\chi^{(2)}_{ikj}(\omega_3; \omega_2, \omega_1)$. This is known as intrinsic permutation symmetry. For real frequencies, $(\chi^{(2)}_{ijk}(-\omega_3; -\omega_1, -\omega_2))^*=\chi^{(2)}_{ikj}(\omega_3; \omega_2, \omega_1)$, while for lossless materials the nonlinear susceptibility also has full permutation symmetry, where $\chi^{(2)}_{ijk}(\omega_3; \omega_1, \omega_2)=\chi^{(2)}_{jik}(\omega_1; -\omega_3, \omega_2)=\chi^{(2)}_{kij}(\omega_2; -\omega_3, \omega_1)$. In addition, the symmetries of the nonlinear susceptibility also have to obey the symmetries of the crystal class to which the material belongs. For crystals with inversion symmetry, $\chi^{(2)}$ is zero since inversion through a point changes the sign of the applied field and induced polarization, while leaving the tensor elements unchanged, leading to $\chi^{(2)}_{ijk}E_jE_k=-\chi^{(2)}_{ijk}E_jE_k$, which can only be satisfiedfor $\chi^{(2)}_{ijk}=0$. For the crystal class to which GaAs (and also AlGaAs) belong, the only nonzero tensor elements are $\chi^{(2)}_{xyz}$ and its permutations.[17] A

180° rotation around one of the four-fold axes reduces $\chi^{(2)}_{iiii}$, $\chi^{(2)}_{iij}$, and $\chi^{(2)}_{ijj}$ to zero, while a mirror reflection about the diagonal plane leads to the equivalence of $\chi^{(2)}_{xyz}$ and its permutations.[14]

This nonlinear polarization is then treated as a source term in the wave equation, leading to the emergence of radiation at frequencies other than that of the applied field. Starting from Maxwell's equations in a nonmagnetic media, the necessary equations are:

$$\vec{\nabla} \times \vec{E} = -\mu_0 \frac{\partial}{\partial t} \vec{H}$$
$$\vec{\nabla} \times \vec{H} = \frac{\partial}{\partial t} \vec{D} \tag{2.6}$$

where **D** is the electric displacement, **H** is the magnetic field, and μ_0 is the vacuum magnetic permittivity. **D** and **E** are related by

$$\vec{D} = \varepsilon_0 \vec{E} + \vec{P}^{tot} \tag{2.7}$$

By taking the curl once again of both equations and substituting, we get

$$\nabla^2 \vec{E} - \vec{\nabla}(\vec{\nabla} \cdot \vec{E}) - \frac{n^2}{c^2} \frac{\partial^2 \vec{E}}{\partial t^2} = \mu_0 \frac{\partial^2 \vec{P}^{NL}}{\partial t^2} \tag{2.8}$$

where $n^2=\varepsilon= \varepsilon_0(1+\chi^{(1)})$, thus accounting for the linear polarization. The nonlinear portion is then the product of two fields, $\mathbf{E}(\omega_1)$ and $\mathbf{E}(\omega_2)$, producing a field at a third frequency, $\mathbf{E}(\omega_3=\omega_1+\omega_2)$.

The solutions to this equation determine the behavior of the nonlinear fields. For most cases of interest, the term $\vec{\nabla}(\vec{\nabla} \cdot \vec{E})$ can be shown to be either zero or negligibly small.[18] The simplest example is for the case of Second Harmonic Generation (SHG) with $\mathbf{E}(\omega_1)=\mathbf{E}(\omega_2)=\mathbf{E}(\omega)$ and $\mathbf{E}(\omega_3)=\mathbf{E}(2\omega)$, with the second harmonic polarized along the y

direction (i.e. only $A_y(2\omega)$ 0) and the fundamental frequency polarized along the x direction (i.e. only $A_x(\omega)$ 0), with both waves travelling in the z direction. For the case of SHG, an extra factor of two needs to be properly accounted for due to a degeneracy in the summation in Eq 2.1 when the two field components are identical. Substituting $\mathbf{E}(\omega)$ into $\mathbf{P}^{NL}$ on the left side of Eq. 2.6, and $\mathbf{E}(2\omega)$ onto the right hand side and solving for $\mathbf{E}(2\omega)$, the result is:

$$[\frac{\partial^2 A_y(2\omega)}{\partial z^2} + 2ik_{2\omega}\frac{\partial A_y(2\omega)}{\partial z} - k_{2\omega}^2 A_y(2\omega) + \frac{n_{2\omega}^2(2\omega)^2}{c^2}A_y(2\omega)]e^{-i(2\omega t - k_{2\omega}z)}$$
$$= \frac{1}{2}\chi_{yxx}^{(2)}\frac{4\omega^2}{c^2}A_x^2(\omega)e^{-i(2\omega t - 2k_\omega z)} \qquad (2.9)$$

By neglecting the second derivative of the amplitude (i.e. the slowly varying amplitude approximation), eliminating common factors, collecting like terms and using $k_{2\omega}=n_{2\omega}\omega/c$, this equation can be simplified to

$$\frac{\partial A_y(2\omega)}{\partial z} = \frac{i\omega^2\chi_{yxx}^{(2)}}{k_{2\omega}c^2}A_x^2(\omega)e^{i(2k_\omega - k_{2\omega})z} = \frac{i\omega\chi_{yxx}^{(2)}}{2n_{2\omega}c}A_x^2(\omega)e^{i(2k_\omega - k_{2\omega})z} \qquad (2.10)$$

and then integrated along z to give

$$A_y(2\omega)(z=L) = (\frac{i\omega\chi_{yxx}^{(2)}}{2n_{2\omega}c}A_x^2(\omega))\frac{1}{i\Delta k}(e^{i\Delta kL} - 1)$$
$$= (\frac{i\omega\chi_{yxx}^{(2)}}{2n_{2\omega}c}A_x^2(\omega))Le^{i\Delta kL/2}\frac{\sin(\Delta kL/2)}{(\Delta kL/2)} \qquad (2.11)$$

where $\Delta k=2k_\omega-k_{2\omega}$.

Converting to intensity, we have

$$I_{2\omega} = \frac{\omega^2(\chi^{(2)})^2 I_\omega^2}{2n_{2\omega}n_\omega^2 c^3 \varepsilon_0} L^2 \mathrm{sinc}^2(\Delta kL/2) \tag{2.12}$$

where sinc(x)=sin(x)/x In the regime of low conversion where pump depletion can be neglected (<20%), the conversion efficiency, η, of the nonlinear process is[19]

$$\eta = \frac{P_{2\omega}}{P_\omega} = \left(\frac{2\omega^2 d^2}{n_{2\omega}n_\omega^2 c^3 \varepsilon_o}\right)\left(\frac{P_\omega L^2}{A}\right)\mathrm{sinc}^2\left(\frac{\Delta kL}{2}\right) \tag{2.13}$$

where the effective nonlinear coefficient is $d=\chi^{(2)}/2$, a convention commonly used in nonlinear optics, P_ω and $P_{2\omega}$ are the pump and second harmonic power respectively, A is the effective interaction area. It is from this expression that the nonlinear optical figure of merit d^2/n^3 is derived, in order to compare the effectiveness of different nonlinear optical materials. Due to the presence of ω^2 in the numerator, the efficiency of mid- to far-IR interactions is typically low compared to those in the visible region of the spectrum.

2.2.1 PHASEMATCHING

The term Δk is a measure of phasematching between the incident fields and the generated nonlinear output. For $\Delta k=0$, the interaction can be very efficient as the intensity grows proportional to L^2. When $\Delta k \neq 0$, the generated intensity will build up over one *coherence* length, L_c, where $L_c = \pi/\Delta k$. For media longer than L_c, power begins to oscillate between the generated and applied fields, resulting in minimal conversion from one frequency to the next. Figure 2.2 is a plot of the $\mathrm{sinc}^2(L/L_c)$ function, showing maximum conversion efficiency for $\Delta k=0$ and nulls for other even values of the coherence length.

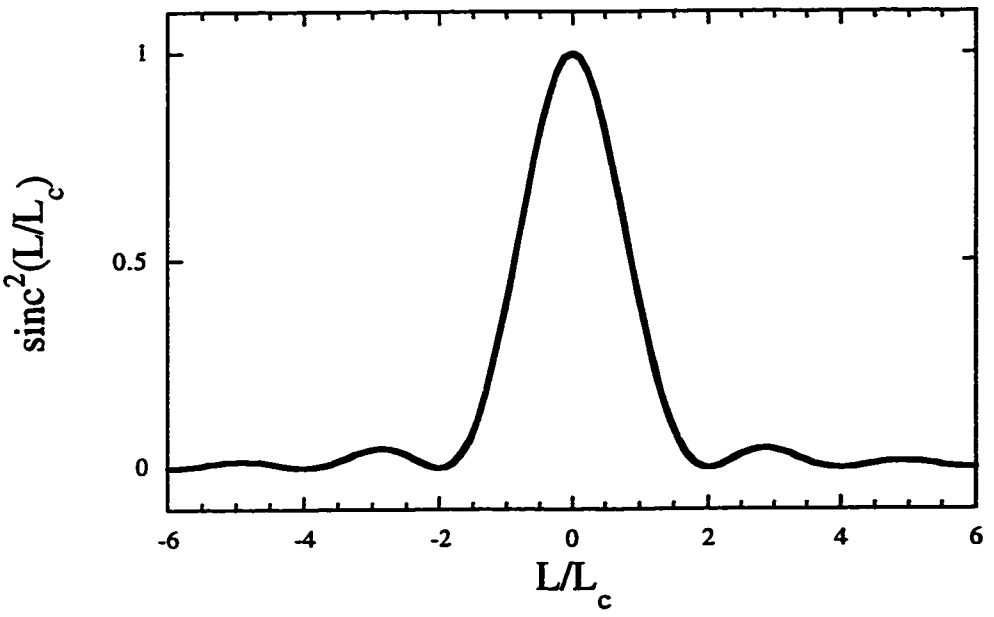

Figure 2.2. $Sinc^2(L/L_c)$ curve showing reduced conversion away from phasematching condition.

Writing Δk in terms of the indices of refraction, we have

$$\Delta k = \frac{2n_{\omega}\omega}{c} - \frac{n_{2\omega}(2\omega)}{c} \tag{2.14}$$

For materials with normal dispersion, where n increases as ω increases ($n_{2\omega} > n_{\omega}$), this equation will not equal zero. Since maximum efficiency occurs when $\Delta k = 0$, much study has gone into ways of achieving this desirable condition. One technique, known as birefringent phasematching, takes advantage of differing indices of refraction for differing polarizations of incident light (see Figure 2.3). By choosing a geometry such that the

highest frequency wave sees the lower of of the two allowed indices, in this case n_e, it is sometimes possible to fulfill the ideal phasematching conditions.

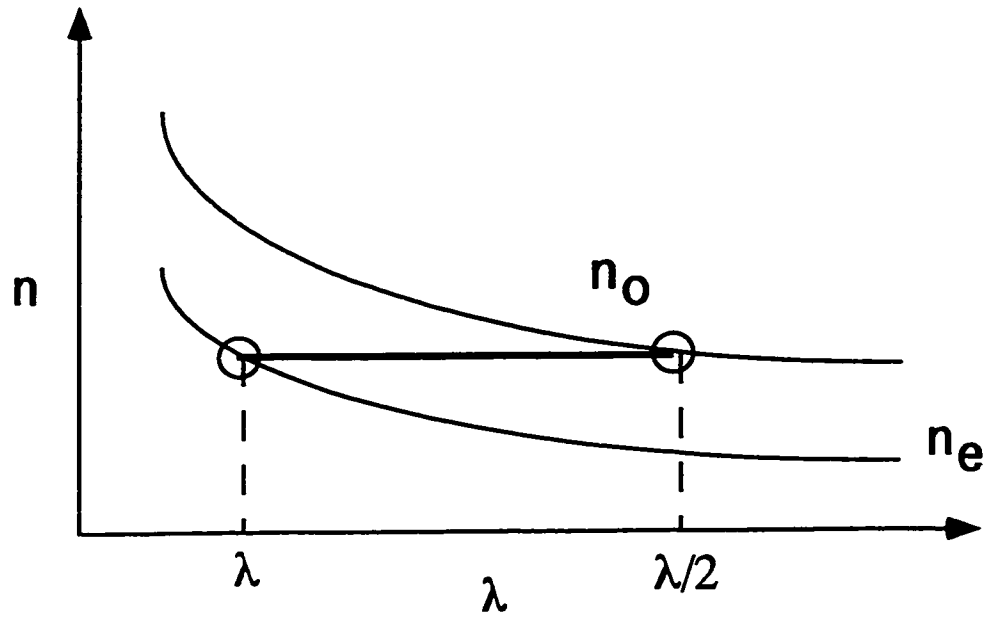

Figure 2.3. Indices of refraction for a negative uniaxial crystal, with n_o greater than n_e.

Birefringent phasematching does have its disadvantages, however. Birefringent walk-off between the pump and signal beam can occur when the Poynting vector **S** and the propagation vector **k** are not parallel, thus limiting the overlap and decreasing the efficiency.[18] Oftentimes, the material of interest (such as GaAs) is not birefringent. Alternatively, the nonlinear tensor $\chi^{(2)}$ may not allow for efficient conversion between two fields polarized in different directions.

Another solution to the phase-matching problem is known as Quasi-PhaseMatching (QPM).[20, 21] If the sign of $\chi^{(2)}$ is alternated every coherence length L_c, then power will continue to flow into the generated frequency instead of back into the fundamental. Mathematically,

$$\Delta K = 2k_{\omega} - k_{2\omega} + K_g = 0 \tag{2.15}$$

where K_g is a k-vector of a Fourier component of the grating, as shown in Figure 2.4.

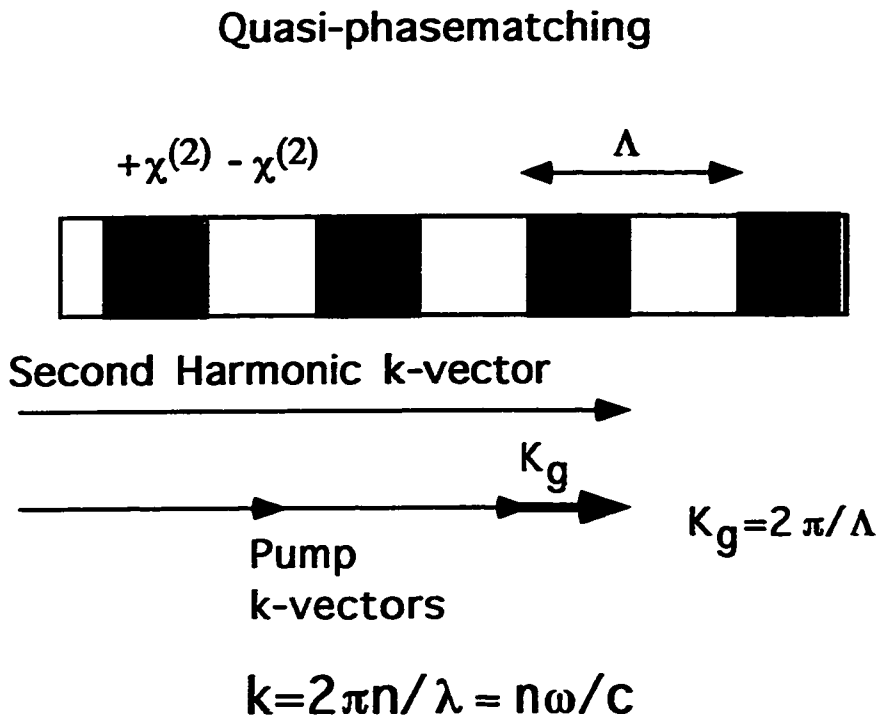

Figure 2.4. Schematic of a quasi-phasematched structure.

Ideally, first-order QPM is desired, as the corresponding Fourier amplitude is the largest. Due to technological difficulties in making gratings with fine enough coherence lengths, however, sometimes higher-order phasematching (third, fifth, etc.) are employed, where the grating period is an odd number of coherence lengths. The Fourier series of such a periodic structure will still have a component at the proper k-vector, since $K_g=2\pi m/\Lambda$, where m is an integer denoting the order of quasiphasematching. Since the Fourier coefficients decrease as 1/m, where m is the order of the grating, the effective nonlinearity decreases as $1/m^2$. Hence third-order QPM is almost an order of magnitude less efficient than first-order QPM. Futhermore, it is not necessary for the duty cycle to be exactly 50%,

although maximum efficiency occurs for this case. On/Off QPM can also be used in situations where it is not possible to change the sign of $\chi^{(2)}$, but rather only modulate it between a maximum value and zero. Figure 2.5 illustrates the nonlinearly generated output power as a function of length for the different cases of perfect phasematching, QPM, and On/Off QPM. For SHG of 2 μm radiation from 4 μm radiation in GaAs, the coherence length is 27 μm. As the wavelengths of interest decrease, the coherence length also decreases as the dispersion increases, while the coherence length increases for wavelengths further out in the mid- to far-IR. Quasi-phasematching techniques are also useful even in instances where the crystal can be birefringently phasematched. For example in lithium niobate d_{33} (QPM) ~ 20 pm/V, while d_{13}, accessible by birefringent phasematching, is only ~4.5 pm/V.[22] Walk-off complications are also avoided.

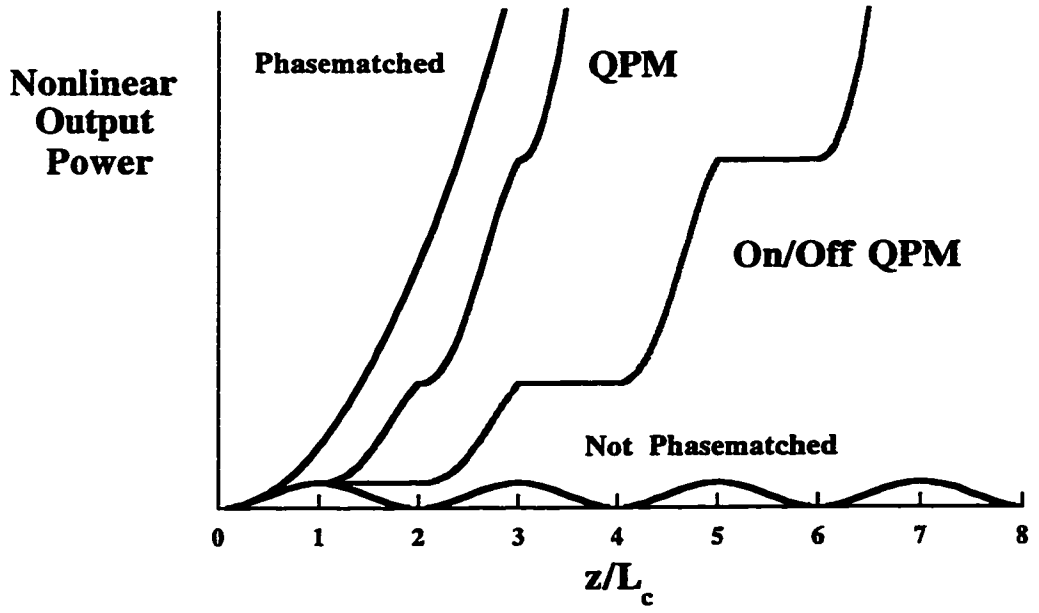

Figure 2.5. Nonlinear output versus length for different phasematching conditions.

2.3 SUM-FREQUENCY GENERATION AND DIFFERENCE-FREQUENCY GENERATION

Difference-frequency (DFG) and sum-frequency generation (SFG) require two applied fields. For SFG, two input photons are destroyed and one output photon created, similar to SHG (Figure 2.6(a)). For DFG, however, one input photon is destroyed and two output photons created(Figure 2.6(b)). One of these photons amplifies the field at the applied input (or signal) frequency, thus DFG can also be thought of as an amplification process, while the other photon is at a new (idler) frequency. The above derivations can easily be extended to the cases of DFG and SFG.

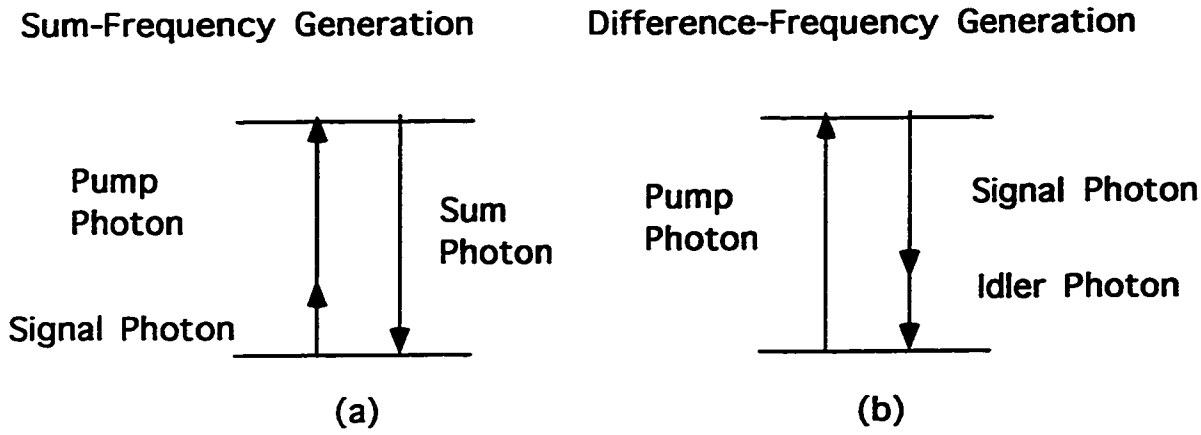

Figure 2.6. Energy-conservation diagrams for (a) Sum-Frequency Generation and (b) Difference-Frequency Generation.

A special case is optical parametric amplification and oscillation. Here, only one field, the pump is applied. Both the signal and idler signals build up from the ever-present quantum noise fluctuations, with their frequencies determined by the phasematching conditions. Growth of the signal frequency stimulates DFG to the idler frequency, and vice versa. The parametric amplification process is greatly enhanced by placing the nonlinear material in a resonator, resulting in an Optical Parametric Oscillator (OPO), as illustrated in Figure 2.7. In order to actually oscillate, the gain of the OPO at the signal and idler frequencies must be greater than the losses. Thus, there is a certain threshhold pump intensity before parametric oscillation begins. The oscillator can either be

singly resonant (SRO), where only one freqeuncy (signal or idler) is resonated, or doubly resonant (DRO), where both frequencies are resonated. Although the threshhold conditions for a DRO are often one hundred times less than that for a comparable SRO, SROs are much more stable and consequently more commonly used. [14] Since the signal and idler frequencies are determined by the phasematching conditions, the output of an OPO can often be tuned. For a birefringently phasematched OPO angle tuning is often used, while for a QPM OPO, temperature tuning or multiple gratings can be employed. In addition, the output can be tuned by tuning the input pump frequency.

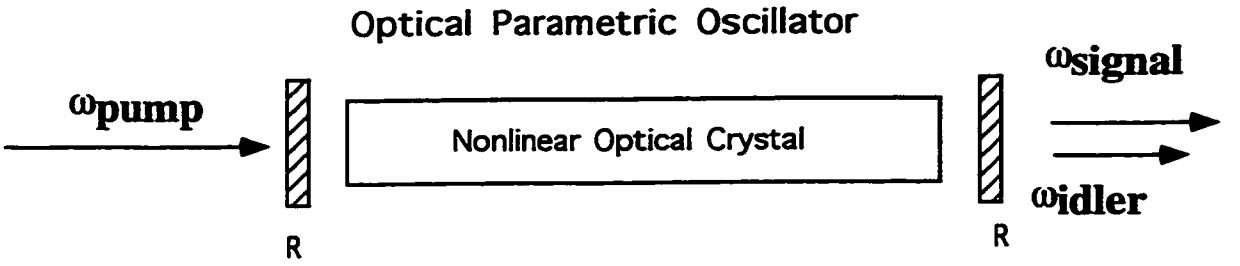

Figure 2.7. Schematic of an Optical Parametric Oscillator.

2.4 WAVEGUIDES

Because nonlinear conversion efficiency depends on the intensity of the applied fields, it is often desirable to tightly focus the applied beam in order to maximize the intensity. As the spot size decreases, however, diffraction increases and hence the effective interaction length decreases. One way to avoid this problem is to use a waveguide. A waveguide is formed when a material with a high index of refraction (known as the core) is surrounded by layers with a lower index (cladding). Due to total internal reflection occuring at the interfaces, the light is then trapped in the core as it propagates (see Figure 2.8). Because the light is confined in a small region, a high intensity can be maintained for an infinite length. Due to boundary conditions, only light reflecting at certain angles will propagate, thus leading to different waveguide modes. Depending on the index difference between the core and cladding, and the physical dimensions of the core with respect to the wavelength being propagated, from zero to multiple modes may be supported by the

waveguide. The effective index of the mode is a measure of the propagation speed of the mode, much as the index of refraction is a measure of the velocity of a plane wave in a material.

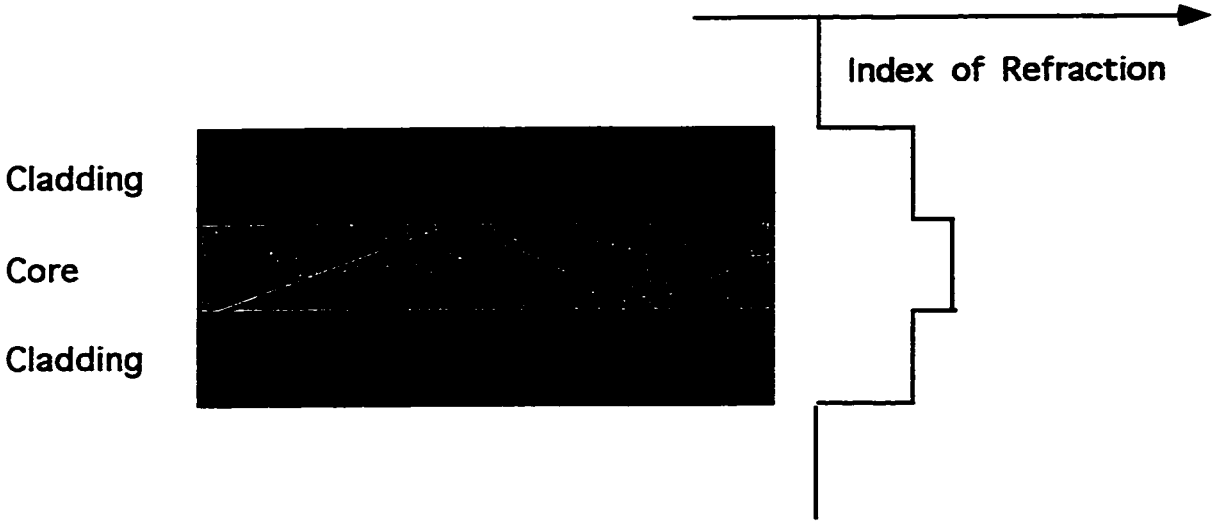

Figure 2.8. Schematic of a waveguide structure, with a high-index core surrounded by low-index cladding layers.

Waveguiding structures can easily be designed in semiconductor materials. The simplest designs call for a high-index core layer separated from the substrate by a low-index cladding layer. The air on top forms the third layer. More typically, a cladding layer is also added on top of the core, in order to create a more symmetric beam profile. In the work presented here, waveguides were fabricated using $Al_xGa_{1-x}As$. The highest index material is GaAs, with AlAs having the lowest index. By alloying the two materials, any value between the two endpoints could be attained. A typical waveguide using these materials consists of a GaAs core, surrounded by AlGaAs cladding layers. For certain applications, where GaAs would be strongly absorbing, the core might consist of a low-percentage AlGaAs, and the cladding a higher-percantage AlGaAs.

Waveguides in the $Al_xGa_{1-x}As$ system do present one complication. GaAs is the highest index material available in this system, and it is also the only available substrate. Thus, the cladding layer between the core and the substrate must completely

shield the wave from the substrate, since any non-zero field at the cladding/substrate interface will leak away and contribute to the waveguide losses. For short wavelengths, this is not a problem. For longer wavelengths, however, the core and cladding must be made thicker. For example, in order to effectively guide 4 μm light, the waveguide/cladding structure needs to be approximately 7 μm thick. Waveguides for even longer wavelengths need to be correspondingly thicker, which increases the complexity of the epitaxial growth process.

In order to transfer the earlier development of nonlinear optics into waveguides, it is necessary to replace the area by the effective area A_{eff}, which is inversely proportional to the square of the overlap integral between the modes. In addition to accounting for the physical dimensions of the waveguide, A_{eff} also takes into account the overlap between the different modes. For example, in a symmetric waveguide, overlap between an even-order pump mode and and an odd-order harmonic would cancel out. For phasematching considerations, it is necessary to use the effective mode indices at each wavelength, instead of the bulk indices. Waveguides thick enough to support long wavelengths will be multi-moded at the shorter wavelengths. Since only one of these modes (preferably the lowest order mode) will be phasematched, any pump light coupled into the higher order modes will be effectively lost. (For second-harmonic generation this is not a severe problem. Light is coupled into the single-moded waveguide at the pump wavelength, and although there will be multiple modes at the harmonic wavelength, only one will be phasematched to the pump.) It is desirable to have the lowest-order modes at each wavelength of interest phasematched with each other, in order to increase the modal overlap.

The symmetry of the third-rank $\chi^{(2)}$ tensor must also be considered, as this determines how the applied beams must be polarized relative to the crystal axes in order to interact. Depending on the point group of the material involved, certain tensor elements can be identified as either zero, or as identical or opposite other elements. Conceptually, fields polarized along one crystallographic axis often induce a nonlinear response upon another axis. For GaAs, the only nonzero components of $\chi^{(2)}$ are $\chi^{(2)}_{xyz}$ and its permuations xzy, yzx, yxz, zxy, and zyx.[16] Thus, in order to induce a nonlinear response, the three fields

involved in the nonlinear interaction must have nonzero components along all three of the crystal axes. To have collinear propagation of the applied and generated fields, all of the beams must additionally be polarized in the plane perpendicular to the direction of propagation. In the case of GaAs waveguides, light is often propagated along a [110] direction in order to take advantage of the (110) cleavage planes, as shown in Figure 2.9. Thus, for SHG the pump could be TE polarized - electric field parallel to the waveguide - in order to provide both x- and y-components simultaneously. The resulting signal would then be TM polarized - electric field in the z-direction. Alternatively, the input radiation could be polarized at 45°, containing equal parts TE and TM componets. The TE and TM components would mix to form a TE polarized output.

Waveguide uniformity is an important issue in order to reduce losses and increase the efficiency of a nonlinear device. Interface roughness between the core and cladding layers, or between a layer and air, can lead to scattering of the pump and/or signal beams. Since the amount of scattering depends on the difference of index between the two materials, it can be particularly severe at either the core/air sidewall or the cladding/air interface. The magnitude of the loss depends also on the field strength at the interfaces and the wavelengths involved. Typically, a shorter wavelength will be more sensitive to a smaller amplitude of roughness. In particular, any periodic fluctuation of a key waveguide parameter (for example index of refraction, width, or core thickness) can lead to very high losses, since the light scattered out in a periodic manner will add coherently in the far field. Thus, it is important that the modulation of $\chi^{(2)}$ for QPM does not also simultaneously modulate any of the linear properties of the waveguide. In addition, any inhomogeneities (i.e width or composition fluctuations) along the length of the waveguide change the effective indices. Since the QPM period depends on the effective indices of the modes, any perturbation in the waveguide structure will decrease the effective phasematching length, as signal photons generated several QPM periods earlier in the structure will accumulate a phase shift relative to those produced latter. The effective coherence length of the device will become finite, and hence the efficiency and power output will decrease as compared to an ideal device. [22]

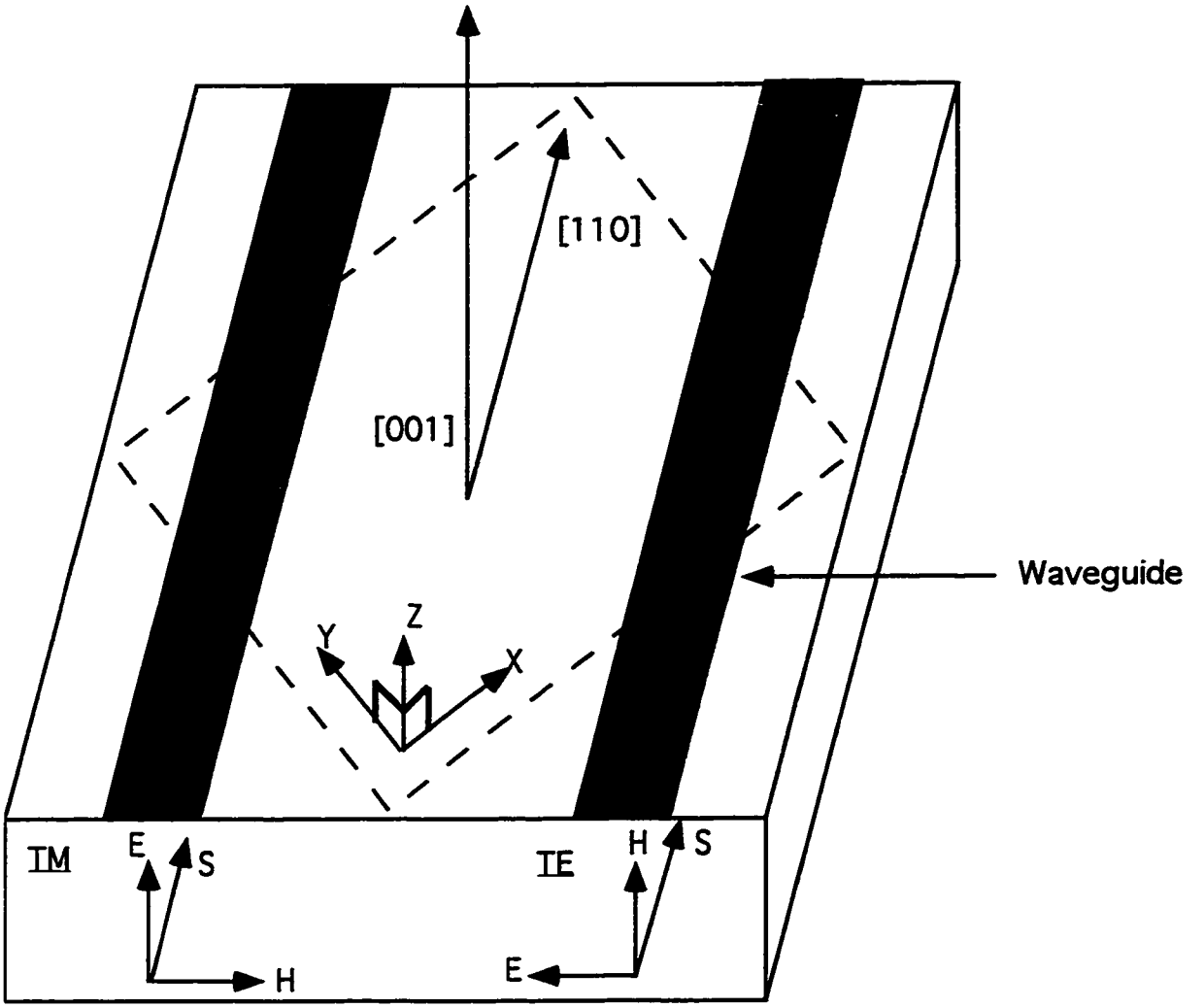

Figure 2.9. Diagram showing TE and TM waves for waveguides fabricated on (001) GaAs.

2.5 CONCLUSION

By combining nonlinear optics with waveguide technology, it is feasible to convert light from one wavelength to another in compact devices with high efficiency. A waveguide geometry is especially necessary in situations where the input power levels would otherwise lead to low conversion efficiencies. In order to be effective, however, the

separate fields must be efficiently coupled into the waveguide core, which is usually only a few microns thick. In addition, the fabrication tolerances must be controlled in order to ensure the device is effective throughout its entire length. There are some applications where bulk interactions are preferred. These include high-power applications, where focussing too tightly may exceed the damage threshhold of the material, or situations where precise coupling alignments would be difficult. To do so, it is necessary to have a suitable nonlinear material, along with a sufficient material technology in order to fabricate low-loss waveguides. GaAs has all the necessary qualifications for such a device, and a method of fabricating quasi-phasematched structures will be described in this thesis.

3. APPROACH

The use of GaAs for nonlinear optics has been limited because of a lack of a method for phasematching the interactions. As mentioned, GaAs is isotropic so birefringent phasematching is not an option. Quasi-phasematching requires some method of modulating the nonlinear response of the material. Ferroelectric materials, such as lithium niobate, can be poled using intense electric fields in order to change the sign of $\chi^{(2)}$, but this option is not available for GaAs.[23] Despite these difficulties, there is still great interest in GaAs as a potential material for nonlinear optics. This is because of its large nonlinear coefficient and corresponding figure of merit (d^2/n^3), a wide transparency range, and the potential for direct integration with laser sources and other opto-electronic devices. Ideally, laser diodes could be fabricated directly on the same chip as the nonlinear waveguide, eliminating many coupling and alignment issues. Alternatively, lasers grown on separate substrates (perhaps to reach wavelengths inaccessible for GaAs lattice-matched materials) could be bonded to a waveguide structure in order to form monolithic devices. High quality GaAs substrates are readily available at a reasonable cost, due to the widespread electronic uses. In addition, a mature body of knowledge concerning GaAs and its processing techniques exists, increasing the feasibility of an integrated product.

Because of these potential advantages, many techniques have been proposed and investigated for nonlinear applications in GaAs. Some have relied upon engineering the nonlinear susceptibility itself, through the proper design of quantum wells and intersubband transitions. Others have sought to utilize the bulk $\chi^{(2)}$ properties, and instead focussed on ways to phasematch the interactions.

3.1 ALTERNATIVE APPROACHES

One technique that has been extensively investigated is to engineer the nonlinear response to have the desired properties, including a method of phasematching. One way to do this is by using the $\chi^{(2)}$ from intersubband transitions created by quantum

wells, instead of the intrinsic $\chi^{(2)}$ of the GaAs material. Using Molecular Beam Epitaxy, the desired structures can be grown with the necessary precision to tailor the nonlinear response to the wavelengths of interest. DFG generation, tunable from 8.66 μm to 11.34 μm, using pumps based at 1.92 μm and 2.39 μm, has been demonstrated using InGaAs/AlAs quantum wells.[3] Analagous to the response due to discrete levels in atoms, a quantum well with discrete energy levels will also have a substantial nonlinear effect. Because of symmetry considerations of the dipole matrix elements, it is necessary to use asymmetric quantum wells in order to have a nonzero $\chi^{(2)}$. High indium-content quantum wells were used to extend the range of intersubband transitions towards 2 μm, compatible with existing laser diode sources. Use of above-band states offers the potential of using even shorter wavelengths as pumps.[24] The interaction can be phasematched by selectively proton bombarding alternating regions, creating traps which nullify the $\chi^{(2)}$ contribution by removing all of the free carriers necessary for excitations in the quantum wells. Although not as efficient as true QPM, this on/off QPM technique still yields a significant enhancement in the nonlinear signal. Although very large values (~ 100,000 pm/V, compared to ~100 pm/V for bulk GaAs) of $\chi^{(2)}$ can be achieved this way, there is also a significant amount of loss due to the linear absorption of the quantum well levels. Alternative geometries, such as a Cerenkov geometry, have been investigated as possible solutions to the loss problem. In a Cerenkov device, the generated beam does not propagate collinear with the pump, but rather radiates out of the core at an angle. If this core is lossy at the signal wavelength, as is the case of quantum well nonlinear optical interactions, this method provides the possibility of increasing conversion efficiency.[25]

Other possibilities focus on using the bulk $\chi^{(2)}$ of GaAs and instead attempting to engineer enough birefringence for phasematching. Although neither GaAs or AlAs is not birefringent by itself, it is possible to induce a birefringence in these materials through a technique known as form birefringence.[26] By alternately layering the two different materials, with thicknesses much less than the wavelengths of interest, it is possible to create an index difference between waves polarized parallel to the layers, and perpendicular to the layers. This effect is known as form birefringence, and is due to the

difference in boundary conditions seen by the two different types of waves. For electric fields perpendicular to the interfaces, the D-field is continuous across the interface, while for fields parallel the E-field is continuous. By increasing the difference in index of refraction between the two materials composing the stack, it is possible to increase the birefringence enough so that nonlinear interactions can be phasematched. The GaAs/AlAs material system, by itself, does not have enough index contrast to phasematch a wide range of interactions. However, by oxidizing the AlAs, this contrast is greatly increased, as seen in Figure 3.1, and the range over which interactions can be phasematched increases dramatically. Disadvantages of this method include polarization sensitivity, poor mechanical stability, and uncertain losses due to a poorly understood oxidation process. DFG of 4 μm light from 1 μm and 1.32 μm pumps has been reported using these structures.[27]

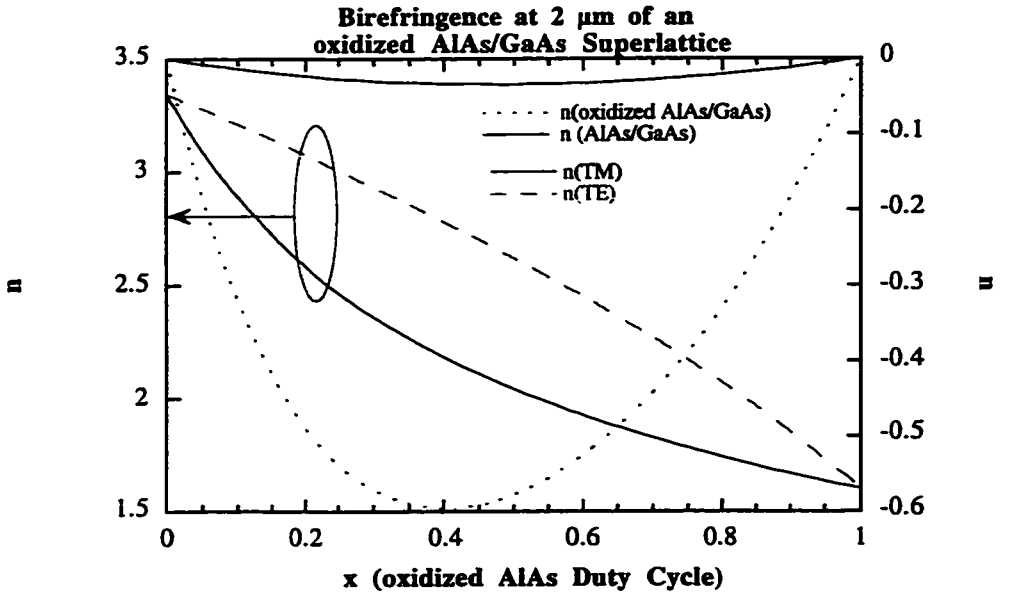

Figure 3.1. Birefringence of AlAs/GaAs multilayer stacks, and oxidized AlAs/GaAs stacks, as a function of (oxidized) AlAs duty cycle. The use of oxidized AlAs increases the birefringence by approximately one order of magnitude.

3.1.1 Quasi-Phasematching

Another possibility is to engineer the GaAs in such as a way as to periodically change the sign of $\chi^{(2)}$ in order to quasi-phasematch a given nonlinear interaction. The sign of $\chi^{(2)}$ is determined by the asymmetry of the electron potential, which in turn is determined by the direction of the Ga-As bond. When the GaAs lattice is observed along one the [110] family of directions, the direction of this bond can clearly be seen. By rotating the crystal lattice 90° around a [100] direction, however, it is observed that the direction of the bond changes. In Figure 3.2(a), the bonds can be seen pointing upwards from the As to the Ga, while in Figure 3.2(b), the bonds point downwards from the As to the Ga. In effect, the Ga and As sublattices exchange positions. This change in bond direction changes the sign of $\chi^{(2)}$. This can also be seen by observing the relation of the tensor elements and applied fields as the crystal is rotated. For $\chi^{(2)}_{xyz}$, applied fields in the x and y directions result in a polarization in the z direction. When the crystal (and $\chi^{(2)}$ tensor) is rotated by 90° around the z axis, x transforms to y, and y to -x. The externally applied fields, however, remain their original (unrotated) orientation,so now the crystal still sees a field applied along y direction, but the field applied along the x direction has changed sign, leading to a change of sign in the polarization. Thus, if it were somehow possible to arrange periodic segments where the crystal lattice was rotated by 90°, a quasi-phasematched device could be realized.

One approach, using wafer bonding methods, is to use (110) oriented wafers, thinned to the coherence length of the interaction. ((110) wafers are chosen so there will be nonzero response of the $\chi^{(2)}$ tensor for light polarized in the plane of the wafer surface.) These wafers are then 'stacked' together, each layer rotated 90° with respect to those on either side, and the entire 'stack' is diffusion-bonded together.[28] There are both advantages and drawbacks to this method, however. The greatest challenge is that the wafer must be thinned and polished to the coherence length of the desired interaction, or alternatively an odd multiple of the coherence length for lower-order QPM. For nonlinear interactions in the near-IR, where the coherence lengths are very short, this would mean very high-order quasi-phasematching due to the impracticality of using wafers only a few

microns thick, with very tight polishing tolerances. Since the efficiency decreases with m^2 (where m is the order of the quasi-phasematching) such a structure would not be very efficient.

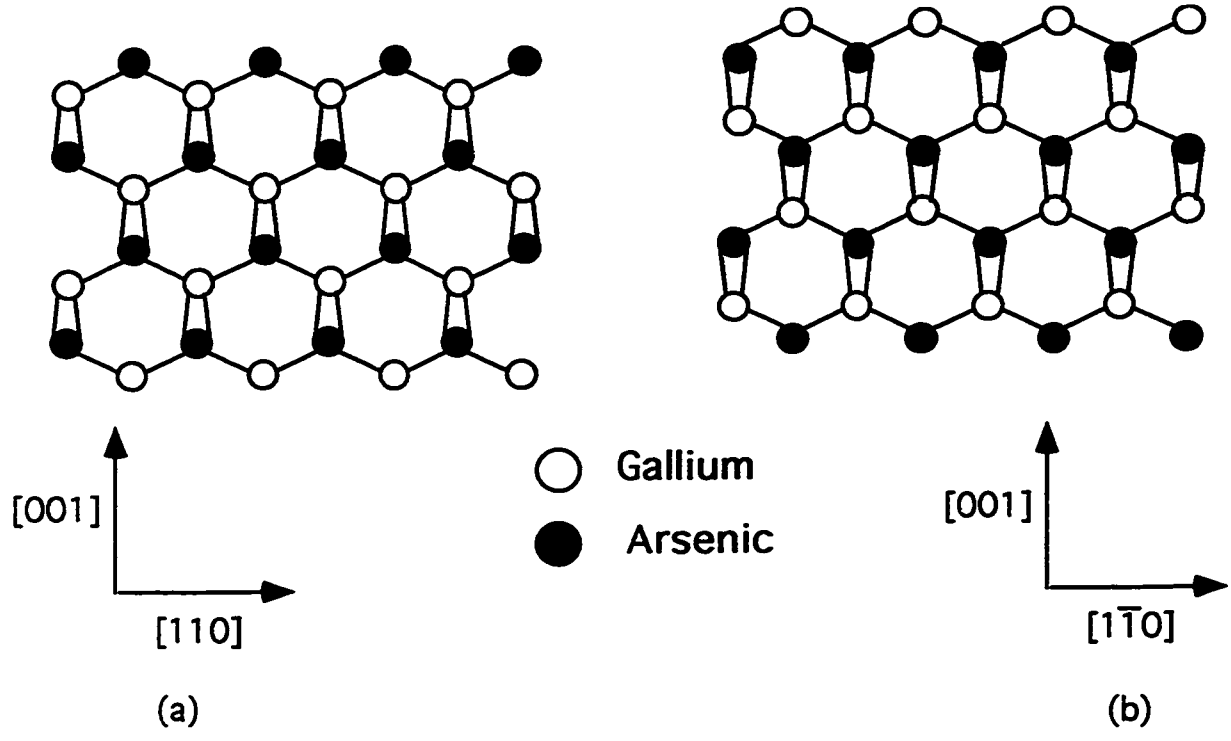

Figure 3.2. GaAs lattice viewed along two different directions, showing change direction of As-Ga bond and also $\chi^{(2)}$.

For interactions in the far-IR, however, where coherence lengths are on the order of 100 μm, first-order devices can be made. Another drawback to this approach is that, even for a first-order device, stacks of approximately 50 layers still need to be made in order to have efficient conversion.[29] As the number of layers in the stack increases, the yield rate of the bonding process decreases and the tolerances on the polishing need to be higher. The major advantage of this technique, however, is that it allows for bulk-like nonlinear optical interactions. The devices are not confined to thin waveguiding layers, making alignment issues much easier. Higher powers can be used since the beam only needs to be loosely focussed, whereas the same amount of power confined in a waveguide

would exceed the damage threshhold of GaAs. Of course, because the intensities are not as high as in a waveguide device, the efficiency is not as high either. One problem being encountered in the fabrication of diffusion-bonded stacks is the tendency of the semi-insulating wafers to convert to p-type during the thermal cycle used in the bonding process.[30] Even a low level of p-type background can lead to high levels of infrared absorption, so tradeoffs must be made between the diffusion bond quality (optimized by using higher temperatures) and the background loss.

Another approach is to create a template, or crystal seed, with alternating regions of (110) and (1-10) GaAs exposed, for subsequent epitaxial growth of waveguiding layers, or even of thick films for bulk-like interactions. One of the major advantages of such an approach would be the ability to quasiphasematch interactions with very short coherence lengths, specifically those on the order of 2-3 μm. In addition, if the coherence length can be easily set via a lithographic process, several structures, all with different coherence lengths, could be fabricated simultaneously. Chirped gratings, for ultrafast NLO applications, could also be easily fabricated, as could wedged gratings in order to provide tunability.

Such templates can indeed be fabricated by bonding two wafers together.[31] In the work of Yoo et al. at Bellcore, two (001) GaAs wafers were bonded to one another, with a 90° rotation about the (001) axis between the two of them, as shown in Figure 3.3.[32] The top wafer was then thinned and etched down to leave a very thin (~2000 Å) layer of rotated material on top of the substrate. This layer was then lithographically patterned, and etched through in some regions to the substrate. A regrowth step was then performed, in which the waveguide cladding layer and core were grown, and ridge waveguides were then etched in the (110) direction. The resulting structure then consists of alternating domains of material, with opposite signs of $\chi^{(2)}$.

This process was also attempted at Stanford University. The work at Bellcore relied on bonding layers of MOCVD-grown InGaP, lattice-matched to GaAs. Diffusion-bonding of GaAs to GaAs is much more difficult than that using indium- and phosphide-based materials, and the difficulties proved insurmountable. In addition, due to economic considerations, work was carried out on wafer pieces instead of whole wafers.

All the debris and particles generated during the cleaving process also contributed significantly to defects in the bonding layer. Small voids would be formed at the bonding interface, which would then etch unpredictably during the patterning stages. Because the grating periods of interest are on the order of 4 μm, even a rather small defect would destroy the features, as the affected area would be significantly increased by the etching. Furthermore, due to the combination of polishing and etching steps, it has only been possible to reduce the initial corrugation of a wafer-bonded template to approximately 1000 Å. Although some planarization takes place during the waveguide regrowth, this corrugation still introduces a periodic modulation into the waveguide core/cladding interfaces and also the upper cladding/air interfaces. As discussed earlier, such a periodic modulation of a waveguide is a very efficient scatterer and leads to very high losses.

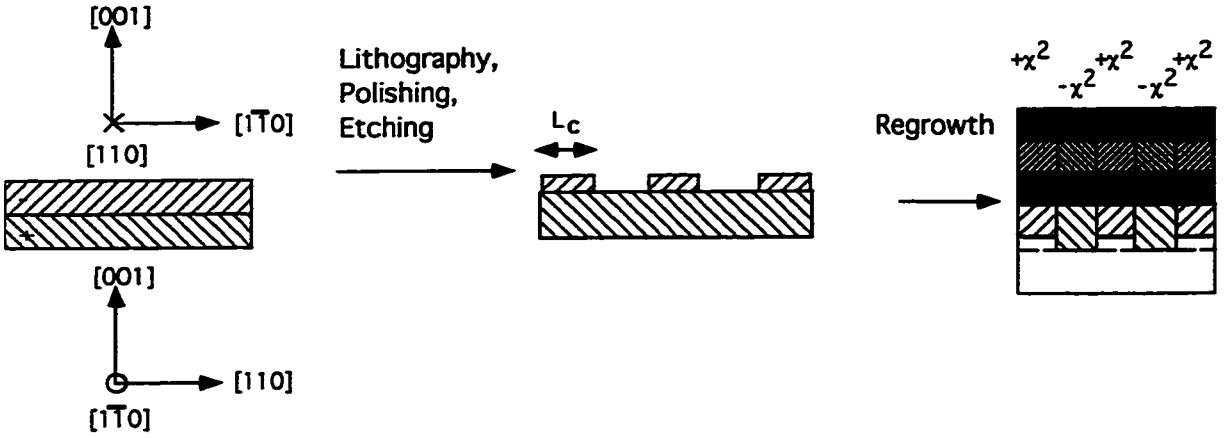

Figure 3.3. Process diagram of wafer-bonding method for creating orientation-patterned structures, after Yoo et al.[32]

3.2 Ge/GaAs APPROACH

In our approach, we have made a structure similar to the wafer-bonded structures, except that we have achieved a 90° rotation in the GaAs crystal lattice through expitaxial techniques instead of physically rotating a wafer. This structure then serves as the template, analagous to the wafer-bonding technique illustrated above. We have relied on a consequence of growing a polar material (GaAs) on a nonpolar material (Ge). (GaAs

and Ge are lattice matched materials, thus eliminating any problems due to strain, such as in the GaAs/Si system.) Because of the reduced symmetry of GaAs with respect to Ge, however, it is possible for two different 'phases' of GaAs to nucleate on a Ge (100) surface, where the phases differ by exchange of the two sublattices (rotation by 90°), and therefore have opposite signs of $\chi^{(2)}$. Simplistically, GaAs has an ABAB... stacking sequence long the (100) direction, and it is possible to begin the GaAs growth on the Ge surface with either the 'A' plane or the 'B' plane, with each case being the opposite phase, or 'antiphase,' to the other. There is little (or no) preference for either phase to nucleate and dominate over the other phase on a regular Ge surface, so if a way of intentionally controlling which phase nucleates on the Ge surface exists, it would be possible to fabricate structures analogous to the diffusion-bonded templates, but using an all-epitaxial approach. Figure 3.4 illustrates the desired crystal structure, where two phases of GaAs are separated by a thin Ge interlayer.

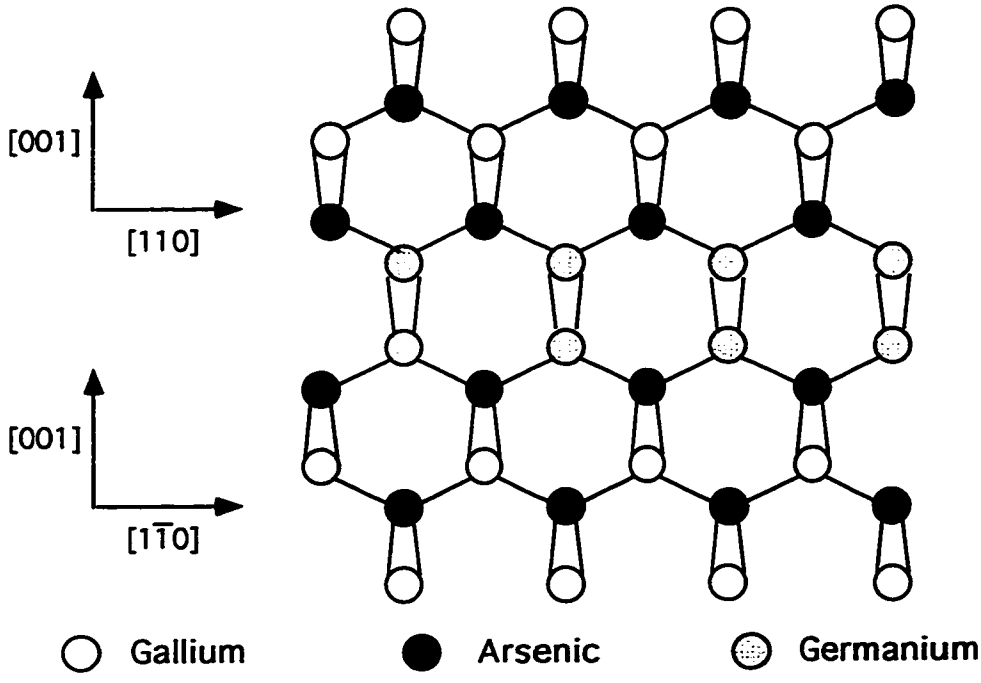

Figure 3.4. Schematic of a GaAs/Ge/GaAs heterostucture with GaAs phases antiphase to one another.

Using all-epitaxial methods, then, the approach to fabricating a quasi-phasematched GaAs waveguide is as follows: First, a template is prepared by growing a thin Ge layer, and then a thin layer of rotated, or antiphase, GaAs. The wafer is then patterned so that in some regions the substrate is exposed, while in others the rotated GaAs layer is left. A waveguide structure is then regrown upon this template. This process is schematically illustrated in Figure 3.5.

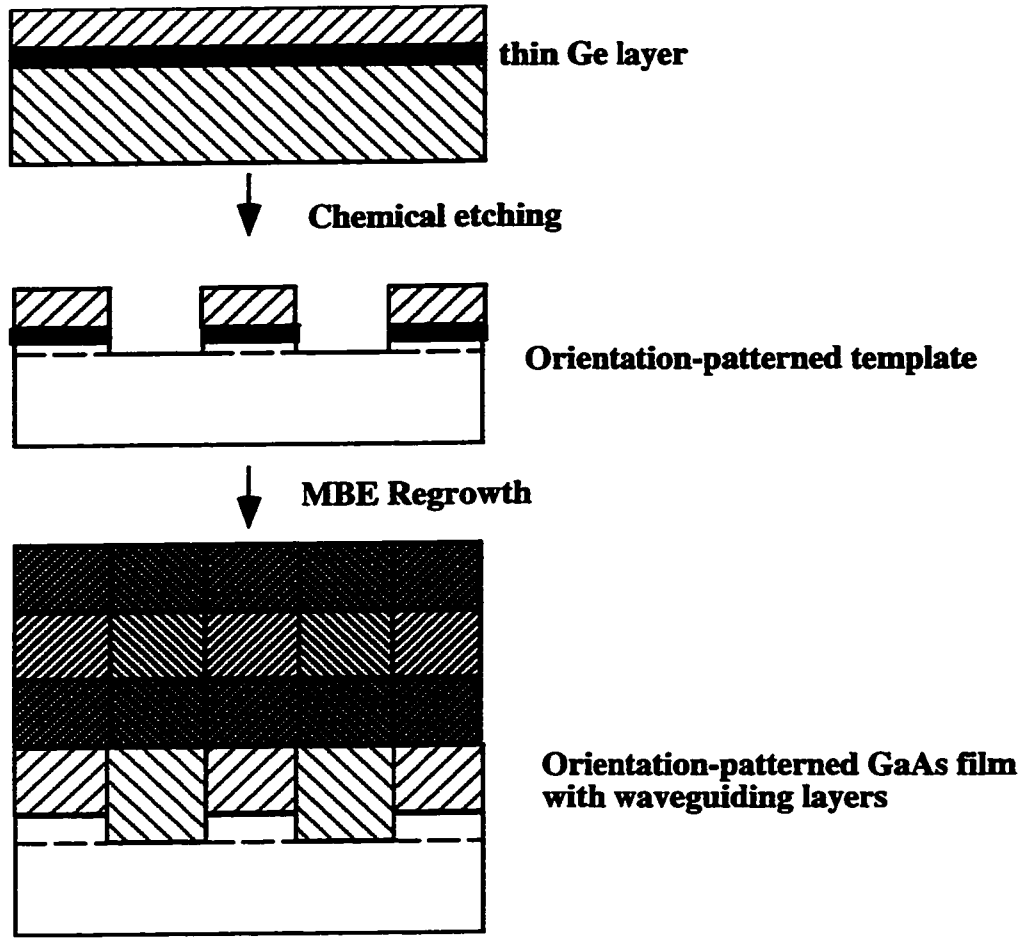

Figure 3.5. Process flow for creating orientation-patterned waveguides using all-epitaxial methods.

At first appearance, this method appears to have few, if any, advantages over the wafer bonding method. The major reason, however, for moving to an all-epitaxial

method of template fabrication is to reduce the starting corrugation, since this corrugation leads to very high losses for near-IR waves. Wafer-bonded templates have initial corrugations on the order of 1000 Å, and with planarization during regrowth the final corrugation will be on the order of 200 Å (although the planarization is a function of the epitaxial growth technique rather than the template fabrication technique). It is hoped that an all-epitaxial template can be fabricated with initial corrugations of less than 500 Å, and it may be feasible to produce nominally zero-corrugation templates through a lift-off technique. An all-epitaxial approach also has the advantage of relying only upon conventional epitaxial growth techniques, which are already required for growth of the waveguide layers, and the addition of a Ge source, rather than requiring any additional apparatus for wafer bonding. An epitaxially fabricated substrate should also be of higher quality, due to the absence of bonding voids formed at the boundaries. The resulting antiphase boundaries will also be more likely to propagate vertically during regrowth, as opposed to the grain boundaries that reult from wafer-bonded templates.

3.3 CONCLUSION

The primary work for this thesis consisted of developing these structures. After initial studies to determine the necessary growth conditions for antiphase GaAs, ways of preparing templates were developed. Finally, both of these pieces were put together in order to grow orientation-patterned GaAs films. Since the coherence length of the structures could be determined by lithographic methods, fabricating different structures for various nonlinear interactions would involve only using a different mask with the necessary period. These films were then tested for the desired nonlinear optical properties, and losses of the waveguide structures were measured in order to provide feedback to improve the process.

4. MOLECULAR BEAM EPITAXY

The microelectronic industry is based upon the ability to control the electrical properties of thin regions of semiconductor materials, typically on the order of 100 Å or less. Oftentimes this is done using diffusion or ion implantation to control the doping of a region. Alternatively, epitaxial growth techniques are also used to create junctions between dissimilar regions. Epitaxial growth is the growth of thin layers of material on a substrate, such that the thin layers continue the crystalline structure of the substrate. By changing the doping of the material as the layers are grown, pn junctions can be fabricated. The same material as the substrate need not be grown, in which case it is known as heteroepitaxy, as opposed to homoepitaxy. Thus, in addition to controlling the doping of the materials, other electronic properties such as the bandgap can also be controlled. In order to grow a heteroepitaxial layer of any appreciable thickness, however, the two materials must be closely lattice-matched, or strain and dislocations will be introduced. One prominent example is the epitaxy of AlGaAs on GaAs substrates. Since AlAs and GaAs are lattice matched to within 1%, any alloy of $Al_xGa_{1-x}As$ can also be grown on a GaAs substrate. As a result, the bandgap of a structure can be tailored from 1.43 eV to 2.16 eV, as well as controlling the index of refraction and doping characteristics of such a structure.

A wide variety of techniques are used to perform epitaxial growth, ranging from Liquid Phase Epitaxy (LPE), through various vapor phase techniques and Molecular Beam Epitaxy, or MBE. In LPE, the substrate is exposed to molten solutions containing the desired material, and the substrate is held at the proper temperature such that the solution nucleates and grows on the substrate[33]. The vapor phase techniques include Vapor Phase Epitaxy (VPE)[34] and Metal-Organic Chemical Vapor Depoition (MOCVD).[35] In this case the constituent materials are provided in gas form, and often a chemical reaction between the gasses is necessary to liberate the proper species for epitaxial growth.

MBE is a growth technique where the constituent materials are supplied to a substrate in the form of atomic beams. Simplistically, MBE can be thought of as high vacuum evaporation, or even 'atomic spray-painting.'[36]

4.1 MBE MECHANICS

The heart of an MBE system is an Ultra High Vacuum (UHV) chamber containing the source effusion cells and a substrate manipulator (see Figure 4.1). A sample is placed on the substrate manipulator and then pointed toward the effusion cells. The manipulator also has the ability to continuously rotate the substrate, in order to average out the radial source distribution. A suitable substrate (GaAs for this work) is placed in a vacuum chamber and heated to approximately 600° C. Molecular beams of Ga and As are then directed towards the substrate, where they combine to form new crystalline material on top of the substrate. Because of the UHV environment, the mean free path of the molecular beams is much greater than the source to substrate distance, so the beams arrive without having undergone any collisions. In addition, there is a shutter in front of each cell that can block the molecular beam. By controlling these shutters, different combinations of alloys can be grown, or the doping controlled. In addition, the interfaces between different regions can be made atomically sharp, due to the fast (~ 100ms) response of the shutters and the direct nature of the beam. Unlike vapor phase techniques, there is no gas that has to be purged from the chamber between interfaces. (Any atoms or molecules that do not deposit on the substrate stick to the cryogenically cooled walls of the chamber.) Because excess As will not incorporate at the growth temperatures, it is usual to grow with an As overpressure. Only when sufficient Ga is present will As be expitaxially incorporated into the growing material, thus maintaining the stoichiometry of the epilayer. The growth rate is determined by the rate at which the Ga (or other group III) element(s) arrive. In order to grow AlGaAs, both the Al and Ga shutters are open, in addition to the As shutter. The growth rate is then merely the sum of the invidual Ga and Al growth rates, and the composition is determined by the ratio of the two growth rates. In order to dope the material, a flux of the appropriate atoms (usually Si, Be, or C) is supplied along with the Ga, Al, and As. By sitting in the proper lattice site, these impurity atoms then donate either an electron (Si) or a hole (Be, C), resulting in either n-type or p-type material. The flux, or

the number of atoms (or molecules) coming from each cell is controlled by the temperature of the cell.[37]

Because of the high vapor pressure of As, a valved cracker was used as the group V source. A cracker consists of two stages: a low temperature sublimator stage and a high temperature cracking stage. The sublimator stage was heated to approximately 415° C in order to provide an adequate flux of As_4 molecules. After passing through a cracking zone at approximately 800° C, these As_4 molecules were cracked into the more reactive As_2, which also happens to be the equilibrium phase of As over GaAs. Because of the large thermal mass of sublimator unit, the source temperature can not be easily changed in order to control the As flux. Instead, the flux was controlled by the controlled aperture opening of a needle valve, hence the term 'valved cracker'. By closing the valve, the As flux could quickly be shut off and the background pressure in the chamber reduced. (While the shutter in front of the As beam is effective in decreasing the flux by about a factor of 20, there is still a high background As partial pressure due to the tendency of As to bounce off of the shutter and hot walls of the cells, instead of stick, as the group III elements do.) [38]

In order to maintain the UHV environment, the chamber is equipped with an ion pump and a large cryopump. Titanium sublimation pumping is also employed on a periodic basis in order to getter any remaining impurities. Furthermore, the chamber employs liquid nitrogen cryoshrouds, which also have a substantial pumping effect in addition to being extremely effective at gettering stray atoms and molecules from the sources. A water/glycol coolant is also run through the source flange to provide additional cooling capabilities, in addition to minimizing thermal cross-talk between the various sources. The base pressure of the chamber is routinely less than 1e-10 Torr. A Load Chamber is utilized in order to introduce new substrates and remove grown wafers, while simultaneously maintaining the UHV environment of the growth chamber. After new substrates are loaded, the chamber is pumped down with a Venturi pump, two-stage sorbtion pump, cryopump, and ion pump. Each substrate is then baked for one hour at 400° C to remove contamination. This temperature is low enough that the integrity of the native oxide is maintained, and no As overpressure is neccessary. The wafers are then transferred into an intermediate chamber, the Transition Tube, from where they can be loaded into one of two MBE chambers. A computer control system is used to open/close

the shutters and change the source or substrate temperatures during the growth of a structure.

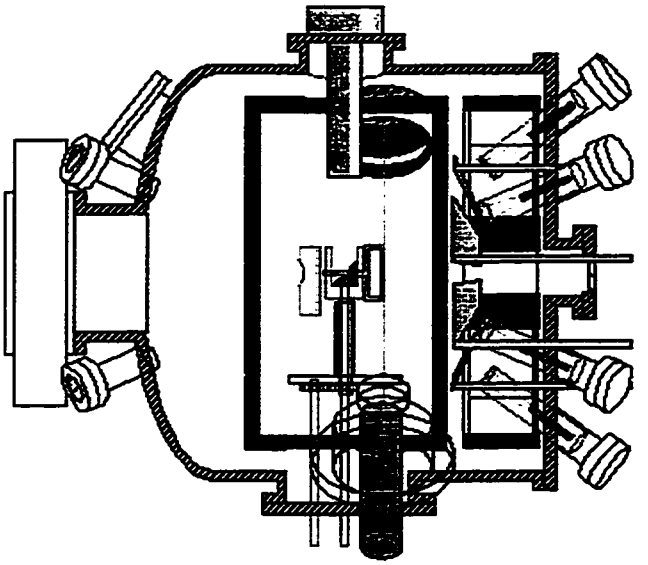

Figure 4.1. Schematic of an MBE machine, showing source furnaces, shutters, substrate manipulator, and RHEED system.[39]

4.2 GaAs MBE

Although this simple picture is oftentimes sufficient, an attempt at understanding some of the details of the actual growth mechanisms are required for this work. Specifically, it is necessary to understand how and where the Ga atoms and As molecules react and combine together in order form the next layer of crystal. One important fact that must be considered is imperfections in the substrate. Because the wafers are not atomically flat, step edges exist with varying degrees of regularity. These step edges provide preferential nucleation sites for new growth to take place. Depending on the growth rates, temperature, and As overpressure, the impinging Ga atoms will have a finite 'lifetime' on the substrate surface, during which they will 'wander' or migrate, searching for suitable sites. Step-flow growth occurs when this migration length is long enough so that incorporation only takes place along step edges. As the Ga adatoms bind to the step

egdes, they react with As to form crystalline GaAs, creating a new step edge displaced by one unit cell. Thus, the step is said to 'flow' across the substrate as the process repeats. This situation occurs when the density of step edges is great enough and the Ga migration length long enough so that the impinging Ga adatoms can find a step edge on which to nucleate. The Ga migration length can be increased by raising the temperature and decreasing the As flux while the density of step edges can be controlled by the orientation of the substrate.[40]

If, however, the Ga migration length, on average, is less than the distance to the next step, island growth will occur. Since the Ga atoms will not have time to find a preferential bonding site before reacting with an As atom, nucleation will take place on a flat region, forming a little island of crystalline material. This island will then provide step edges for the nucleation of additional Ga atoms. Eventually, the islands will coalesce together and the surface will once again become flat. The process then starts over when a new island is nucleated. It can be seen that, for step flow growth, the surface maintains a relatively constant amount of disorder. For island growth, in contrast, the surface goes through maxima and minima of roughness , as illustrated in Figure 4.2.

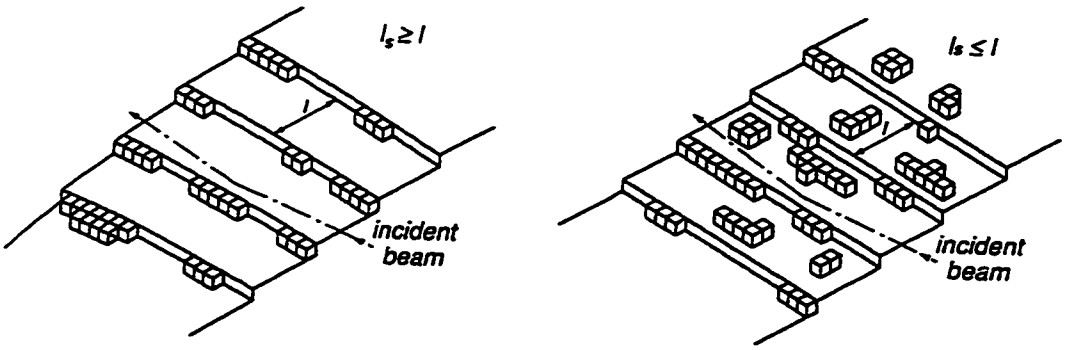

Figure 4.2. Step-flow growth vs. island nucleation.[41]

For most applications, normally oriented (001) substrates are used. Within the precision of the wafer saw, these substrates are aligned with the (001) plane of GaAs,

so no regular or periodic step structure results, only random steps resulting from the imperfections of the sawing and polishing process. Oftentimes it is desirable to introduce an intentional step structure into the substrate by introducing a small angle between the substrate surface and the (001) crystal plane. The spacing of the steps depends upon the amount of misorientation, and the nature of the steps depends on the direction of the miscut. Starting from the (001) plane, substrates can be misoriented towards the (111)A, (111)B, or a (110) plane, each exposing different combinations of steps. Traditionally, growth on wafers misoriented towards (111)A is preferred for MBE, as opposed to wafers misoriented towards (111)B. This is because of the differing reactivity of the two types of steps. Surfaces misoriented towards (111)A expose dangling Ga bonds, and surfaces misoriented towards (111)B expose dangling As bonds. Because of the higher sticking coefficient at the dangling As bonds, growth proceeds rapidly from (111)B steps. For substrates misoriented towards (111)A, the only place where (111)B steps are exposed are at kink sites. Hence, growth proceeds in the 'step-flow' mode, where the steps flow in the direction of the misorientation, one over the other (Figure 4.3). For substrates misoriented towards (111)B, growth can occur anywhere along the exposed step edge. In addition, the growth rate is much lower along any exposed (111)A step. As a result, growth proceeds in long, finger-like projections from the (111)B steps (Figure 4.4). It is easy to see why growth on (111)B can lead to rough surfaces, a problem that was encountered in this work. Substrates misoriented towards a <110> plane have a combination of A-type and B-type steps.

A growth technique that was widely used in the project is known as MEE, or Migration Enhanced Epitaxy. In this technique, the group III elements and the group V element are supplied separately (Figure 4.5). By doing this, the Ga migration length is increased in the (brief) As-free environment.[42] For example, the Ga shutter is opened for a time adequate to deposit ~1 - 1.5 monolayers (1 monolayer = 2.83 Å). A pause of approximately 3-5 seconds then allows the Ga atoms to migrate to all available sites. The As shutter is then opened long enough to supply enough As to stabilize the surface. At this point one monolayer of GaAs has been grown. The process is then repeated until the desired thickness of material has been deposited.

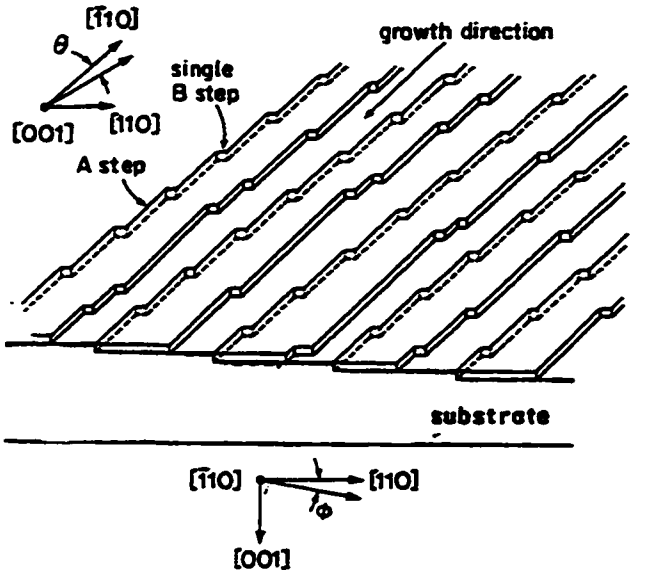

Figure 4.3. Schematic of growth on a surface misoriented towards (111)A.[43]

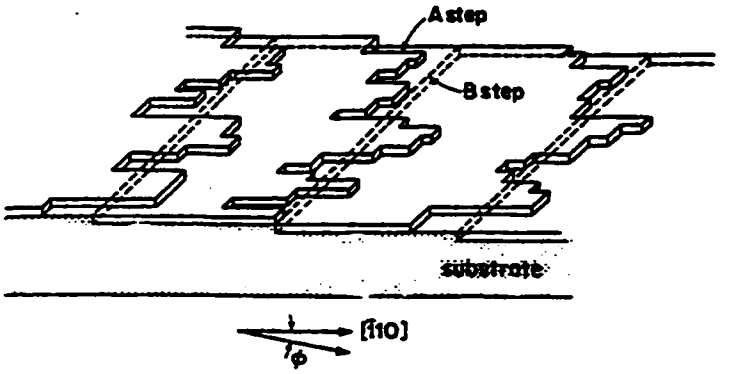

Figure 4.4. Schematic of growth on a surface misoriented towards (111)B, illustrating rough growth front.[43]

The major disadvantage of this approach is the extremely low overall growth rate. MEE, however, can be performed at temperatures too low for normal MBE growth. Thus, it has found applications in situations where low temperatures are desired to inhibit diffusion, either of dopants, or in order to maintain sharp interfaces to enhance quantum confinement effects. In addition, MEE is often used to 'smooth' rough surfaces, because of the long Ga migration lengths. This long Ga migration length promotes step-flow growth, which is smoother than the alternative island-growth. MEE growth occurs by the repeated formation and annihilation of small Ga droplets on the (2x4) As-stable surface. MEE was employed in this work in an attempt to help smooth out the corrugation left after patterning wafers and to minimize any p-type doping that would result from Ge diffusing into the GaAs.

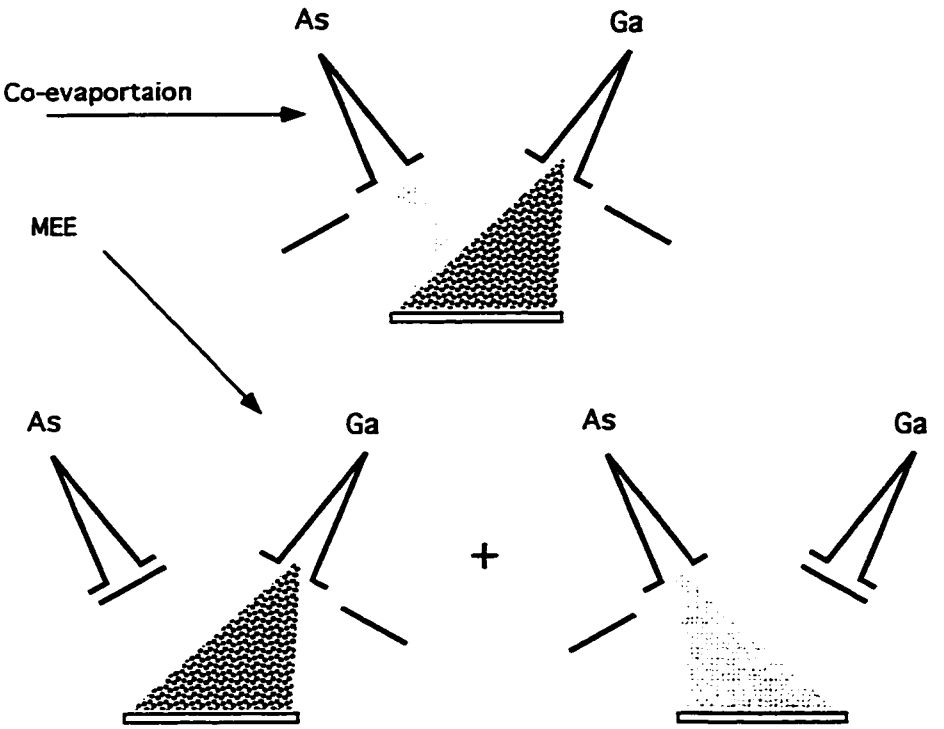

Figure 4.5. Co-evaporation vs. MEE.

For the applications of this work, the growth of $Al_xGa_{1-x}As$ is similar to GaAs. The major difference is that due to the increased reactivity of Al as compared to Ga, the migration length for Al is much shorter. Oftentimes AlGaAs is grown at a higher temperature than GaAs in order to help combat this problem.

4.3 RHEED

Because MBE growth takes place in a UHV environment, it is possible to perform Reflection High Energy Electron Diffraction, or RHEED, on the wafer while it is growing. RHEED relies upon coherent scattering from the 2-dimensional surface reconstruction of the growing sample to create patterns that can be interpreted with regards to crystal quality, growth processes, etc. During RHEED, a beam of high energy (8keV - 15 keV) electrons is directed at a glancing angle to the substrate. The beam is then diffracted by the substrate, with the diffraction pattern imaged on a phosphorous screen opposite the gun (see Figure 4.1). Because of the glancing angle, only the 2-D surface structure of the sample is probed. The diffraction results can be thought of in similar terms as X-ray diffraction, with reference to Ewald spheres and reciprocal lattice space (Figure 4.6). Because the surface is only a 2-D structure, however, the reciprocal space is now a series of rods, instead of discrete points. Any intersection of the Ewald sphere with one of these rods results in a spot or streak in the RHEED pattern.[39]

RHEED patterns provide information concerning both the structure of the surface and its quality. As the surface roughens and becomes more 3-D, the diffraction pattern becomes 'spotty'. Conversely, long streaks are indications of smooth, good quality surfaces with 2-D characteristics. In addition, different surface reconstructions can be seen. A surface reconstruction is a periodic arrangement of surface atoms that differs from the underlying bulk, in order to minimize the energy of the dangling bonds at the substrate-vacuum interface. In observing a RHEED pattern along a particular azimuth, a periodic pattern of streaks, known as principal streaks, is observed. These streaks are due to diffraction of the beam by the underlying bulk structure. When the surface structure has a period greater than the bulk period - i.e. when surface atoms are further apart than the bulk lattice sites - streaks appear in between the principal streaks. This is because a larger period in real space results in a closer spacing of the reciprocal lattice rods. If, for example, only

one minor streak is observed halfway between two principal streaks, the determining surface structure has a period (in this direction) twice that of the bulk. According to the nomenclature, this is known as a 2-fold pattern. Three equally spaced minor streaks would result in a 3-fold pattern, etc. Usually the pattern is observed along one azimuth, and then 90° off. If one direction yielded a 3-fold pattern, and 90° off yielded a 1-fold, then the surface reconstruction would be named a (3x1). For a well characterized material such as GaAs, the growth conditions (temperature, V/III ratio) which lead to various reconstructions are well-known and studied. Thus, by observing the different patterns, one can calibrate temperature, fluxes, determine if the native oxide has been removed, or determine if growth conditions are As-rich or Ga-rich.[44]

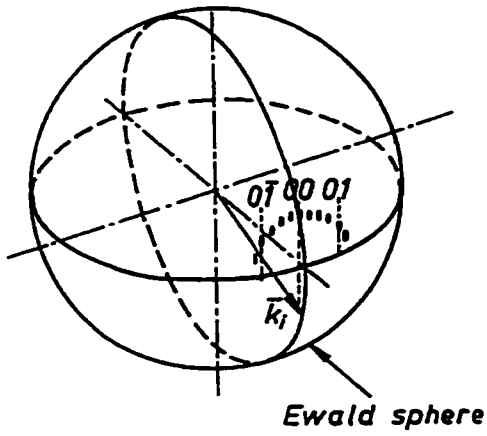

Figure 4.6. Schematic of Ewald sphere, showing principal streaks and minor streaks. In this direction a 4-fold reconstruction is seen.[41]

Of particular relevance to this project is the (2x4) surface reconstruction of (001) GaAs under typical MBE growth conditions with a substrate temperature of approximately 600 °C and an As overpressure. Along the [110] direction, in these conditions, a 2-fold pattern will be observed. Along a [1-10] direction, a 4-fold pattern will be observed. One possible schematic of the 2x4 surface reconstruction is shown below in Figure 4.7. A misoriented wafer will also have what is known as a 'horizon',

due to the step edges. In a wafer misoriented towards (111)B, the [1-10] direction will appear above the horizon, the [-110] direction will be below the horizon, and the [110] and [-1-10] directions will be on the horizon. Thus, the 4-fold patterns will appear either above or below the horizon, and the 2-fold patterns on the horizon. By identifying the relation of the 2-fold and 4-fold directions with respect to the horizon, we were able to determine the orientation of the epilayer GaAs with respect to the underlying substrate. This is an important capability for studying GaAs/Ge/GaAs growth, as discussed later.

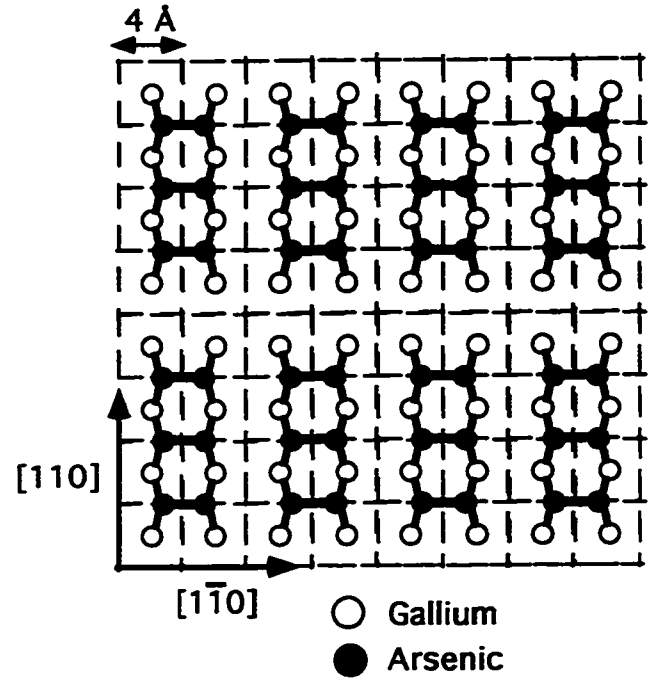

Figure 4.7. Proposed model of (2x4) surface reconstruction during GaAs growth.[39]

RHEED can also give valuable information concerning growth rates. For example, in the island-growth mode, the reflected intensity of the RHEED beam will go through minima and maxima, as the surface roughens and flattens. These oscillations correspond to one monolayer of growth, and can be used to calibrate the machine. RHEED can also indicate when the native oxide of the substrate has been adequately removed, as the pattern will change from a diffuse glow characteristic of an amorphous surface to one

that is characteristic of an ordered surface. This is important for growing high-quality epitaxial material, and it can also be used to help calibrate temperatures as the oxide is known to desorb at approximately 580° C. Many of the different reconstructions also display temperature, growth rate, or As flux dependencies, and their existence or absence can provide even more data points for proper calibrations.[40]

4.4 Ge EPITAXY

Ge epitaxy, due to its elemental nature, is a much simpler affair than that for compound semiconductors. All that was necessary to grow epitaxial Ge was to install a high-temperature cell loaded with pure Ge. Because of the low vapor pressureof Ge, however, the growth rates were extremely low - ~ 200 Å/hr. was the rate commonly used during this work (as compared to ~ 1 μm/hr. for III-V growth). Because of the thin layers needed, ~30-100 Å, this was not a major issue. A substrate temperature of 350° C was used during the growth of all the Ge layers. The scarcity of Ge MBE growth is largely due to the high background doping that results in chambers used for Ge deposition, due to the amphoteric nature of Ge in GaAs, rather than any difficulty in growing Ge itself.

4.5 REGROWTH

The second important step for the fabrication of orientation-patterned nonlinear waveguides was to successfully regrow GaAs on a patterned substrate. Although MBE is sensitive to surface contamination of the substrate, it is possible to regrow material that has been processed in one form or another. One common example would be the fabrication of DFB lasers, where a grating is etched in the sample to act as a mirror, and then the rest of the structure is grown.[6] Regrowth techniques are also often employed to fabricate quantum wires and other nanostructures.[45] In addition, before the ready availability of epi-ready wafers, substrates had to be prepared for growth through a combination of polishing, etching, and cleaning steps. It is important to remove any organic contamination from the wafer. Carbon, in addition to doping the sample, also serves as a nucleation site for Ga, resulting in a higher local growth rate and results in faceting during growth. It is also crucial to leave the surface smooth. An etch that results

in a rough, irregular surface will not yield good regrown material. Finally, there is the issue of the oxide. An oxide can be useful for protecting the sample from further contamination during atmospheric exposure before insertion into the MBE system, but it must be able to be removed in situ before regrowth.

Two difficulties can arise in the regrowth in this particular case. First is the difference in growing on surfaces misoriented both towards (111)A and (111)B simultaneously. Optimizing the growth conditions for one surface may not be ideal for the other. In addition, it is desirable to choose a growth regime where the corrugation will be smoothed out. Slightly different growth rates on the two surfaces could make the corrugation worse, or lead to composition fluctuations in the AlGaAs waveguide layers. In an attempt to reduce the corrugation, the regrowths were started with a layer of GaAs grown by MEE. As discussed above, the Ga migration length is greatly enhanced in MEE growth, so this should promote smoothing of the layers. Also, it was found necessary to carefully prepare and clean the sample, especially when using AlGaAs etch stop layers, in order to get good quality regrowth.

5. ANTIPHASE GROWTH: BACKGROUND, RESULTS AND DISCUSSION

In order for the all-epitaxial approach to work, it is necessary to grow a layer of epitaxial GaAs on a thin Ge interlayer, such that the epitaxial GaAs is of the opposite phase, or rotated by 90°, compared to the original substrate. In addition, the GaAs must all be of the same phase across the surface of the wafer - any regions of opposite phase would negate any desired phasematching effects. Since the ability to grow high quality, antiphase GaAs was crucial to our approach, much work and time were spent investigating the necessary growth conditions. In addition to the direct applicability to the work presented here, it is hoped that this research will also be beneficial to other researchers studying polar-on-nonpolar epitaxy for other uses.

5.1 BACKGROUND

Polar-on-nonpolar epitaxy has many potential applications and as such is widely studied. Heterojunction Bipolar Transistors (HBTs), using Ge as a base material, were widely studied because of the high hole mobility of Ge, and GaAs/Ge solar cells also have many useful properties.[46] By using materials of differing bandgaps to collect light from differing regions of the spectrum, the efficiency can be vastly improved. In addition, the ability to use Ge substrates, instead of more costly GaAs wafers, could have a substantial economic benefit, especially for space-based solar arrays. GaAs/Si heteroepitaxy, in the hopes of directly integrating GaAs optoelectronic devices with Si-based circuitry, encounters the same problems in addition to the lattice-mismatch (4%) problem. Using Ge_xSi_{1-x} as a buffer layer to accomodate the strain is one potential solution. Growth of GaP on Si has also been studied.[47]

As a result, there is a large body of literature - both theoretical and experimental - concerning polar-on-nonpolar epitaxy. In order to make suitable device grade material, two difficulties need to be overcome. First is the tendency of the polar material to form AntiPhase Domains (APDs) and AntiPhase Boundaries (APBs), when growth is nucleated on the nonpolar material. Because of the higher symmetry of the nonpolar material(Ge) it is possible for two different phases of the polar material (GaAs) to

nucleate on the nonpolar surface, so that growth may commence with either the cation plane or the anion plane. These regions of different phase are known as APDs, and are separated by APBs, as shown in Figure 5.1 by the dashed line. Since the APBs consist of charged Ga-Ga or As-As bonds, their existence would degrade the performance of any electronic device. In addition, there is also the problem of cross-contamination resulting in unintentional doping between the two materials (i.e. Ge doping of GaAs). Since this second matter was not a concern for our ultimate (optical) devices, it will not be discussed in detail.

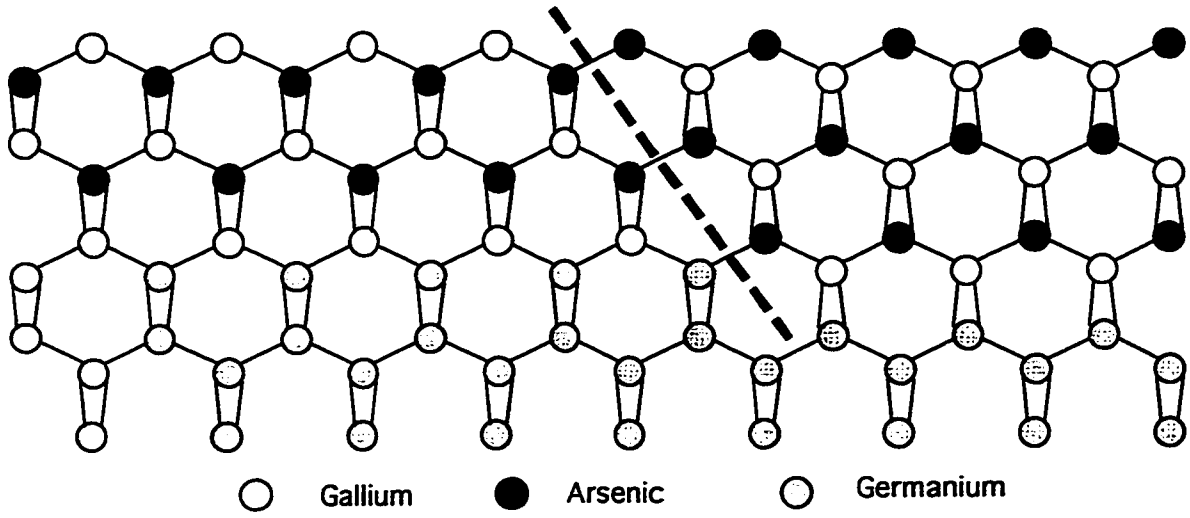

Figure 5.1. Antiphase Boundary (APB) and Antiphase Domains (APDs) resulting from a single step in the Ge surface.

Not surprisingly, it was found that APDs and APBs do indeed occur under standard growth conditions, most likely due to the occurrence of single steps in the nonpolar material, or incomplete prelayers. Calculations also showed that the nonpolar/polar interface must be nonplanar in order to avoid the buildup of significant electric fields.[48] Several researchers tried various surface treatments (high-temperature anneals, etc.) in order to promote the existence of double steps over single steps. Still

other researchers tried growing on nonstandard crystal planes - such as (211) - in order to alleviate APDs.[49] It was observed that, instead of growing on a nominally flat (001) substrate, APD free material could be grown by using substrates with a deliberate misorientation introduced.[46, 50] This result may be due either to the tendency of the misoriented wafers to form double steps, given the proper treatment, or to preferential bonding of one particular species of the polar material at the step edges, thus breaking the symmetry between the two. Based on the double-stepped model of APD-free growth, two essential conclusions can be reached. First, growth must be initiated with a monolayer of one species, as incomplete coverage will result in APDs. Second, the phase of the epilayer should be controlled by choosing which species to deposit first - i.e. a sample grown with an initial As monolayer should have the opposite phase than one initiated with a Ga monolayer. One major difficulty with controlling the phase with the appropriate prelayer is avoiding As contanimation of a Ga prelayer, since the chambers used for the growth of GaAs usually have a significant background pressure of As unless careful measures are taken. Any incomplete prelayer coverage can lead to a high APD density.

Kroemer pointed out the improbability of a surface spontaneously double-stepping, unless there was a preference for one kind of step edge over another. Otherwise, as single steps coalesce into double steps, there should be a 25% chance that the two nearest-neighboring steps might move away, leaving behind a finite density of single steps. For a Ge (or Si) film, the only difference between steps is whether the dangling bonds are oriented parallel or perpendicular to the step edges, and it was speculated that this difference might be enough to create all double steps if one type of bond were of lower energy.[51]

Strite and co-workers reported good quality, APD-free material for growth on substrates misoriented 4° towards (111)A using an As prelayer. This material was in-phase with the underlaying substrate. If a Ga prelayer was used for a misoriented substrate, the material was also in phase with the underlying substrate, but APDs were seen. For nominally (001) oriented substrates, APDs were observed at the initiation of growth, and then annihilated after about 500 Å of growth, based on RHEED and TEM studies. This occured independent of whether a Ga or an As prelayer was used. When a Ga prelayer was used, however, the topmost layer was antiphase to the substrate - i.e.

rotated by 90°. These results were explained by postulating preferential, nonequivalent bonding sites for Ga and As adatoms at the step edges of the Ge. For the misoriented wafers the step density was large enough so that the As and Ga atoms were able to find their suitable bonding sites at the step edges, and even exchange positions if necessary. For the nominally (001) case, however, the density of step edges was not large enough to allow any exchange mechanism to take place. As a result, APDs were formed, which then annihilated. For a Ga prelayer, the dominant domain that resulted is antiphase to the substrate.[52, 53]

Strite termed the growth mechanism for misoriented wafers *step-dominated*, while nominally (001) growth was termed *terrace-dominated*. It can be seen that these two methods have many parallels with the step-flow growth and island-growth mechanisms discussed for traditional III-V growth. In the first case, the growth mechanism is dominated by effects occuring at step edges, while in the second case nucleation is taking place at nonfavored sites. Thus, it is not surprising that changing the prelayer has a much stronger effect in the terrace-dominated growth regime, as nothing else exists to differentiate between As and Ga. In the step-dominated regime, the two species are discriminated between by their preferential bonding sites at the Ge step edges. The increased incidence of APDs observed when Ga, as opposed to As, prelayers are used was explained as residual As resulting in incomplete prelayer coverage.

Pukite and Cohen investigated conditions for growing APD free GaAs on Ge. They reported the interesting result that changing between As_2 and As_4 resulted in the domain of the GaAs, with respect to the Ge misorientation, switching. No clear explanations for this result was given.[54, 55] Sieg et. al. also reported some intriguing results for GaAs/Ge heteroepitaxy.[56] They were able to grow APD free material on Ge substrates misoriented 6° towards the (111) plane, using either a Ga or an As prelayer. (It is important to remember that GaAs substrates can be misoriented towards either the (111)A or (111)B planes, while for Ge substrates the two (111) planes are equivalent.) Crucial to obtaining this result, however, was a 20 min., 640° C anneal before growing the GaAs. It is postulated that this anneal results in a double-stepped Ge surface, thus supressing APD formation. The independence on prelayer species is more evidence that some type of exchange mechanism, most likely at the step edges, is taking place. It is

important to note that Sieg et al. used Ge substrates and not thin Ge films on GaAs, an important distinction because thin films are often observed to behave differently than bulk material. For example, the GaAs surface is naturally double-stepped, thus any thin Ge film deposited on top might also be double-stepped, whereas a Ge substrate will be a mixture of single and double steps unless explicit steps are taken to insure otherwise. In addition, Sieg et al. also observed a phase dependence on the As species - as for Pukite and Cohen, films nucleated with As_2 and As_4 gave opposite phases.

One valuable tool for determining both the quality of the films and their dominant orientation is the use of RHEED, and this was in fact done in the works mentioned above. As explained earlier, the [110] and [1-10] directions can be determined by identifying the 2-fold and 4-fold patterns, respectively. In addition, the presence of a horizon for a misoriented wafer also helps to establish directions. It is relavent to note that both Strite et al. and Sieg et al. reported RHEED data that is consistent with one another. Sieg reported seeing the 2-fold reconstruction above the horizon, and the 4-fold pattern on the horizon for Ge wafers misoriented towards the in-plane [110] direction. Likewise, with Strite et al. using GaAs wafers misoriented towards (111)A, the final 2-fold pattern was above or below the horizon, and the 4-fold pattern on the horizon. When growing with As_2, the results of Pukite and Cohen are consistent with Strite and Sieg. [52-56]

The consistency of the results between Strite et al. and Sieg et al. strengthens the argument for preferential bonding sites created by the misorientation. On a Ge surface misoriented towards a (111) plane, it appears that GaAs prefers to grow with its [110] direction parallel to the misorientation, and its [1-10] direction perpendicular. In other words, the GaAs prefers to misorient itself towards its (111)A plane instead of its (111)B plane.

It was decided to use the results of Strite et al. as a starting point towards growing antiphase GaAs, using a Ge interlayer. Their results indicated that single-domain GaAs could be grown on thin (~20 Å) Ge layers deposited on substrates misoriented 4° towards (111)A. In this particular instance, the epitaxial GaAs was the same phase as that of the substrate, as shown in Figure 5.2(a). It can be seen that misorienting the GaAs wafer either towards (111)A or (111)B will result in the same misorientation (towards (111)) and step structure in the Ge epitaxial layer, due to its higher symmetry. If a wafer

misoriented towards (111)B is chosen, however, the epitaxial GaAs will be antiphase to that of the substrate (Figure 5.2(b)). This is exactly the effect that is desired. Another way of illustrating the matter is to consider the case of GaAs grown on Ge misoriented towards (111). Assume that the GaAs grows single-domain and with a fixed orientation with respect to the misorientation (i.e. the top GaAs is misoriented towards its (111)A plane). Then, by placing a misoriented GaAs substrate 'beneath' the Ge, we can create the GaAs/Ge/GaAs heterostructure. Since a substrate misoriented towards either (111)A or (111)B can be placed beneath the Ge misoriented towards (111), the top layer will either be in-phase or antiphase to the substrate, depending on which one is chosen.

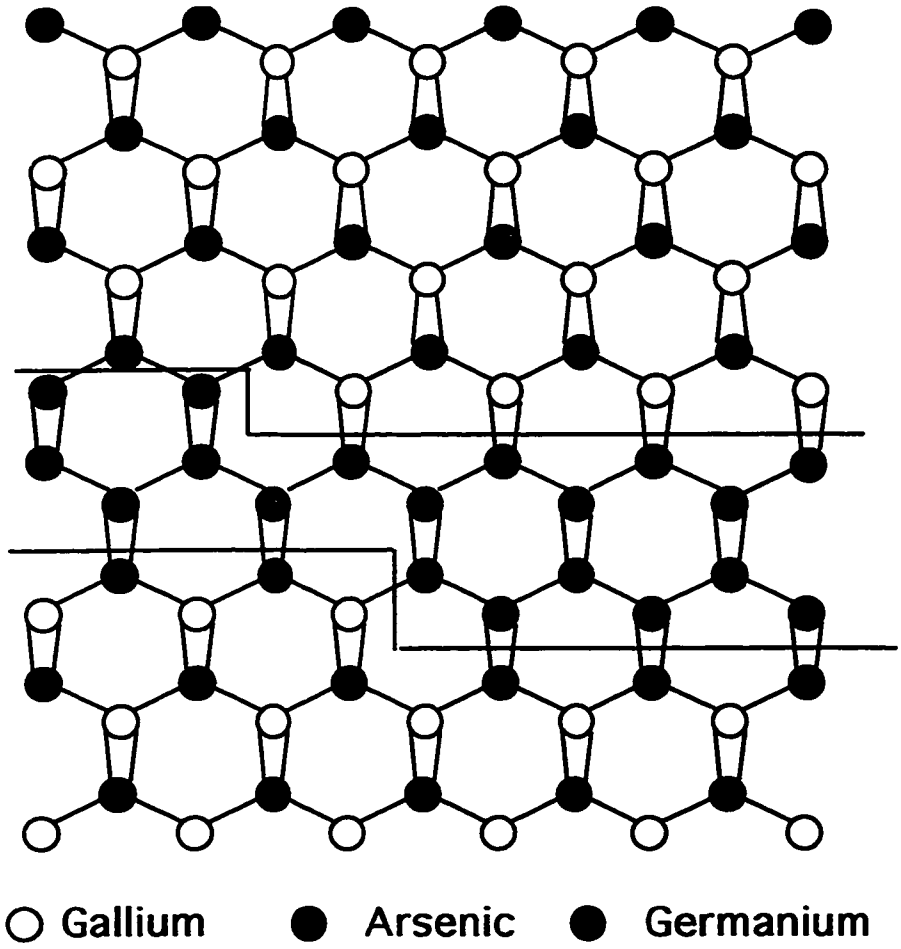

(a)

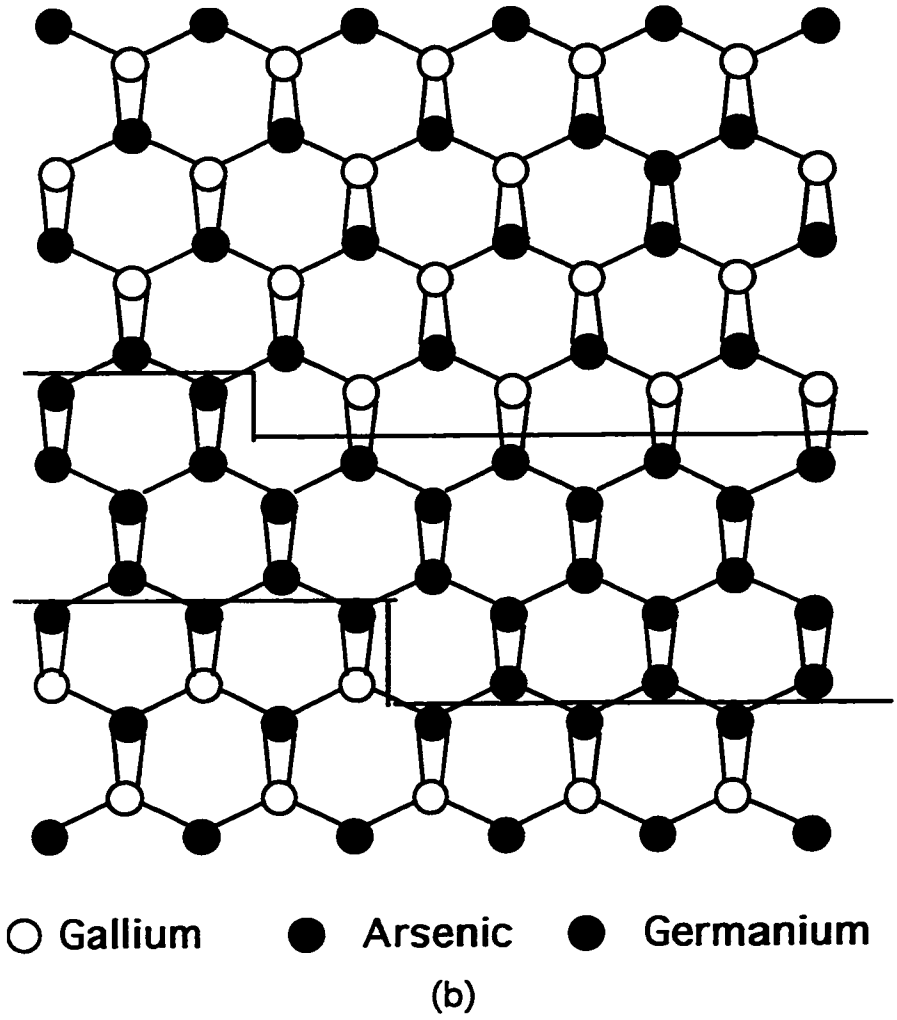

Figure 5.2. Schematic of growth of GaAs/Ge/GaAs heterostructures on surfaces misoriented towards (a) (111)A and (b) (111)B, following model of Strite et al.

Just by observing the misoriented Ge surface, however, it is not possible to see that a fixed orientation of GaAs will nucleate every time. That it does so was merely an observed experimental fact, reported by one research group. For our research to be successful, we would have to find the necessary growth conditions that would also allow us to grow APD free GaAs on thin Ge films. Then, by changing the misorientation direction by 90°, we should be able to grow antiphase films. We were mindful, however,

available to the growing wafer, the orientation of the RHEED beam compared to the major flat on the wafer can be used as a reference point. The easiest reference point, however, is the horizon due to the misorientation of the substrate. If the 4-fold pattern is seen above or below the horizon for the substrate and on the horizon for the GaAs epilayer, with the converse for the 2-fold pattern, then the GaAs epilayer is antiphase to the substrate. This is exactly the situation pictured in Figure 5.3.

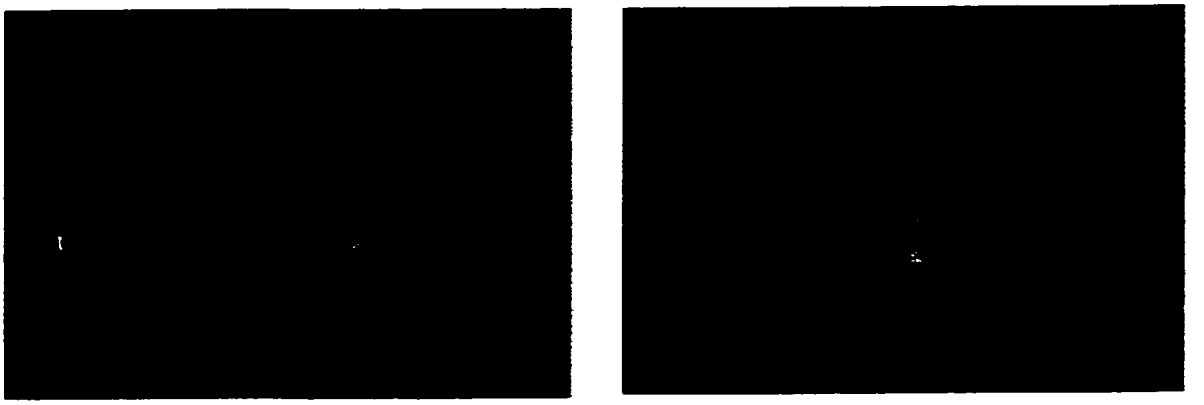

[110] [1$\bar{1}$0]

GaAs RHEED Patterns before Ge deposition

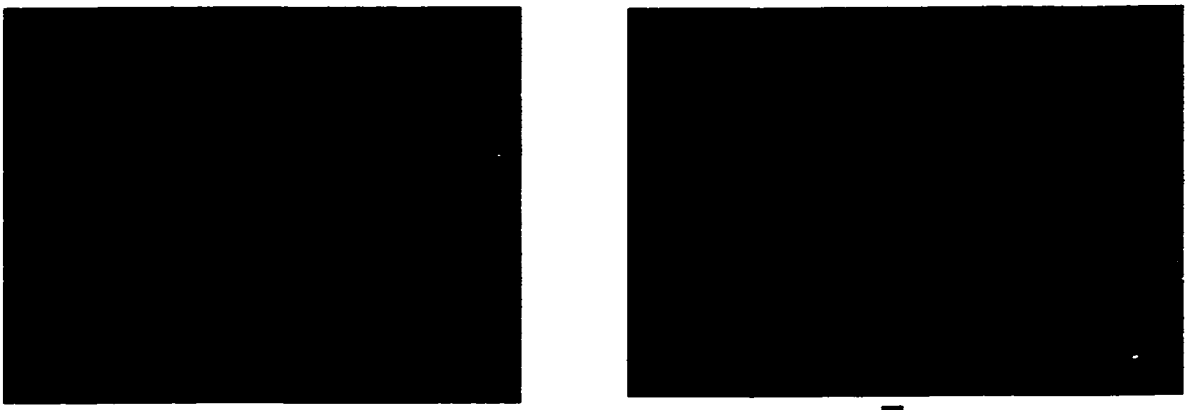

[110] [1$\bar{1}$0]

GaAs RHEED Patterns after Ge deposition and GaAs growth

Figure 5.3. RHEED pictures before and after Ge deposition, showing that the 2-fold and 4-fold patterns have switched directions.

Once the wafer is removed from the growth chamber, RHEED can no longer be used to probe the orientation of the film. In addition, the RHEED beam only probes a small spot of ~ 1mm^2 near the center of the wafer. For *ex situ* measurments, and in order to characterize large areas, an anisotropic etching technique was developed. For the anisotropic etching, ridges were lithographically defined, along the [110] and [1-10] directions. The samples were then etched using a 1:1:6 $NH_4OH:H_2O_2:H_2O$, a preferential etchant that leaves the sidewalls either slanted along the {111} planes for ridges in the [1-10] direction, or slightly undercut for ridges in the [110] direction.

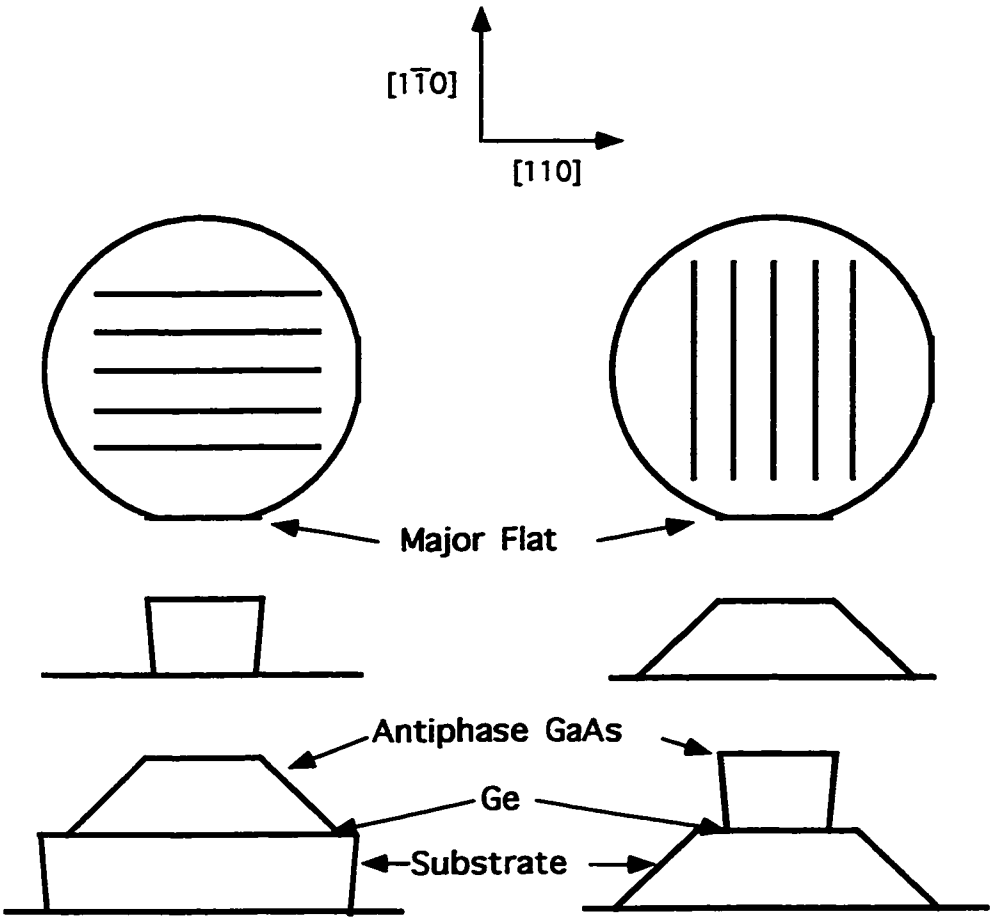

Figure 5.4. Etch profiles for features defined along in-plane [110] and [1-10] directions of a (001) wafer.

For antiphase GaAs epilayers, the sidewall profile will change as the etchant briefly stops and then goes through the Ge interlayer, while for in-phase material the sidewall angle will remain unchanged. For material with large numbers of APDs, severe disorder along the etching fronts could be detected under SEM examination, since a random mixture of V-groove and undercut etching would occur. A qualitative feel for the height of the APD propagation could also be obtained by comparing the heights of the disordered regions. Diagrams of the expected etch profiles are illustrated in Figure 5.4.

5.3 TEST STRUCTURE

In order to test the necessary conditions for antiphase growth, the following test structure (Figure 5.5) was used, while varying only one parameter at a time. After growing a 1000 Å GaAs buffer layer via conventional MBE, a 100 Å Ge layer was deposited at 350° C. The Ge surface was then annealed for 15 min. at 640° C. Next, 10 ML of GaAs were deposited via the MEE technique, at nucleation temperatures ranging from 350° C to 500° C. Next, 1000 Å of GaAs were deposited via coevaporation at 500° C, after which the substrate temperature was raised to 620° C and another 9000 Å deposited.

Most of the materials characterization studies were done on substrates misoriented 4° towards (111)A, but samples were also grown on wafers misoriented 4° towards (111)B for comparison purposes. Samples were grown with and without an As_2 flux during the Ge anneal in order to study its effect on material phase. In addition, samples were grown with both As and Ga prelayers in order to discern any dependence there.

The first study done was to determine the effect of the MEE nucleation temperature on the phase of GaAs epilayer. Because our earlier studies had shown the tendency of a Ge film to roughen at high temperatures in the absence of As, an As_2 flux was supplied during the anneal. Using wafers misoriented towards (111)A, films nucleated at 350° C yielded material antiphase to the substrate (Figure 5.6), while films nucleated at 500° C yield material in phase with the substrate (Figure 5.7). It should be noted that this nucleation temperature refers only to the first 10 MLs of MEE on the Ge, the rest of the structures are identical. Furthermore, films grown on wafers misoriented

towards (111)B show the expected opposite behavior - 350° C nucleation results in in-phase material, while 500° C nucleation results in antiphase material. In both cases, the epitaxial GaAs [1-10] direction is perpendicular to the misorientation-induced steps for low-temperature nucleation, while for high-temperature nucleation the [1-10] direction is parallel to the steps. No appreciable difference in material quality due to the difference in substrate misorientation was observed.

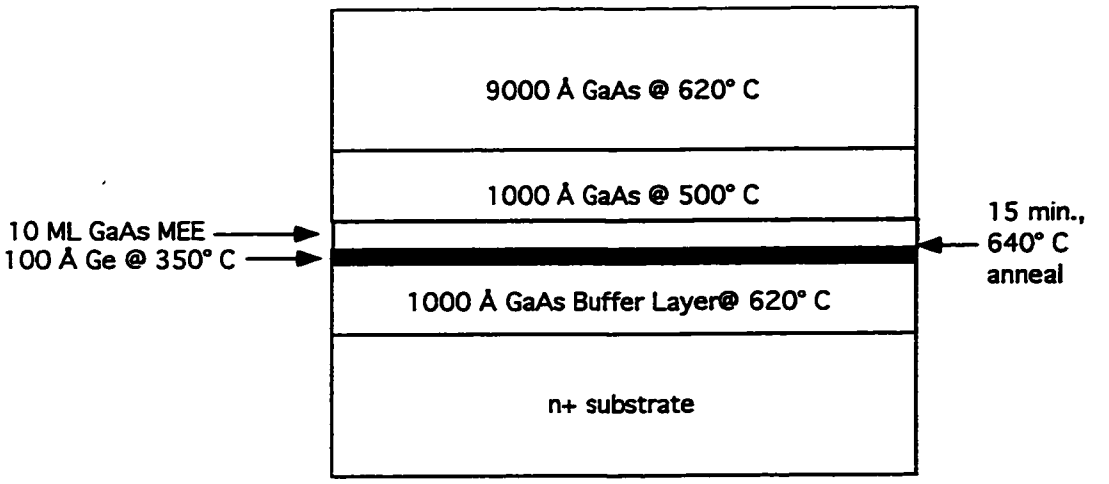

Figure 5.5. Schematic of test structure used for antiphase growth studies. Effect of nucleation temperature of the 10 ML MEE layer, substrate misorientation, and use of As during the anneal of the Ge surface were all studied.

The critical temperature appears to be at approximately 400° C, where the film becomes mixed domain. Optically, the surface appearance is quite cloudy, and preferential etching reveals evidence of a large density of APDs (Figure 5.8). It is important to compare samples etched for comparable amounts of time, as overetching in the preferential etch solution tends to exacerbate any defects in the material and give a false impression as to its quality.

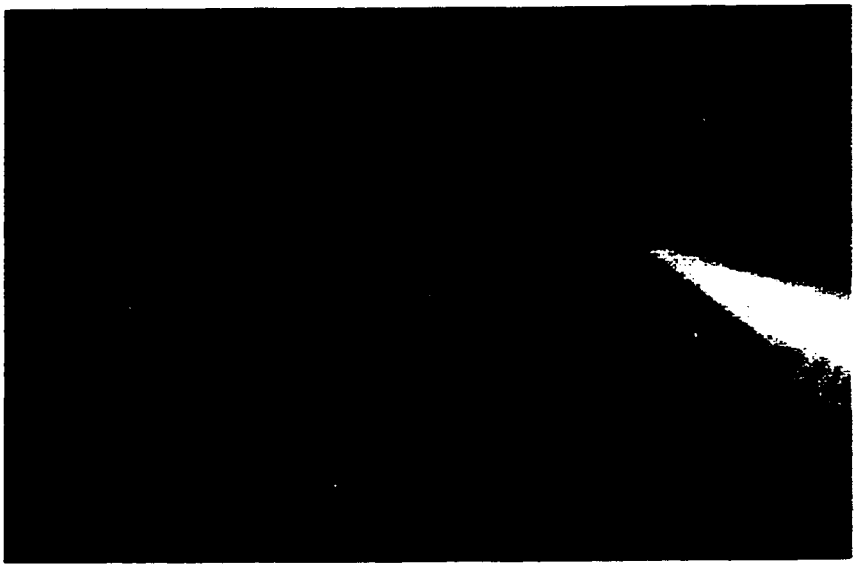

(a)

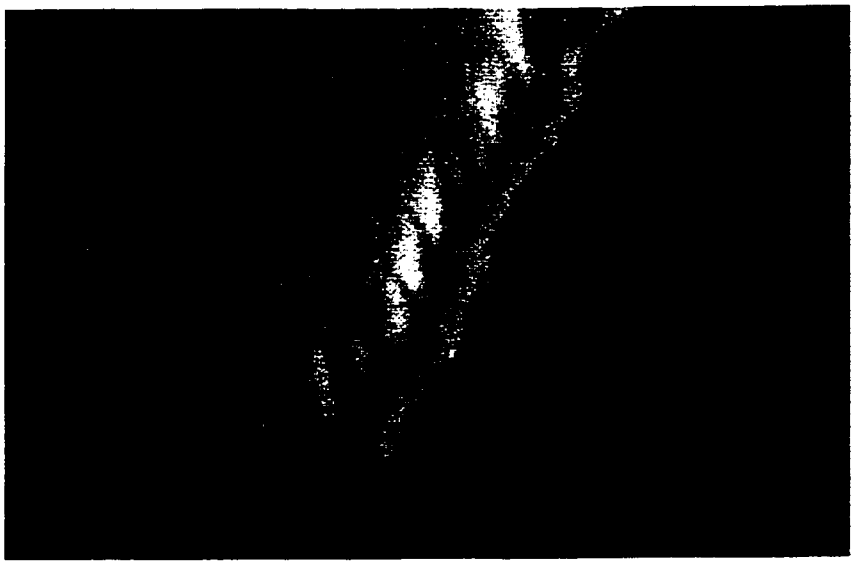

(b)

Figure 5.6. Cross section of film nucleated at 350° C, (a) showing epilayer GaAs antiphase to the substrate, and (b) showing smooth sidewall with small initial APD density. Substrate is (001) GaAs misoriented 4° towards (111)A.

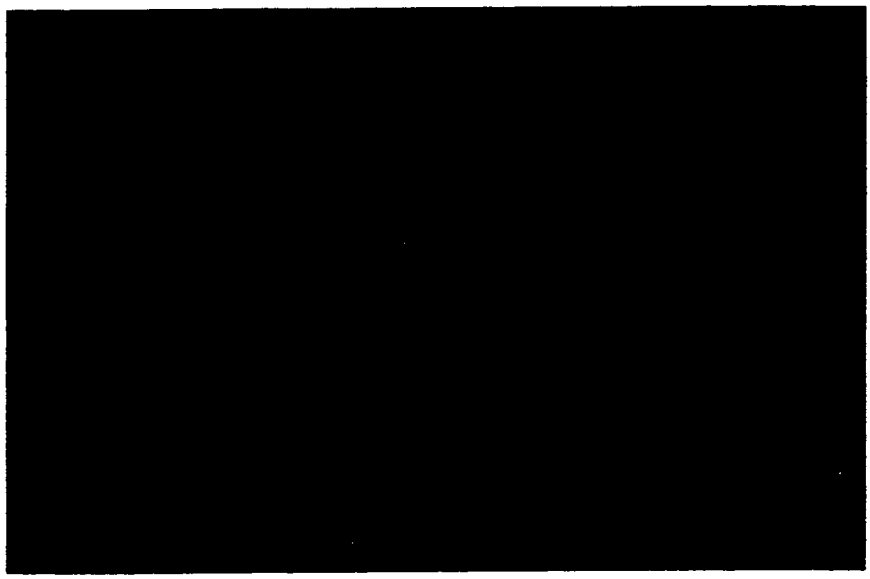

(a)

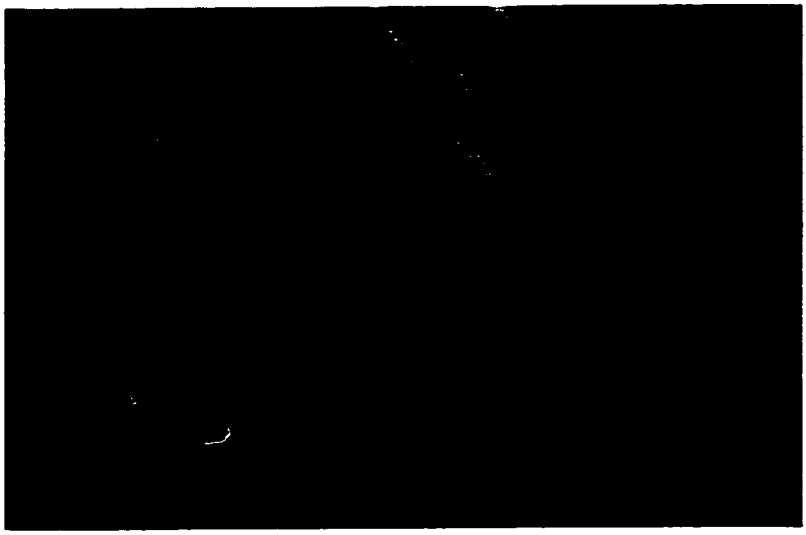

(b)

Figure 5.7. Cross-section of film nucleated at 500° C, showing (a) epilayer GaAs in-phase with substrate, and (b) smooth sidewalls indicative of low APD density. Substrate is (001) GaAs misoriented 4° towards (111)A.

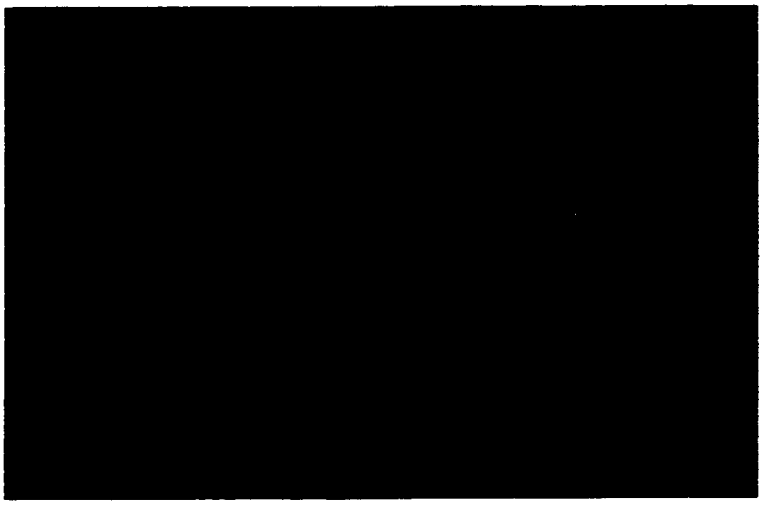

(a)

(b)

Figure 5.8. Cross-section of film nucleated at 400° C, showing (a) poorly defined profile, and (b) high APD density. Substrate is (001) GaAs misoriented 4° towards (111)A.

By simply changing the nucleation temperature, it is possible to grow alternating layers of antiphase and in-phase material on the same substrate. Starting with a substrate misoriented towards (111)B, a thin Ge layer was deposited, followed by 10ML MEE GaAs at 500° C in order to grow antiphase material. After approximately 1 μm of GaAs growth, another Ge layer was deposited, and this time the 10 ML MEE GaAs were deposited at 350°C, because the antiphase material was now misoriented towards (111)A. The structure was then capped with 1 μm of GaAs. Photographs illustrating this double phase reversal are shown in Figure 5.9. Although such a structure might be useful for surface-emitting nonlinar optical devices, it cannot be used for normal-incidence interactions due to the symmetry of the $\chi^{(2)}_{xyz}$ tensor; however it does clearly illustrates the control over the GaAs phase for growth on a Ge surface.[17]

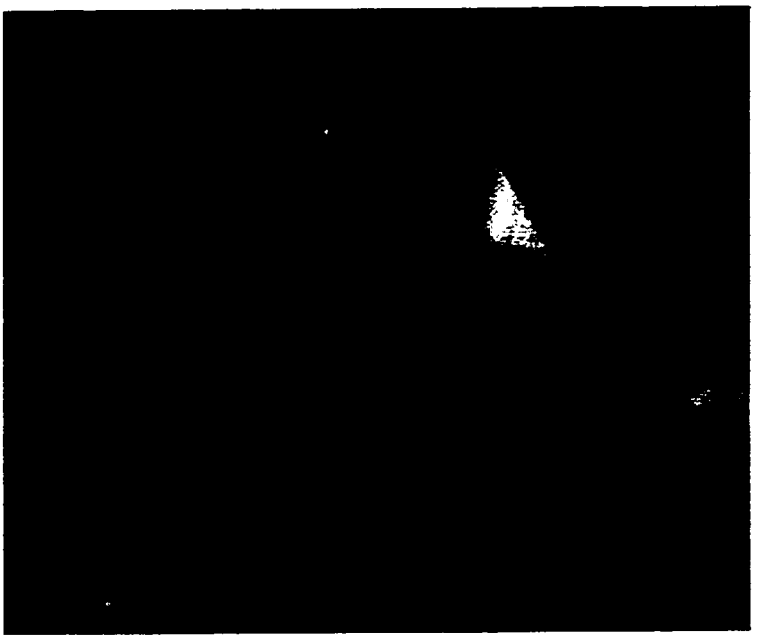

(a)

(b)

Figure 5.9. Cross-section views of samples containing layers of alternating phase. (a) is in the in-plane [110] direction, and (b) is in the in-plane [1-10] direction. Substrate is (001) GaAs misoriented 4° towards (111)B.

Although our studies had shown a tendency of thin Ge layers to roughen during a high temperature anneal in the absence of a stabilizing As flux, the results of Sieg et al. were obtained by annealing without an As flux. Furthermore, an As flux had been reported to significantly change the nature of the Ge surface, making direct comparison of our results impossible with those of the other researchers.[54] Consequently, we decided to attempt growth on samples annealed in the absence of an As flux to see if high quality material could still be obtained, and if the same temperature dependences were observed. For growths with an As flux, the As valve and shutter were left open after the 640° C anneal had ended and until the substrate stabilized at the nucleation temperature. The valve and shutter were then closed and the first Ga layer of the 10 MEE cycles was deposited. For samples annealed without an As flux, the first layer in the MEE cycle could be chosen to be either Ga or As, since the As valve and shutter were closed for approximately 40

minutes for the Ge growth and anneal. Four samples were grown without an As flux during the high temperature anneal (all on substrates misoriented towards (111)A): 1) Ga prelayer and 10 ML MEE GaAs at 350° C, 2) Ga prelayer and 10 ML MEE GaAs at 500° C, 3) As prelayer and 10 ML MEE GaAs at 350° C, and 4) As prelayer and 10ML MEE GaAs at 500° C.

For samples with a Ga prelayer, nucleation at both 350° C and 500° C resulted in epilayers which were in-phase with the substrate. It should be noted, however, that the film nucleated at 500° C had a high density of large APDs, as evidenced by preferential etching. Films nucleated with an As prelayer showed similar behavior to those annealed with As: 350° C nucleation resulted in growth misoriented towards (111)B, and 500° C nucleation resulted in growth misoriented towards (111)A.

Substrate Misorientation	As during Anneal?	Nucleation Temperature (C)	Prelayer	Phase
4° -> (111)A	Yes	350	---	-> (111)B (antiphase)
4° -> (111)B	Yes	350	---	-> (111)B (in phase)
4° -> (111)A	Yes	397	---	mixed
4° -> (111)A	Yes	500	---	-> (111)A (in phase)
4° -> (111)B	Yes	500	---	-> (111)A (antiphase)
4° -> (111)A	No	350	Ga	-> (111)A (in phase)
4° -> (111)A	No	500	Ga	-> (111)A (in phase)
4° -> (111)A	No	350	As	-> (111)B (antiphase)
4° -> (111)A	No	500	As	-> (111)A (in phase)

Table 1. Growth conditions for various samples grown for antiphase growth studies.

5.4 DISCUSSION OF ANTIPHASE GROWTH

The temperature-dependence of the phase of GaAs growth on Ge has been observed and reported before while other researchers have observed a dependence on either prelayer type (As vs. Ga) or As species (As_2 vs. As_4). Li et al. explained this phenomenon

through competing mechanisms of terrace-dominated vs. step dominated nucleation.[57] Nucleation occurs on both the steps and terraces simultaneously, but with competing domains. For high temperature growth (or large misorientation angle) the step-nucleated islands have time to coalesce, thus resulting in single-domain material. For lower temperatures (or smaller misorientation angle) the step-nucleated islands and terrace-nucleated islands do not have time to coalesce, thus the terrace-nuclei overgrow the step-nuclei, resulting in single-domain material that is of opposite phase compared to that of the high temperature scenario. It should be noted that the second case always results in a nonzero APD density, while the first case can theoretically result in completely APD-free growth. According to their definitions, GaAs-B (with its [1-10] direction parallel to the steps) nucleates at low temperature, while GaAs-A (with its [1-10] direction perpendicular to the steps) is the high temperature phase. The GaAs-A phase nucleates at the steps edges due to the combination of Ge surface dimers running parallel to the step edges and an As layer used to initiate growth. GaAs-B nucleates on the terraces, following Kroemer's model for Ga-dominated growth while maintaining electric neutrality at the interface.[51, 57] Our results are in direct contrast with those presented by Li et al., since we observe GaAs-A to be the low-temperature phase and GaAs-B to be the high-temperature phase. The use of MOCVD with its high H_2 concentration, as opposed to MBE, may explain this apparent contradiction, due to the different nature of the Ga precursors and temperature regimes of these two processes.

The effect, if any, of As during the 640° C anneal of the Ge surface is harder to ascertain. Since the two samples grown with As prelayers behaved identically to those grown with As during the anneal, the only effect of the anneal might be to insure an As prelayer. In contrast, the samples with Ga prelayers do not show the same temperature dependence as the other samples, with both the 350° C nucleation and the 500° C nucleation samples having the same phase. Two possible explanations can be proposed. One possibility is that in the absence of an As monolayer, the Ga mobility is high enough even at 350° C that the sample is growing in the step-nuclei regime instead of the terrace-nuclei. For either the As anneal or the As prelayer sample, there is enough As around to reduce the Ga mobility enough so that the terrace nuclei dominate. An alternative explanation would also assume that the high temperature (500° C) growths grow in the step-nuclei regime, due to the greater Ga mobility at that temperature. The difference between the low temperature

(350° C) Ga and As prelayer samples would be due to the difference of the prelayer itself, as would be expected for a perfectly flat or double-stepped surface.

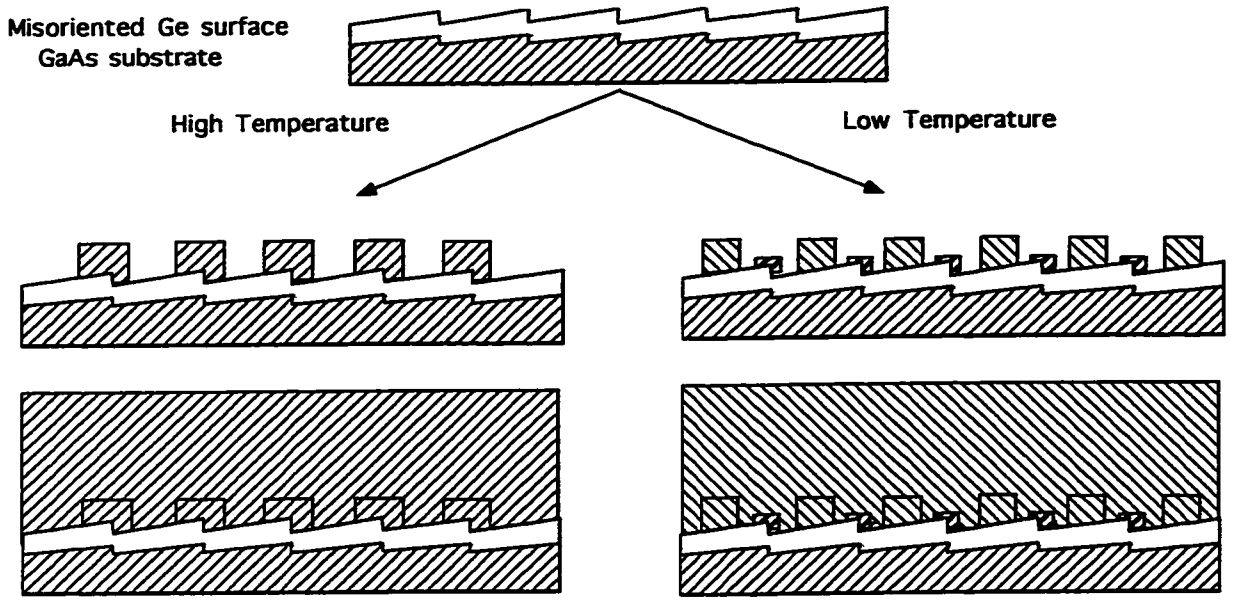

Figure 5.10. Step- vs. Terrace-nucleation model proposed by Li et. al to explain temperature dependence of phase.[57]

5.5 CONCLUSION

Through the above studies, we were able to determine the proper conditions for APD-free growth of material suitable for template formation. Two important conclusions were established that were necessary in order to fabricate orientation-patterned GaAs samples. First, it was learned that through the proper combination of substrate misorientation and nucleation temperature antiphase GaAs could be realiably grown on thin Ge interlayers. Second, it was determined that the phase is established by as little as 10 ML of growth on the Ge interlayer. Although a finite number of APDs may exist, they eventually grow out and the desired phase will dominate. Using this second piece of

knowledge, suitable templates could be designed using thin antiphase GaAs epilayers, instead of growing for several thousand Angstroms to insure APD-free films.

6. GROWTH OF ORIENTATION-PATTERNED WAVEGUIDES AND NONLINEAR OPTICAL RESULTS

Once the growth of APD-free, antiphase GaAs was well studied and understood, the next step was to fabricate actual oreintation-patterned GaAs waveguide structures designed to quasiphasematch a specific nonlinear optical interaction. To do this, a template structure had to be developed that would allow for alternating regions of opposite phase to be exposed for regrowth. Next, these templates were used as substrates for the subsequent growth of a waveguiding structure.

Channel waveguides were then defined on these structures for the optical experiments. In order to characterize the waveguides, second harmonic generation measurements were made in order to determine the phase matching peaks. In addition, various loss mechanisms will be discussed.

6.1 TEMPLATE GROWTH

A template optimized for regrowth should have a minimal (or no) corrugation, leave surfaces suitable for epitaxial regrowth, and involve a minimum of processing. Properly preparing the surface for regrowth and maintaining a minimal corrugation are often two contradictory goals, since traditional surface preparation techniques usually rely on backetching significant amounts of material, typically on the order of microns, in order to achieve a good surface.[40] Consequently, any initial corrugation on the order of several hundred Angstroms would be completely eliminated by such a step. In order to reproducibly fabricate a corrugation of known depth, it was decided to use a pair of AlGaAs etch stop layers, combined with selective etching, in order to selectively expose alternating phases of GaAs. Because initial results had indicated antiphase growth was only possible on wafers misoriented towards (111)B, these substrates were used for the growth of all template wafers due to a greater supply, even though subsequent investigation led to the possibility of using substrates misoriented towards (111)A as templates.

6.1.1 Buffer Layer Studies

Early on during the growth experiments, it was noticed that epilayers grown on wafers misoriented towards (111)B had a cloudy or hazy final appearance, while the same structure grown on wafers misoriented towards (111)A would appear specular and mirror-like. This was due to the different nature of the growth mechanisms occuring on the two misorientations, as discussed earlier. For substrates misoriented towards (111)A, Ga bonds are left dangling, while substrates misoriented towards (111)B have As dangling bonds. Arsenic dangling bonds are more reactive, leading to finger-like growth projections. In contrast, step-flow growth occurs more readily for substrates misoriented towards (111)A, resulting in a smoother surface. Since the mechanisms for APD-free growth rely on a controllably-stepped surface, the roughening that occurs during growth on surfaces misoriented towards (111)B is extremely detrimental since it results in steps of varying types. In order to grow antiphase material on substrates misoriented towards (111)B, it was necessary to overcome this problem, and several different buffer layer designs were investigated.

The first attempts focussed on depositing approximately 500 Å of GaAs by MEE in hopes of smoothing out the growth surface. In order for a lift-off technique to be viable, a buffer layer of only a few hundred Angstroms would have to suffice. Unfortunately, these thin MEE buffer layers were inadequate, resulting in the same hazy or cloudy appearance. Next a buffer layer consisting of a GaAs/AlAs superlattice was employed, approximately 1 μm thick. AlAs/GaAs interfaces have a tendency to getter impurities, specifically oxygen, and it was hoped this would lead to a smoother growth front.[40] This was indeed the case, and this buffer layer was employed for subsequent growths of template structures on substrates misoriented towards (111)B. This buffer layer was also employed during the regrowth of the waveguide structures, for the same reasons.

6.1.2 Template Design

A typical template consisted of the following structure (Figure 6.1):

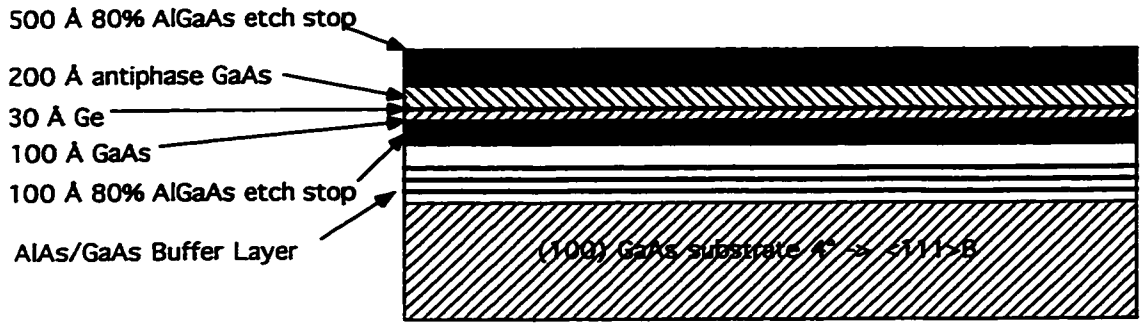

Figure 6.1. Schematic of template structure used for patterned regrowth.

The 1 μm buffer layer consisted of a 50Å AlAs/ 450Å GaAs superlattice (with three 500 Å AlAs marker layers inserted to help with SEM analysis). Since the substrate was misoriented 4° towards (111)B, the 200 Å GaAs layer on top of the Ge was deposited at 500° C, in order to achieve growth antiphase to the substrate. The 80% AlGaAs layers served as etch stops in order to selectively expose regions of alternating phase, as explained in the next section.

6.2 TEMPLATE PATTERNING AND REGROWTH PREPARATION

The templates were then lithographically patterned with the desired gratings, in order to quasi-phasematch the particular interaction of interest for that sample. A mask with several different grating lengths was used, in order to ensure the waveguide was phasematched in the available pump band. Typically the entire template wafer would go through the lithography step as one piece, after which it was quartered. One quarter was often used for calibration samples in order to accurately measure etch times, while the other three were processed for regrowth. Either whole, half, or quarter wafers were ideal for regrowth, as these shapes could easily be accomodated in our substrate holders by changing the inserts.

The use of selective etching and etch stop layers allowed for the reproducible fabrication of a specific, known, corrugation depth. A 1:1 HCl:H_2O mixture was used to selectively etch only the 80% AlGaAs layers, and to stop on the GaAs layers.

A mixture of 4:1 citric acid:H_2O_2 was then used to etch through GaAs and Ge layers, while stopping on the AlGaAs layers. Using these techniques, the depth of the corrugation was determined by the placement and thickness of the various layers.

The template was prepared for regrowth through the following steps (Figure 6.2):

1. Lithographically define the desired grating patterns on the substrate, using conventional techniques.

2. Pattern top etch stop layer with 1:1 HCl:H_20 (typically 30-45 s etching time), followed by a 5 minute running DI rinse.

2. Strip photoresist, 3-solvent clean (hot degreaser, acetone, and hot isopropanol), and O_2 plasma clean.

3. Pattern structure down to bottom etch stop layer using 4:1 citric acid:H_2O_2 (1:00 - 1:15 etching time), followed by a 10 minute running DI rinse.

4. Remove top and bottom etch stops simultaneously with 1:1 HCl:H_20 (1:00 etching time), followed by a 10 minute running DI rinse.

5. Blow dry and load into machine.

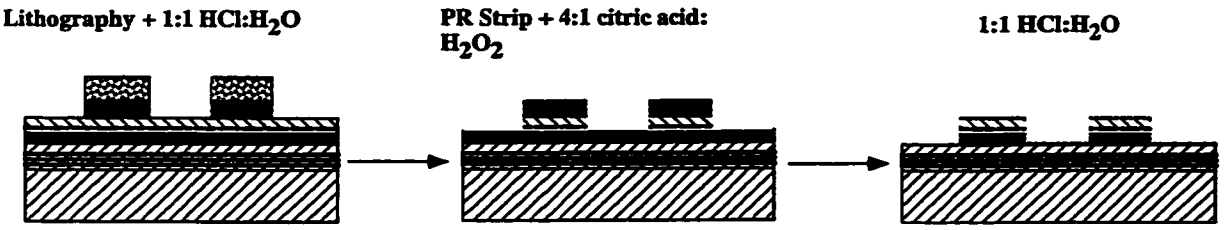

Figure 6.2. Etch sequence used to pattern templates.

Once again, the parameter space of variables to be investigated was quite large: etch stop thicknesses, etching times, final cleaning procedure, etc. Test samples were typically etched and measured with a profilometer in order to determine etching times. Equally important, however, was observing the color changes of the sample as the etch goes through the different layers, as this could be used to adjust the etching times as necessary on the larger pieces. Due to thin layers used, and the index contrast between GaAs and AlGaAs, these changes were quite noticeable as the sample color changed from dark blue to green to pink through the various processing steps. It was observed that it was necessary to overetch with the 1:1 $HCl:H_2O$ mixture on the last step in order to assure good quality material in the subsequent MBE regrowth. In general, all of the steps were overetched in order to ensure complete removal of the layer. Unfortunately, this leads to noticeable lateral etching, which decreased the duty cycle of the grating from the ideal 50%.

The above template structure (Figure 6.1) is not ideal, as it leaves a residual corrugation of over 400 Å. This could be reduced by decreasing the thickness of the layers, however some finite corrugation would still remain. This structure was chosen because of the well-characterized selective etching processes that could be employed using AlGaAs etch stop layers, and the ready availability of the necessary selective etches. In addition, the final HCl-based etch leaves a nice surface for regrowth, devoid of any oxide, after removing simultaneously the top and bottom etch stop layers. Thus, both regrowth surfaces remained protected from contamination until the final step. Logistically, the use of only two etches (and three total etching steps) simplified the process so the whole procedure could be done quickly to minimize any contamination before the wafer was reloaded into the MBE chambers.

6.2.1 Alternative Template Designs

As mentioned, the current template structure could be improved. Another, perhaps better, possibility would be to use a lift-off technique. For example, a dielectric layer is deposited on a misoriented substrate. The dielectric layer is then patterned with the appropriate grating periods, and the substrate is backetched to a depth of 500 - 1000 Å. After the appropriate cleaning, the wafer is loaded into the MBE system, where the appropriate buffer layer/Ge/antiphase GaAs structure can be grown on the exposed regions, with the dielectric layer serving as a growth mask. The sample is then removed from the

machine and the dielectric layer lifted off, exposing alternating regions of antiphase and substrate-phase material. The desired waveguide structure can then be grown on the template. Ideally, the thickness of the buffer layer/Ge/antiphase GaAs structure will be equal to the depth of the backetching, so that no corrugation should result in the final template.

6.3 REGROWTH

Once the template was patterned and reloaded into the MBE machine, it was necessary to find a set of growth conditions that resulted in high quality material suitable for waveguide devices. Issues to be considered include the quality of the surface after etching and regrowth preparation, growth on a corrugated sample, and the simultaneous growth on surfaces misoriented towards both (111)A and (111)B.

RHEED examination of the processed template, once inside the UHV growth chamber, showed little evidence of any oxide on the surface. Even so, the samples were annealed for 10 minutes at 700° C, under an As_2 flux, in order to remove any traces of oxide before growth. In an attempt to smooth out any initial corrugation and also to inhibit any Ge diffusion, the first 500 Å of the regrowth were deposited via the MEE technique. Due to the increased Ga mobility, it was expected that the longer migration length would facilitate the filling in and smoothing out of the initial corrugation from the template. It was also necessary to remember that growth was occuring on surfaces misoriented towards both (111)A and (111)B simultaneously. As mentioned earlier, growth on surfaces misoriented towards (111)A is generally preferred, as the dangling bonds and step structure generally promote the step-flow regime of growth, in contrast to the finger-like growth found on substrates misoriented towards (111)B. Just as it was found necessary to grow an AlAs/GaAs superlattice buffer layer for the template growth, the same buffer layer structure was also employed during the waveguide regrowth and once again gave similar improvement. In both cases, this is probably in part due to the tendency of GaAs/AlAs superlattice to pin impurities and other crystal defects at the interfaces .

6.4 PHASE-BOUNDARY PROPAGATION

In order for successful devices to be realized, it was crucial that the intentionally formed antiphase boundaries (induced by the template) propagated vertically during subsequent growth of thicker layers. In other words, it was necessary for them to propagate along a vertical [110] direction. Other researchers, especially those utilizing MOCVD growth, had observed a tendency of the APD boundaries to propagate along {011} planes at a 45° angle to the (001) surface.[58] This would result in the domains closing over, which would nullify the desired QPM effects of such a structure. MBE growth, however, is much more kinetically driven than MOCVD growth, so the situation could indeed be quite different. Figure 6.3 shows a cross-section of an orientation-patterned film grown via MOCVD (using a wafer-bonded template), where closure of the domains can be seen.[32]

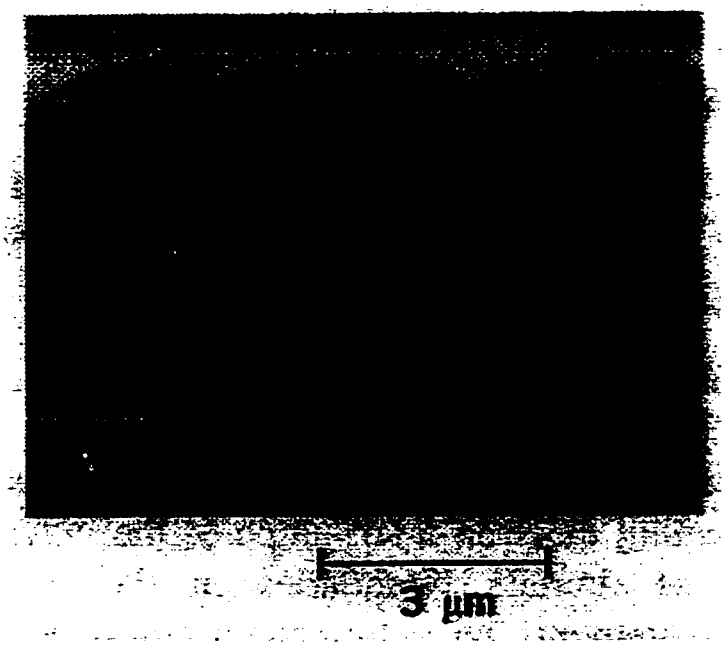

Figure 6.3. Cross-section of orientation-patterned GaAs film grown via MOCVD using a wafer-bonded template. Note the tendency of the domain boundaries to wander.[32]

On some of the first samples, thick (2-3 μm) GaAs layers were grown for characterization purposes, instead of AlGaAs waveguide structures. Stripes were than patterned perpendicular to the gratings, and the samples etched in the 1:1:6 $NH_4OH:H_2O_2:H_2O$ preferential etchant. Since regions of different domains should etch differently - with alternating slanted and undercut sidewalls (Figure 6.4), it was quite clear that indeed the template orientation was preserved on the surface, even after 2-3 μm of growth, and that the vertical propagation lines (as seen in Figure 6.6) were not due to any residual effects from a corrugation.

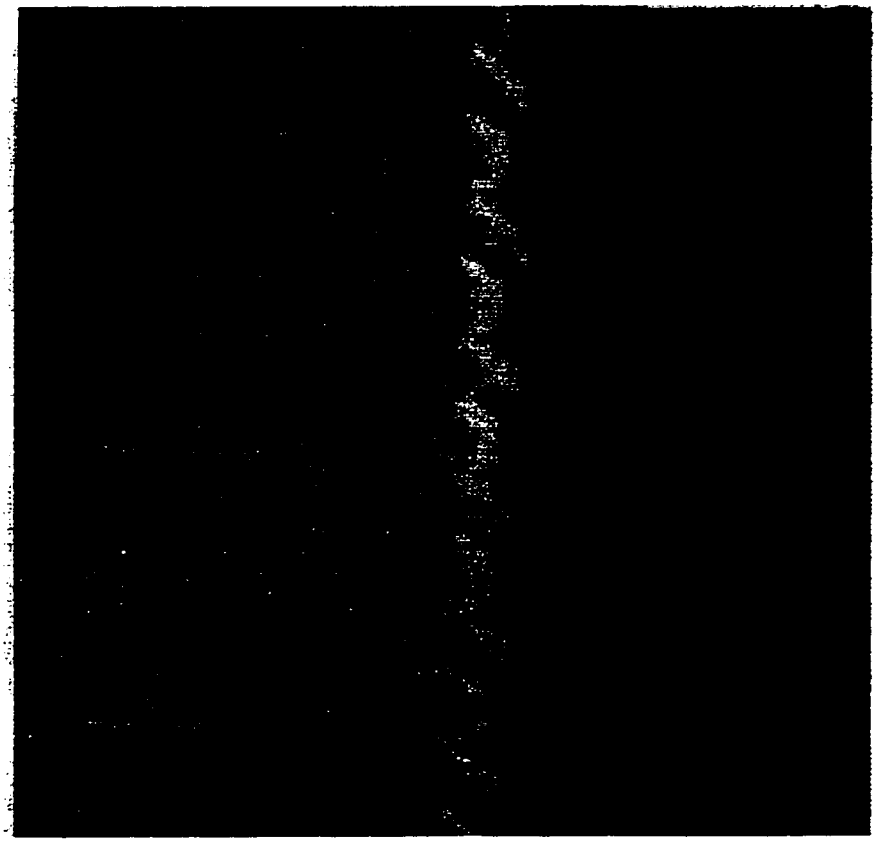

Figure 6.4. SEM micrograph of anisotropically etched orientation-patterned GaAs film, showing alternating regions of slanted and undercut sidewalls.

6.5 WAVEGUIDE GROWTH

Once it was demonstrated that the domains were propagating in the desire manner, waveguide structures were then grown using the patterned templates. For SHG of 775 nm light from a 1550 nm pump (and hence also DFG of 775 nm and 1550 nm light), the structure consited of 500 Å GaAs MEE (for smoothing purposes), 1 μm AlAs/GaAs buffer layer (to pin impurities and defects), followed by 2 μm of 60% AlGaAs (lower cladding), 1 μm of 50% AlGaAs (core), and 1 μm of 60% AlGaAs (top cladding) (Figure 6.5).

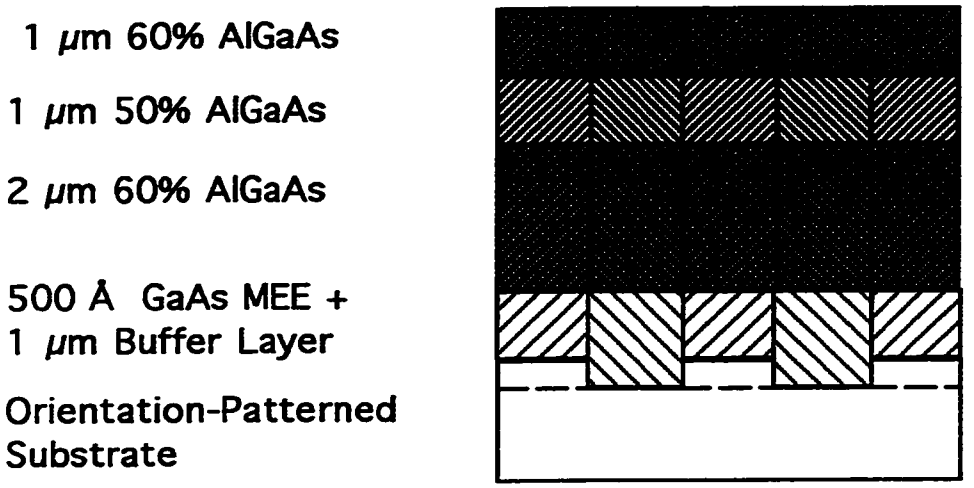

Figure 6.5. Waveguide structure used for SHG of 1550 nm pump.

In order to better examine the propagation of the boundaries during growth, some of the waveguide samples were cleaved perpendicular to the grating, stain etched, and then observed under the SEM (Figure 6.6). The stain etching acts to highlight the AlAs layers, and also brings out the AntiPhase Boundary between the two regions. In order to facilitate observation of the corrugation, 100 Å AlAs marker layers were added between the waveguide core and cladding layers (such thin layers have no appreciable effect on the waveguide modes of IR light). Using this technique, domain aspect ratios of 10:1 (0.5 um domains propagating 5 um high) were observed to propagate vertically. In addition, the

evolution of the corrugation can be seen, especially its impact on the core/cladding interfaces.

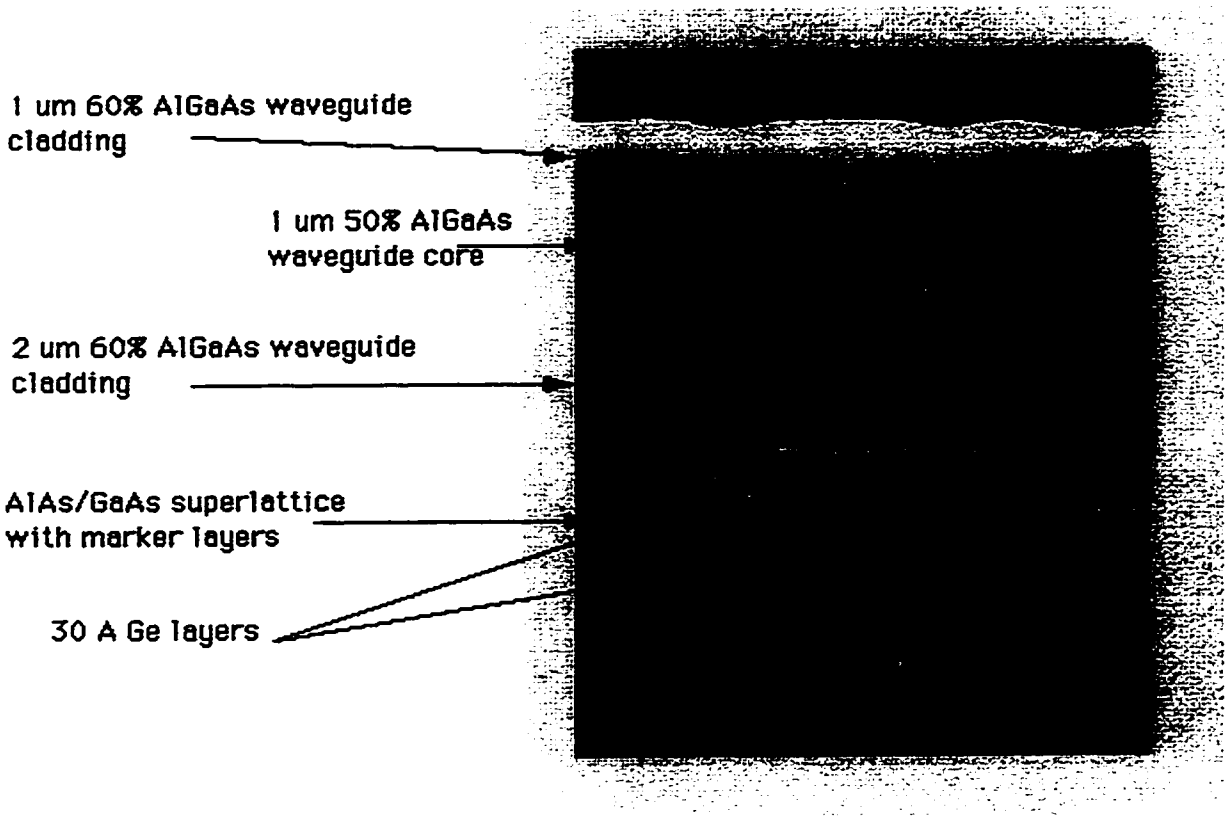

Figure 6.6. Cross section SEM micrograph of orientation-patterned GaAs film, stain-etched to highlight APBs.

These pictures also provided invaluable feedback concerning the template fabrication procedure. It can be seen that the final duty cycles of the patterned material are significantly less than the ideal 50%. This was due to overetching the top AlGaAs etch stop during template fabrication. It was observed that in order to get a clear, smooth surface, longer etch times in 1:1 HCl:H_2O were desirable. Etching times of approximately 45 s - 1 min. were used, although the first etch stop cleared (marked by a noticeable change in color of the template) in only about 10 seconds. As a result of the long etch time, the photoresist pattern was undercut, resulting in a duty cycle of less than 50%. After the

photoresist was stripped, the remaining AlGaAs than acted as the mask for the next etch in the process.

6.6 WAVEGUIDE FABRICATION

After the waveguide structures were grown, the samples were then etched in 80:4:1 HCl: H_2O_2:H_2O, a diffusion-limited etch, to smooth out any roughness introduced during the growth. Total amount of material removed was ~3000 Å. Channel waveguides with widths of 3 μm, 4 μm, 6 μm, 8 μm, 30 μm, and 60 μm were lithographically defined, and the sample was then etched using the same diffusion-limited etch to a depth of 8500 Å, so that the upper cladding was completely removed, along with 1500 Å of the core (see Figure 6.7). This etchant was chosen to reduce sidewall roughness, and hence the associated scatter. In order to reliably cleave the samples in to the appropriate sizes, the substrates were thinned to a few hundred microns first, and then cleaved along (110) facets.

Figure 6.7. Profile of a waveguide fabricated in orientation-patterned GaAs. Alternating phases of GaAs can be seen, despite smoothing etch.

6.7 NONLINEAR OPTICAL MEASUREMENTS

Next, nonlinear optical measurements were performed on selected samples. It is easiest to characterize and identify the phasematching conditions of a sample using second harmonic generation, as only one beam needs to be coupled in, instead of two as for SFG or DFG, and no resonant cavity is required, as for an OPO. In order to determine the phasematching conditions, it was necessary to solve for the waveguide modes and effective index, n_{eff}, at each wavelength, given the waveguide structure that had been fabricated. Once this was done, the phasematching wavelength, assuming a fixed period grating, could be determined, or conversely the necessary phasematching period could be calculated for a given pump wavelength. Any variation in the waveguide growth from the ideal structure, however, would necessarily change the phasematching conditions. To overcome this uncertainty, a tunable pump source was employed in order to help identify the phasematching peak.

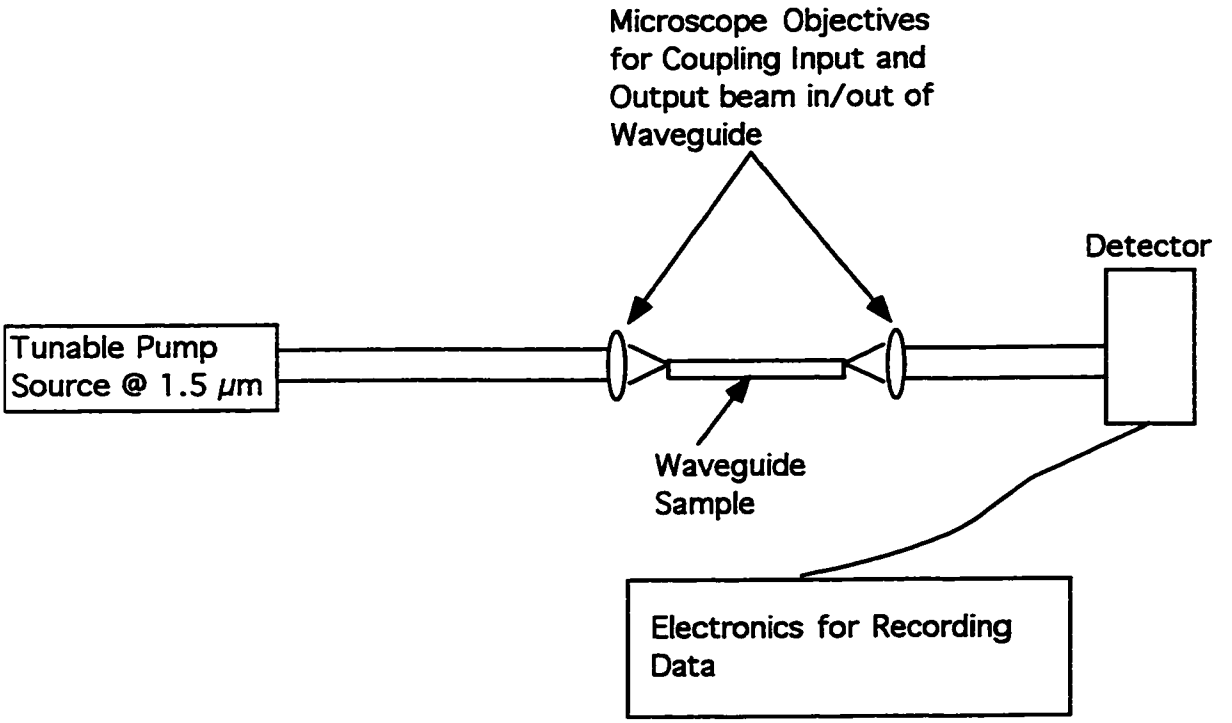

Figure 6.8. Schematic of setup used to measure SHG from patterned waveguide samples.

The pump beam was end-fire coupled into the waveguide through the use of a microscope objective, and collected from the output facet in a similar manner and refocused onto a detector (Figure 6.8). As explained in Chapter 2, the proper input polarization (in this case TE) had to be used in order to successfully generate any second harmonic. The choice of input polarization also had an effect on the phasematching conditions, since the TE and TM modes of the waveguides have slightly different effective indices (i.e. modal birefringence).

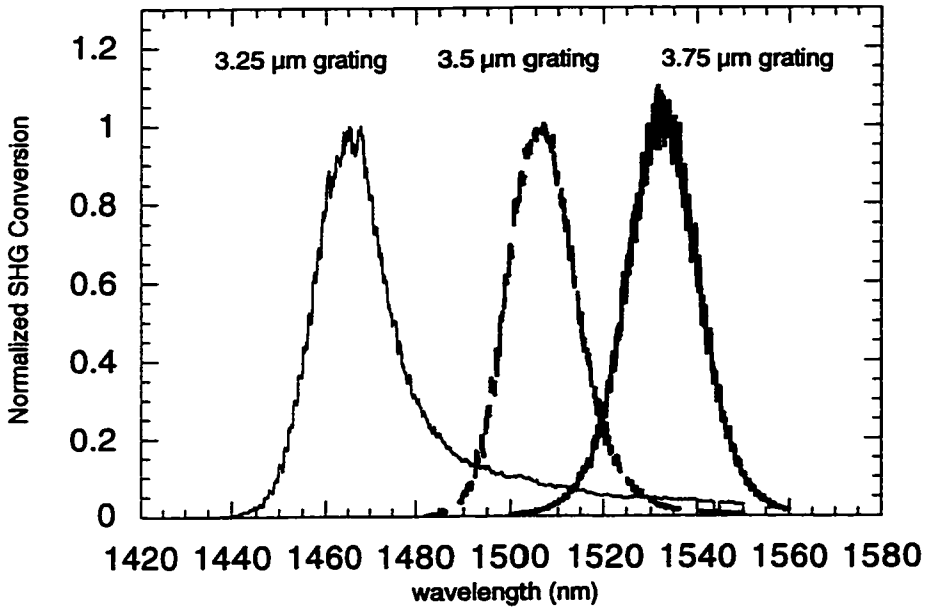

Figure 6.9. SHG Phasematching peaks for three different gratings. Linewidth of ~20nm is set by mode locked source, not gratings.

The curves in Figure 6.9 were taken with a pulsed OPO optimized for ultrafast optics. As a result, the pulses were very short with a linewidth of ~20nm, so this determined the linewidth of the tuning curves. This source was used because its large tuning range allowed for the determination of the phasematching peak for several different

grating periods, whereas the other available source only had enough tuning range to find the peak for one grating period.

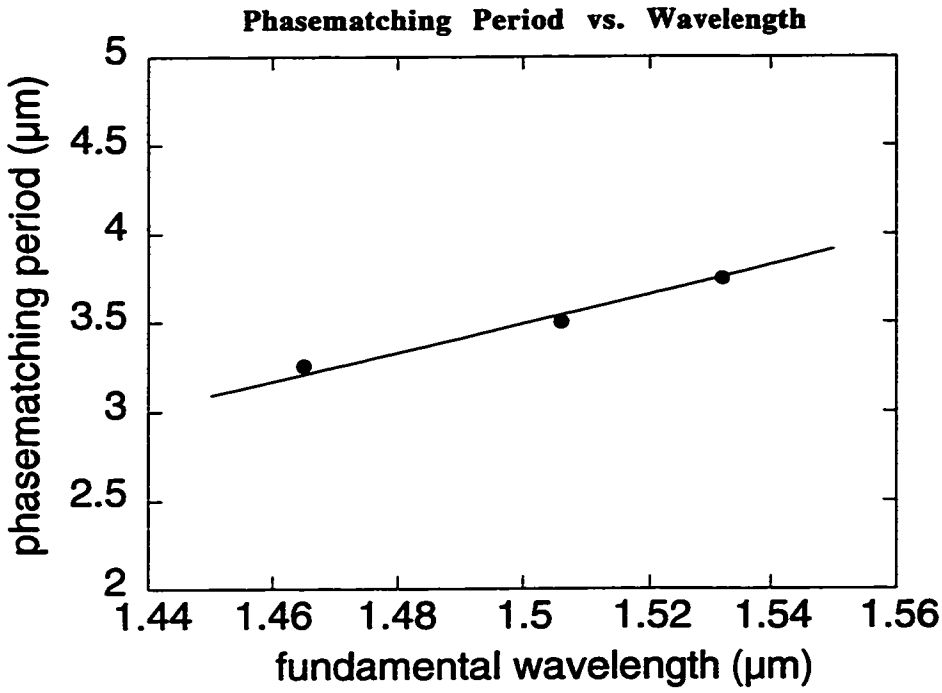

Figure 6.10. Plot showing predicted phasematching period vs. wavelength. Line is calculated values, points are actual data.

Using the phasematching points found above, it was possible to compare the predicted phasematching peak, as a function of wavelength, with the measured values. As Figure 6.10 illustrates, the agreement between experiment and theory are quite good. This confirms many aspects of the waveguide fabrication process, such as the accuracy of the layer thicknesses and the grating periods as defined by lithography.

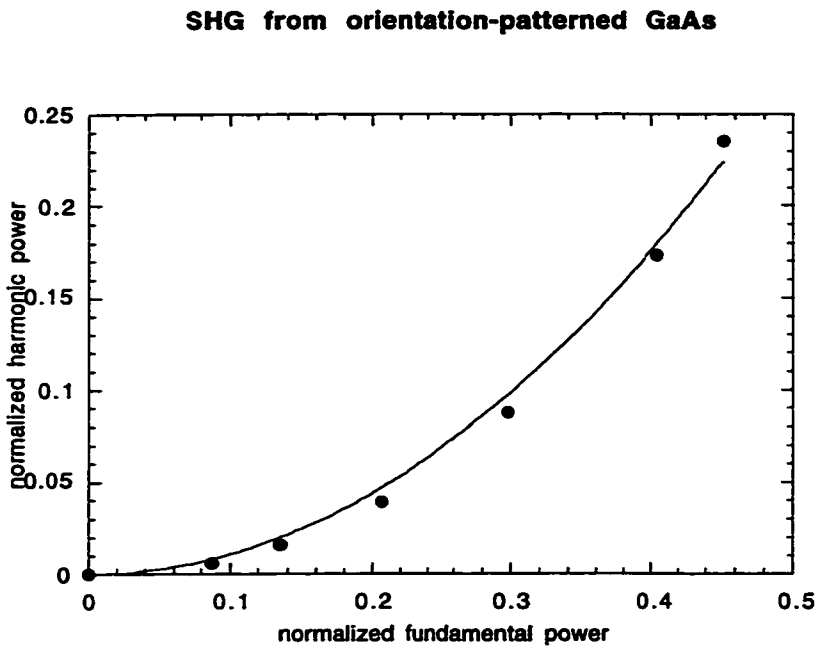

Figure 6.11. Output power vs. Input power for SHG, showing expected parabolic dependence.

Using Eq. 2.12, it can be seen that the second-harmonic intensity should scale quadratically with the input power. This is indeed the case, as seen in Figure 6.11.

6.7.1 Loss Mechanisms in Orientation-Patterned GaAs Waveguides

Although these waveguide did exhibit the desired nonlinear optical properties, namely phasematching at the predicted wavelength, they also exhibited extremely high losses. For any practical device, such as a wavelength mixer or an OPO for the generation of mid-IR light, these losses will have to be significantly reduced in order to maximize the conversion efficiency.

As mentioned several times, the dominant cause of loss in these type of waveguides will be the corrugation. For example, a 200Å corrugation height can lead to losses of 40 db/cm., thus driving the development towards zero-corrugation waveguides.[4]

These scattering losses are worse for the shorter wavelength applications (i.e. 1550nm -- 775 nm mixing) than for mid- to far-IR applications, since the coupling into the long wavelength modes is not as efficient as the coupling into the shorter wavelength modes for the periods and amplitudes typically encountered. [59]

Other potential loss sources include poor material quality of the antiphase material (the GaAs grown over the Ge) or perhaps Ge doping. If half of the domains are doped p-type , high losses could result from high levels of free-carrier absorption. Another possibility is poor quality of the antiphase material, perhaps due to residual APDs propagating upwards from the Ge layer, or from poor surface preparation. Both of these causes have been eliminated, however, by fabricating waveguides only of antiphase material, and comparing their losses to waveguides fabricated of substrate-phase material (since the Ge layer was removed before regrowth in these regions, no subsequent Ge doping could occur during regrowth).

As seen in Figure 6.12, the losses between the two types of waveguides do not show any discernible differences. The losses were measured by ratioing the input power, incident on the waveguide facet, with the power measured exiting the wavguide and corrected for a 3dB loss at the air/semiconductor interface. Figure 6.12 also illustrates the large variation in waveguide losses, even when comparing nominally identical waveguides. This is due to inhomogeneities across the sample which appear after the regrowth but are likely introduced during the processing stage. Because of these variations, though, it is difficult if not impossible to draw meaningful conclusions regarding other sources of loss, as any trends (i.e. loss vs. length, loss vs. number of interfaces) are obscured by the error levels of the data. Unfortunately, the method used does not take into account the coupling efficiency into the waveguide. More sensitive loss measurement echniques, such as Fabry-Perot techniques, provide a more accurate picture of the waveguide losses and will be presented in future work.[60]

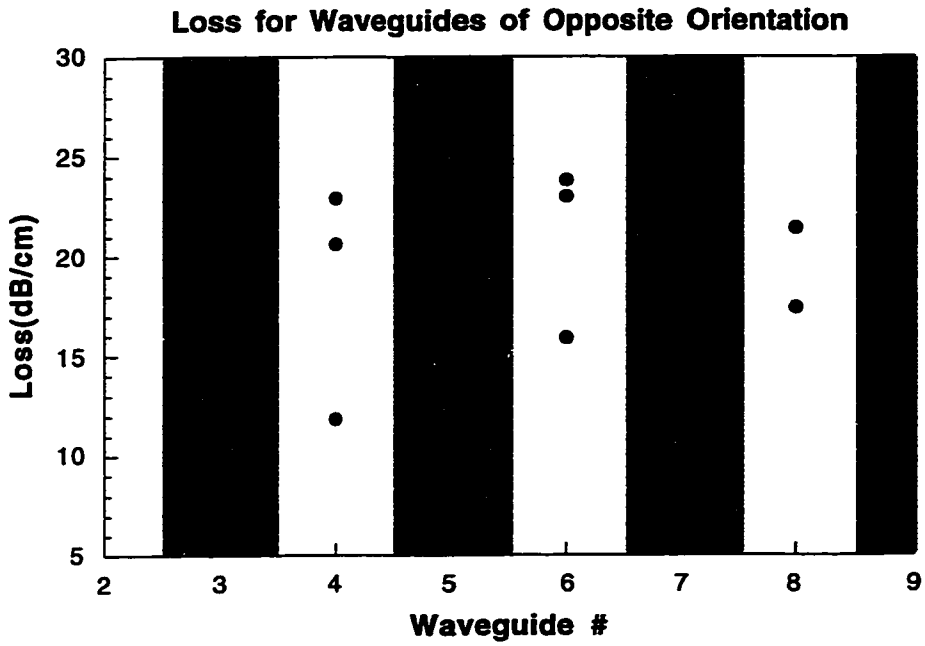

Figure 6.12. Loss (in dB/cm) for waveguides patterned entirely of substrate-phase and antiphase material. Even and odd numbered waveguides are of opposite phases.

6.8 CONCLUSION

Using the knowledge of antiphase growth on GaAs developed earlier, template structures were designed, grown, and patterned. Waveguiding layers were then regrown on these templates, and selective etching and SEM analysis confirmed that the alternating phase orientation of the templates was indeed preserved through the waveguiding layers. The observed aspect ratios and domain dimensions are sufficient to quasi-phasematch any nonlinear interaction within the transparency range of AlGaAs.

After successfully fabricating orientation-patterned GaAs films, several optical experiments were performed to determine both their linear and nonlinear optical properties. Various loss mechanisms were studied in the hopes of determining the major

source of loss so that it could be significantly reduced. Finally, second harmonic generation experiments were performed, confirming that the nonlinear optical output intensity is greatly enhanced by the quasiphasematching. The predicted phasematching values agree well with the those predicted by theory.

7. FUTURE WORK AND CONCLUSION

7.1 FUTURE WORK

Using this thesis as a starting point, there is a wide variety of future work that can be performed. The field of polar-on-nonpolar epitaxy still has many unanswered questions. Although the work here demonstrated it is possible to control the phase of the GaAs grown on Ge, through the nucleation temperature, there are still many theories as to why this is so. Further exploration of the growth conditions, such as anneal, nucleation temperature, and nucleation species, should help to focus on what are the key factors in determining the phase and quality of a GaAs epilayer grown on a Ge film. A thorough understanding of the processes involved may lead to the ability to control the phase on (110)-oriented wafers, thus allowing for the direct epitaxial fabrication of quasi-phasematched structures for normal incidence interactions. In addition, perhaps there are other applications for structures in which phase of the material is important.

For the growth of orientation-patterned films, the area of greatest improvement lies in perfecting a robust template fabrication technique. The use of etch stop layers,while successful, suffered from the difficulty of consistently removing the AlGaAs layers. In addition, the high reactivity of high-percentage AlGaAs also had the tendency to react with the photoresist during patterning, creating another set of problems. In order for the use of dielectric growth masks and lift-off to be successful, a viable way of consistently and cleanly lifting off the mask and polycrystalline deposits, without contaminating the rest of the surface, must be addressed.

Once a template technique is perfected, work can begin on minimizing the corrugation. One potential barrier may be the thickness of antiphase GaAs, on top of the Ge, necessary to successfully 'seed' the growth of the subsequent antiphase regions. Although preferential etching studies indicated the tendency of APDs to propagate upward approximately ~1000Å before finally growing out, it was found a 200Å film was sufficient to seed the growth of the subsequent layers. In fact, the nucleation studies, using MEE, described in Chapter 5 indicate that as few as 10 ML may be all that is necessary. The

minimum thickness, however, that will suffice will also have to survive any processing and regrowth preparation techniques. Finally, the thin antiphase GaAs layer will also need to be stable under any oxide blow-off or other thermal anneals it may be subjected to prior to regrowth. At elevated temperatures a thin film with high APD density might roughen in an attempt to reduce its surface energy. This research will obviously require a detailed understanding of the nucleation process of GaAs on Ge, and why which phases dominate under the conditions they do.

Provided high-quality templates can be reliably fabricated, one logical extension of this work is the use of orientation-patterned templates as substrates for thick-film growths. Provided that material of sufficient quality can be epitaxially grown on a template, GaAs films of 100 μm or greater thickness would provide the opportunity for bulk-like nonlinear optical interactions. This would allow for easier coupling into the material, reducing the difficulty of coupling into thin waveguides with cores only a couple microns thick. In addition, high-power applications could be pursued, where the intensity would exceed the damage threshold for GaAs if tightly confined into a waveguide but would be acceptable in a loosely-focussed beam. Although a minimal-corrugation template is not necessary for such thick-film applications, the all-epitaxial templates still have the advantage of not requiring any specialized wafer-bonding seteup but can intead be leveraged using standard epitaxial techniques and should yield higher quality interfaces. For growing such thick films, one promising technique appears to be Vapor Phase Epitaxy, or VPE, while Close-spaced Vapor Tranport techniques are also an option.[61] Of course, the propagation of the APBs over much greater thicknesses, and under much different growth conditions, will need to studied to determine if the desired aspect ratios can be obtained.

Another logical extension of this work would be to transfer, either in part or in whole, the growth technology to other epitaxial techniques, mainly MOCVD. Because of its high growth rates and *in situ* cleaning capabilities, MOCVD would be ideally suited to the regrowth of the waveguide structures. The higher purity and greater interface control of MBE are not necessary for the growth of mid- to far-IR waveguide structures, and with waveguide thicknesses of 5 μm or greater, material depletion becomes significant. MOCVD, by contrast, has much faster growth rates, almost an infinite supply of material,

and the presence of H_2 and metallo-organics to reduce the surface contamination and etch the surface.[62] The possibilities of MOCVD in the growth of orientation-patterned waveguides could vary widely. At a minimum, regrowth on patterned templates, with the initial Ge/antiphase GaAs layers grown by MBE, should be relatively straightforward, and it is conceivable even the whole process could be done via MOCVD, as the ability to control the phase of GaAs on misoriented (001) Ge substrates with MOCVD has already been demonstrated.[57, 63] One complication would be the tendency of the surfaces with different misorientations (towards (111)A vs. towards (111)B) to exhibit different growth rates, but this can be controlled through the V/III ratio, and also could be utilized to help minimize any corrugation.

7.2 ACCOMPLISHMENTS AND CONCLUSION

The capability to reliably control the phase of GaAs epitaxially grown on a Ge surface was developed, and the effects of such growth parameters as substrate misorientation, nucleation temperature, annealing conditions, and prelayer species was studied. Samples were characterized *in situ* using RHEED and *ex situ* using preferential etching and SEM analysis. Nucleation temperatures of 350° C yielded films that were misoriented towards the (111)B plane, unless a Ga prelayer was used. Films nucleated at 500° C were misoriented towards (111)A, regardless of anneal type and prelayer species. Other researchers, however, have not seen any phase dependence on nucleation temperature, or have seen the opposite behavior, with material misoriented towards (111)A for lower nucleation temperatures and material misoriented towards (111)B for higher nucleation temperatures.[56, 57] More research into the exact mechanisms of phase determination needs to be performed in order to resolve these discrepancies.

Combining this capability to control the GaAs phase with standard semiconductor processing techniques, template structures were grown and fabricated such that alternating phases of GaAs were exposed. Waveguide structures were then regrown on these templates, and further preferential etching and SEM analysis confirm the desired phase patterning (from the template) was maintained throughout the several microns of growth. Furthermore, the phase boundaries were observed to propagate vertically, as is necessary for the proper device performance. The necessary control over domain sizes

was demonstrated in order for this technique to be sufficient to creater quasi-phasematched structures throughout the transparency region of AlGaAs.

Second-harmonic generation of 1.5 μm light has been observed using an orientation-patterned GaAs waveguide grown on a template fabricated through epitaxial techniques. The phasematching peaks for three different grating periods correlate well with the predicted values. Structures designed to phasematch other nonlinear optical interactions of interest can easily be fabricated with the use of masks with the proper period and regrowth of the correct waveguide structure on the template. Using thick-film techniques, bulk-like structures can be fabricated to allow for high-power applications.

8. BIBLIOGRAPHY

1. P.A. Franken, A.E. Hill, C.W. Peters and G. Weinreich, "Generation of Optical Harmonics," *Phys. Rev. Lett.*, **7**, p. 118 (1961).

2. D.H. Chow, R.H. Miles, T.C. Hasenberg, A.R. Kost, Y.-H. Zhang, H.L. Dunlap and L. West, "Mid-wave infrared diode lasers based on GaInSb/InAs," *Appl. Phys. Lett.*, **67**, p. 3700 (1995).

3. H.C. Chui, G.L. Woods, M.M. Fejer, E.L. Martinet and J.S. Harris, "Tunable mid-infrared generation by difference frequency mixing of diode laser wavelengths in intersubband InGaAs/AlAs quantum wells," *Appl. Phys. Lett.*, **66**, p. 265 (1995).

4. S.J.B. Yoo, C. Caneau, R. Bhat, M.A. Koza, A. Rajhel and N. Antoniades, "Wavelength conversion by difference frequency generation in AlGaAs waveguides with periodic domain inversion achieved by wafer bonding," *Appl. Phys. Lett.*, **68**, p. 2609 (1996).

5. G.A. Pasmanik, A.Z. Matveyev, D.G. Peterson, A.A. Shilov and I. Yakovlev, "Nonlinear optical technique for advanced tunable IR lidar," in *Nonlinear Optical Engineering* (SPIE, San Jose, CA, 1998), Vol. 3263, p. 74.

6. G.P. Agrawal and N.K. Dutta, *Semiconductor Lasers* (Van Nostrand Reinhold, New York, 1993).

7. H.K. Choi, G.W. Turner and H.Q. Le, "InAsSb/InAlAs strained quantum-well lasers emitting at 4.5 μm," *Appl. Phys. Lett.*, **66**, p. 3543 (1995).

8. Z. Shi, M. Tackle, A. Lambrecht and H. Böttner, "Midinfrared lead salt multi-quantum-well diode lasers with 282 K operation," *Appl. Phys. Lett.*, **66**, p. 3543 (1995).

9. J. Faist, F. Capasso, D.L. Sivco, A.L. Hutchinson, C. Sirtori, S.N.G. Chu and A.Y. Cho, "Quantum Cascade laser: Temperature dependence of the performance characteristics and high T_0 operation," *Appl. Phys. Lett.*, **65**, p. 2901 (1994).

10. C. Sirtori, J. Faist, F. Capasso, D.L. Sivco, A. L. Hutchinson and A.Y. Cho, "Long Wavelength infrared ($\lambda \equiv 11$ μm) quantum cascade lasers," *Appl. Phys. Lett.*, **69**, p. 2810 (1996).

11. J. Faist, F. Capasso, C. Sirtori, D. L. Sivco, J.N. Baillargeon, A.L. Hutchinson, S.N.G. Chu and A.Y. Cho, "High Power mid-infrared ($\lambda \sim 5$ μm) quantum cascade lasers operating above room temperature," *Appl. Phys. Lett.*, **68**, p. 3680 (1996).

12. J. Faist, C. Gmachl, F. Capasso, C. Sirtori, D. L. Sivco, J.N. Baillargeon and A.Y. Cho, "Distributed Feedback quantum cascade lasers," *Appl. Phys. Lett.*, **70**, p. 3680 (1997).

13. W.R. Bosenberg, A. Drobshoff, J.I. Alexander, L.E. Myers and R.L. Byer, "93% pump depletion, 3.5-W continuous-wave, singly resonant optical parametric oscillator," *Opt. Lett.*, **21**, p. 1336 (1996).

14. Y.R. Shen, *The Principles of Nonlinear Optics* (Wiley, New York, 1984).

15. T.H. Maiman, "Stimulated Optical Radiation in Ruby," *Nature*, **187**, p. 493 (1960).

16. A. Yariv, *Quantum Electronics, 3rd. edition* (John Wiley and Sons, New York, 1989).

17. R. Lodenkamper, "Surface Emitting Second Harmonic Generation: Vertical Resonance and Theory of Efficiency," Ph.D. thesis, Stanford University, 1995.

18. R. W. Boyd, *Nonlinear Optics* (Academic Press, Boston, 1992).

19. E. Lim, "Quasi-Phasematching for Guided-Wave Nonlinear Optics in Lithium Niobate," Ph.D. thesis, Stanford University, 1992.

20. J.A. Armstrong, N. Bloembergen, J. Ducuing and P.S. Pershan, "Interactions between light waves in a nonlinear dielectric," *Phys. Rev.*, **127**, p. 1918 (1962).

21. P.A. Franken and J.F. Ward, "Optical harmonics and nonlinear phenomena," *Rev. Mod. Phys.*, **35**, p. 23 (1963).

22. M.M. Fejer, G.A. Magel, D.H. Jundt and R. L. Byer, "Quasi-phase-matched second harmonic generation: tuning and tolerances," *IEEE J. Quant. Elect.*, **28**, p. 2631 (1992).

23. G.D. Miller, R.G. Batchko, W.M. Tulloch, D.R. Weise, M.M. Fejer and R.L. Byer, "42%-efficient single-pass cw second-harmonic generation in periodically poled lithium niobate," *Opt. Lett.*, p. 1834 (1997).

24. B. Sung, "Quantum Well Above-Barrier States and Short Wavelength Intersubband Transitions in InGaAs/AlGaAs Quantum Wells," Ph.D. thesis, Stanford, 1998.

25. G.L. Woods, "Nonlinear Optical Frequency Conversion Devices Based On Intersubband Transitions in Semiconductor Quantum Wells," Ph.D. thesis, Stanford University, 1997.

26. J.P. van der Ziel, "Phase-matched harmonic generation in a laminar structure with wave propagation in the plane of the layers," *Appl. Phys. Lett.*, **26**, p. 60 (1975).

27. A. Fiore, V. Berger, E. Rosencher, P. Bravetti, N. Laurent and J. Nagle, "Phase-matched mid-infrared difference frequency generation in GaAs-based waveguides," *Appl. Phys. Lett.*, **71**, p. 3622 (1997).

28. L. Gordon, G.L. Woods, R.C. Eckardt, R.R. Route, R.S. Feigelson, M.M. Fejer and R.L. Byer, "Diffusion-bonded stacked GaAs for quasi-phase-matched second-harmonic generation of a carbon dioxide laser," *Elect. Lett.*, **29**, p. 1942 (1993).

29. D. Zheng, "Tunable Infrared Generation with Diffusion-Bonded-Stacked Gallium Arsenide," Ph.D. thesis, Stanford University, 1998.

30. Y.S. Wu, R.S. Feigelson, R.K. Route, D. Zheng, L.A. Gordon, M.M. Fejer and R.L Byer, "Improved GaAs Bonding Process for Quasi-Phase-Matched Second Harmonic Generation," *J. Electrochem. Soc.*, **145**, p. 366 (1998).

31. L. A. Eyres, C. B. Ebert, Jr. J. S. Harris, M. M. Fejer and H. C. Chui, "Fabrication of GaAs Orientation Template Substrates for Quasi-Phasematched Guided-Wave Nonlinear Optics," in *Nonlinear Guided Waves and Their Applications* (Optical Society of America, Dana Point, 1995), Vol. 6, 1995 OSA Technical Digest Series, p. 156.

32. S.J.B. Yoo, R. Bhat, C. Caneau and M.A. Koza, "Quasi-phase-matched second-harmonic generation in AlGaAs waveguides with periodic domain inversion achieved by wafer bonding," *Appl. Phys. Lett.*, **66**, p. 3410 (1995).

33. H. Nelson, "Epitaxial Growth from the liquid state and its applications to the fabrication of tunnel and laser diodes," *RCA Rev.*, **24**, p. 603 (1963).

34. D.W. Shaw, "Kinetics of transport and epitaxial growth of GaAs with a Ga-$AsCl_3$ system," *J. Cryst. Growth*, **8**, p. 117 (1971).

35. H.M. Manasevit and W.I. Simpson, "The use of metal-organics in the preparation of semiconductor materials. 1: Epitaxial gallium-V compounds," *J. Electrochem. Soc.*, **116**, p. 1725 (1969).

36. D.G. Schlom, "Molecular Beam Epitaxial Growth of Cuprate Superconductors and Related Phases," Ph.D. thesis, Stanford, 1990.

37. S.M. Koch, "Studies of the Nucleation and Growth of Gallium Arsenide on Silicon by Molecular Beam Epitaxy," Ph.D. thesis, Stanford, 1988.

38. R.A. Kubiak, S.M. Newstead and P. Sullivan, "The Technology and Design of Molecular Beam Epitaxy Systems," in *Molecular Beam Epitaxy: Applications to Key Materials*, edited by R. F. C. Farrow (Noyes Publications, Park Ridge, N.J., 1995), p. 1.

39. J.P.A. van der Wagt, "Reflection High-Energy Electron Diffraction During Molecular-Beam Epitaxy," Ph.D. thesis, Stanford University, 1994.

40. E.C. Larkins and J.S. Harris, "Molecular Beam Epitaxy of High-Quality GaAs and AlGaAs," in *Molecular Beam Epitaxy: Applications to Key Materials*, edited by R. F. C. Farrow (Noyes Publications, Park Ridge, N.J., 1995), p. 114.

41. M.A. Herman and H. Sitter, *Molecular Beam Epitaxy: Fundamentals and Current Status* (Springer, Berlin, 1996).

42. M. Kawashima, T. Saku and Y. Horikoshi, "Characteristics of AlGaAs/GaAs heterostructures grown by migration-enhanced epitaxy at high temperatures," *Semicond. Sci. Technol.*, **10**, p. 1237 (1995).

43. Y. Horikoshi, "Migration-enhanced epitaxy of GaAs and AlGaAs," *Semicond. Sci. Technol.*, **8**, p. 1032 (1993).

44. P.I. Cohen, G.S. Petrich and G.J. Whaley, "Reflection High Energy Electron Diffraction Studies of the Dynamics of Molecular Beam Epitaxy," in *Molecular Beam Epitaxy: Applications to Key Materials*, edited by R. F. C. Farrow (Noyes Publications, Park Ridge, N.J., 1995), p. 669.

45. D.J. Miller and J.S. Harris, "50nm GaAs/AlAs structures grown on corrugated GaAs," *JVST B*, **12**, p. 1286 (1994).

46. R. Fischer, W.T. Masselink, J. Klem, T. Henderson, T.C. McGlinn, M.V. Klein and H. Morkoç, "Growth and properties of GaAs/AlGaAs on nonpolar substrates using molecular beam epitaxy," *J. Appl. Phys.*, **58**, p. 374 (1985).

47. S.L. Wright, H. Kroemer and M. Inada, "Molecular beam epitaxial growth of GaP on Si," *J. Appl. Phys.*, **55**, p. 2916 (1984).

48. W.A. Harrison, E.A. Kraut, J.R. Waldrop and R.W. Grant, "Polar Heterojunction Interfaces," *Phys. Rev. B*, **18**, p. 4402 (1978).

49. P.N. Uppal and H. Kroemer, "Molecular beam epitaxial growth of GaAs on Si(211)," *J. Appl. Phys.*, **58**, p. 2195 (1985).

50. W.T. Masselink, T. Henderson, J. Klem, R. Fischer, P. Pearah and H. Morkoç, "Optical Properties of GaAs on (100) Si using molecular beam epitaxy," *Appl. Phys. Lett.*, **45**, p. 1309 (1984).

51. H. Kroemer, "Polar-on-Nonpolar Epitaxy," *J. Cryst. Growth*, **81**, p. 193 (1987).

52. S. Strite, D. Biswas, N.S. Kumar, M. Fadkin and H. Morkoç, "Antiphase domain free growth of GaAs on Ge in GaAs/Ge/GaAs heterostructures," *Appl. Phys. Lett.*, **56**, p. 244 (1990).

53. S. Strite, M.S. Ünlü, K. Adami, G.-B. Gao, A. Agarwal, A. Rockett, H. Morkoç, D. Li, Y. Nakamura and N. Otsuka, "GaAs/Ge/GaAs heterostructures by molecular beam epitaxy," *J. Vac. Sci. Technol. B.*, **8**, p. 1131 (1990).

54. P.R. Pukite and P.I. Cohen, "Suppresion of Antiphase Domains in the Growth of GaAs on Ge(100) by Molecular Beam Epitaxy," *J. Cryst. Growth*, **81**, p. 214 (1987).

55. P.R. Pukite and P.I. Cohen, "Multilayer Step Formation after As adsorption on Si(100):Nucleation of GaAs on vicinal Si," *Appl. Phys. Lett.*, **50**, p. 1739 (1987).

56. R.M. Sieg, S.A. Ringel, S.M. Ting, E.A. Fitzgerald and R.N. Sacks, "Anti-Phase Domain-Free Growth of GaAs on Offcut (001) Ge Wafers by Molecular Beam Epitaxy with Suppressed Ge Outdiffusion," *J. Elect. Mat.*, **27**, p. 900 (1998).

57. Y. Li, L. Lazzarini, L.G. Giling and G. Salviati, "On the sublattice location of GaAs grown on Ge," *J. Appl. Phys.*, **76**, p. 5748 (1994).

58. Y. Li and L.J. Giling, "A closer study on the self-annihilation of antiphase boundaries in GaAs epilayers," *J. Crystal Growth*, **163**, p. 203 (1996).

59. D. Marcuse, *Theory of Dielectric Optical Waveguides* (Academic Press, Boston, 1991).

60. R. Regener and W. Sohler, "Loss in Low-Finesse Ti:$LiNbO_3$ Optical Waveguide Resonators," *Appl. Phys. B*, **36**, p. 143 (1985).

61. G. Lalande, N. Guelton, D. Cossement, R.G. Saint-Jacques and J.P. Dodelet, "Optimum growth conditions for the epitaxy of GaAs on Ge by close-spaced vapor transport," *Can. J. Phys.*, **72**, p. 225 (1994).

62. L. Li, S. Gan., H.-K. Han, H. Qi and R.F. Hicks, "The reaction of carbon tetrachloride with gallium arsenide (001)," *Appl. Phys. Lett.*, **98**, p. 951 (1998).

63. A.H. Khan and J.J. Santiago, "Epitaxial films of germanium by MOCVD," in *Epitaxy of Semiconductor Layered Structures: Symposium*, edited by R. T. Tung, L. R. Dawson and R. L. Gunshor (USA Mater. Res. Soc., Pittsburgh, 1988), p. 279.

IMAGE EVALUATION
TEST TARGET (QA-3)

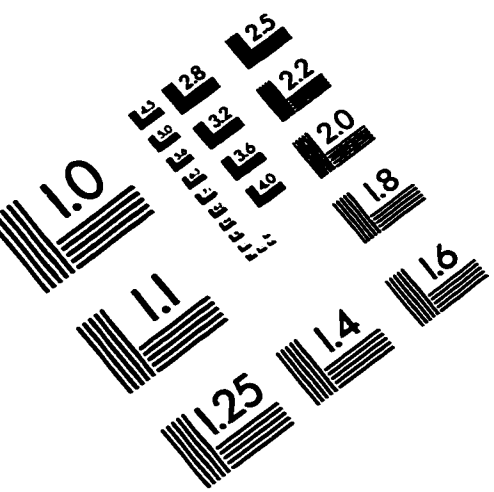

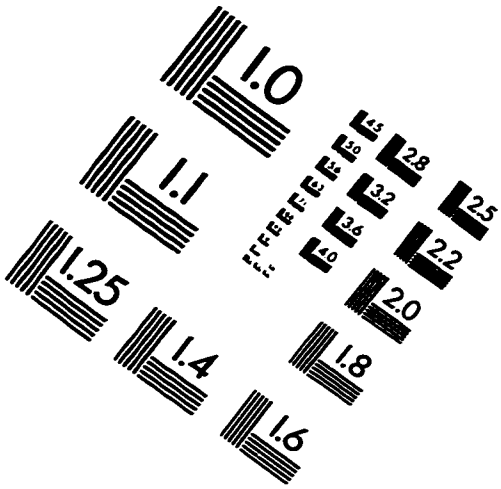

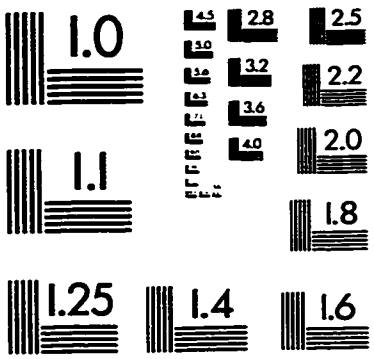

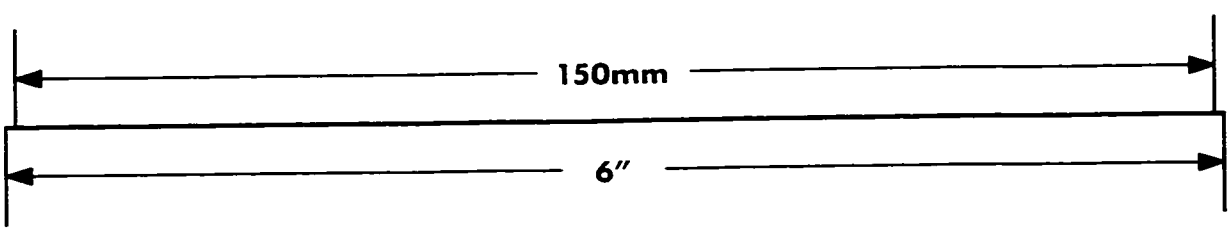

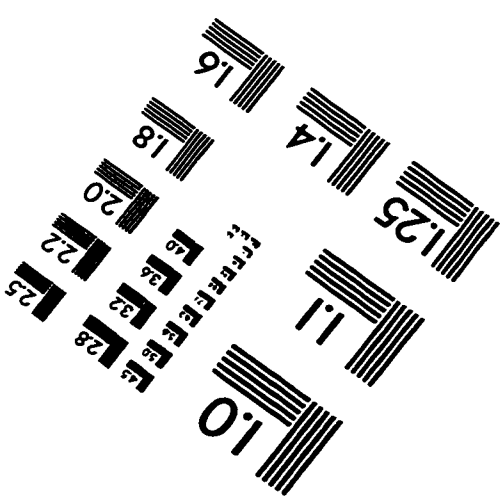

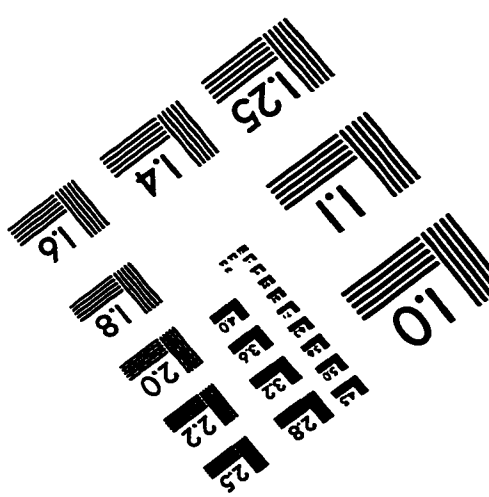

APPLIED IMAGE, Inc
1653 East Main Street
Rochester, NY 14609 USA
Phone: 716/482-0300
Fax: 716/288-5989

© 1993, Applied Image, Inc., All Rights Reserved